CALIFORNIA INSTITUTE OF TECHNOLOGY

Pasadena U.S.A.

A new look at some closure problems of turbulent boundary layers

by

A. E. Perry

1992

G.A.L.C.I.T. Report

FM-92-4

Summary

A new look at the closure problem of turbulent boundary layers is made here using recently derived analytical expressions for the shear stress distributions. These expressions are further simplified here and are based on the law of the wall , the law of the wake formulation of Coles (1956) with the mean continuity and the mean momentum differential and integral equations. The concept of equilibrium layers of Clauser (1954,1956) is extended and using similar ideas as Rotta (1962) for self similarity, a closure scheme is proposed for layers developing in arbitrary adverse pressure gradients for the case where the streamwise derivative of the Coles wake factor is not too large. For a given flow case, this Coles wake condition can be tested with internal consistency checks.

The mathematical framework is most suitable for incorporating the attached eddy hypothesis of Townsend (1976) as recently developed by Perry, Li and Marusic (1991) for closure. This gives an opportunity to incorporate coherent structure concepts into closure schemes. Possible ways of handling the difficult case where the streamwise derivative of the Coles wake factor is significant are discussed.

Many of the important relations are in analytical form and were derived using Mathematica.

1. Introduction

In this work, a new look is taken at the closure problem for turbulent boundary layers in the light of new and more complete analytical expressions recently derived for the shear stress profiles. These derivations are based on the well accepted similarity laws such as Prandtl's law of the wall and law of the wake of Coles (1956). The insights gained from this analytical approach open up new possibilities for simple and plausible closure hypotheses. This is done here using extensions of the equilibrium layer concept of Clauser (1954,1956) and the self preserving flow analyses of Rotta (1962) and Townsend (1976). The results here are intended to be applicable to a wide class of turbulent boundary layers subjected to arbitrary streamwise pressure gradients. It is hoped that the results here will be tested experimentally and are found to be applicable to a wide class of turbulent boundary layers subjected to arbitrary streamwise pressure gradients.

To the author's knowledge, the first attempt to derive shear stress profiles from the law of the wall and law of the wake was Coles (1957). This was for equilibrium layers where the Coles wake factor is invariant with streamwise development. Rotta (1962) attempted the more general non equilibrium flow cases but he made too many approximations and assumptions to give a convincing or reliable result. The author in 1968 carried out the equilibrium layer analysis and tested more hypotheses than were considered by Coles. This work was not published. However, because of a growing need to refer to it in recent years it has been released in its original form as a University of Melbourne internal report. The author's students have extended this analysis to the non equilibrium flow cases and their work is in the theses by Li (1990) and Marusic (1991). An internal report by Perry and Li (1991) extends and applies these analyses to the experimental data of many workers. Rough wall boundary layers were included. These analyses have all been done by hand and the amount of algebra is considerable. The possibility of error is high. Marusic's (1991) result was expressed as the sum of 18 terms, these terms represented a plethora of non-dimensional parameters made up of mean velocity profile variables and associated streamwise derivatives of such quantities. Perry and Li (1991) expressed the result more compactly but it is equivalent to the Marusic (1991) result. The author in this present work, carried out at G.A.L.C.I.T., has repeated and checked all of the above analyses with

the help of *Mathematica* and the results are in agreement with these earlier works and so no errors are apparent. The final result is further simplified here with the help of further relationships derived from the law of the wall, law of the wake and the momentum integral equation. Although the final result is complex in detail and was tedious to arrive at, its overall structure is extremely simple and the insights given are worthwhile rewards for the effort.

One motivation for this work was to incorporate the attached eddy hypothesis of Townsend (1976) as further developed by Perry, Henbest and Chong (1986) into a closure scheme. Some initial steps towards this are given by Perry, Li and Marusic (1991). This represented one of the first attempts to incorporate coherent structure concepts into closure schemes for wall turbulence and avoids the use of local exchange coefficients. This has prompted the following questions for this work:

1.) What sort of mathematical framework would be needed to house such a scheme? Closure schemes such as the attached eddy hypothesis in Perry, Li and Marusic (1991) use convolution integrals and so differential field methods are clearly inappropriate. Hence an integral scheme is the obvious choice.

2.) What high quality information and what reliable assumptions can we use to feed into this framework so as to miminize arbitrary assumptions for closure?

3.) At what point in the framework does closure naturally enter and what are the most natural non-dimensional parameters to use?

For 2 above, the following have been chosen:

(a). The law of the wall and the law of the wake.

(b). The mean momentum differential and integral equations.

(c). The mean continuity equation.

(d). The assumption that streamwise derivatives of the normal Reynolds stresses are negligible.

(e). Close to two-dimensional mean flow is possible.

(f). The belief that if theoretical conditions can be found from the mean momentum and continuity equations which give self similarity in both the velocity defect and shear stress profiles then when these conditions are applied, such self similarity will indeed occur (e.g.

see Rotta 1962).

Using assumptions (a) to (e) above, the shear stress relationships have been derived. Further, with the aid of (f) above, evolution equations for the streamwise development of equilibrium layers have been derived. This is extended to quasi equilibrium layer development where the Coles wake factor is permitted to vary slowly with streamwise distance. The required relationships for closure and the most appropriate nondimensional parameters to use are devised. The form of these closure relationships would need to be obtained from a series of systematic "once and for all" experiments. It might also be possible to use the attached eddy hypothesis in conjunction with this. An example of this is illustrated later in the report.

For the case of Coles wake factor undergoing rapid streamwise development, the quasi equilibrium assumptions breakdown. Problems with this are left to future work but possible directions are briefly discussed.

2. Shear Stress Profiles in Turbulent Boundary Layers

We start with the Coles (1954) "law of the wall, law of the wake" formulation. This can be written as

$$\frac{U}{U_\tau} = \frac{1}{\kappa}\ln\left[\frac{zU_\tau}{\nu}\right] + A + \frac{\Pi}{\kappa}W_c[\eta,\Pi] \tag{1}$$

where U is the mean velocity in the streamwise direction (i.e., the x direction), z is the distance normal to the wall, U_τ is the friction velocity given by $U_\tau = (\tau_0/\rho)^{\frac{1}{2}}$ where τ_0 is the wall shear stress and ρ is the fluid density, ν is the fluid kinematic viscosity, κ is the Kármán constant (later assumed to be 0.41), A is the universal smooth wall constant (later assumed to be 5.1), Π is the Coles wake factor which generally varies with streamwise distance and W_c is the Coles wake function. Traditionally W_c is a universal function of η alone where $\eta = z/\delta_c$ where δ_c is the boundary layer thickness. However we will use the Lewkowicz (1982) formulation, equation (2), which ensures that $\partial U/\partial z = 0$ at $\eta = 1$, i.e.

$$W_c[\eta,\Pi] = 2\eta^2(3-2\eta) - \frac{1}{\Pi}\eta^2(1-\eta)(1-2\eta) \tag{2}$$

An alternative formulation, which also satisfies the above condition, was used by Perry

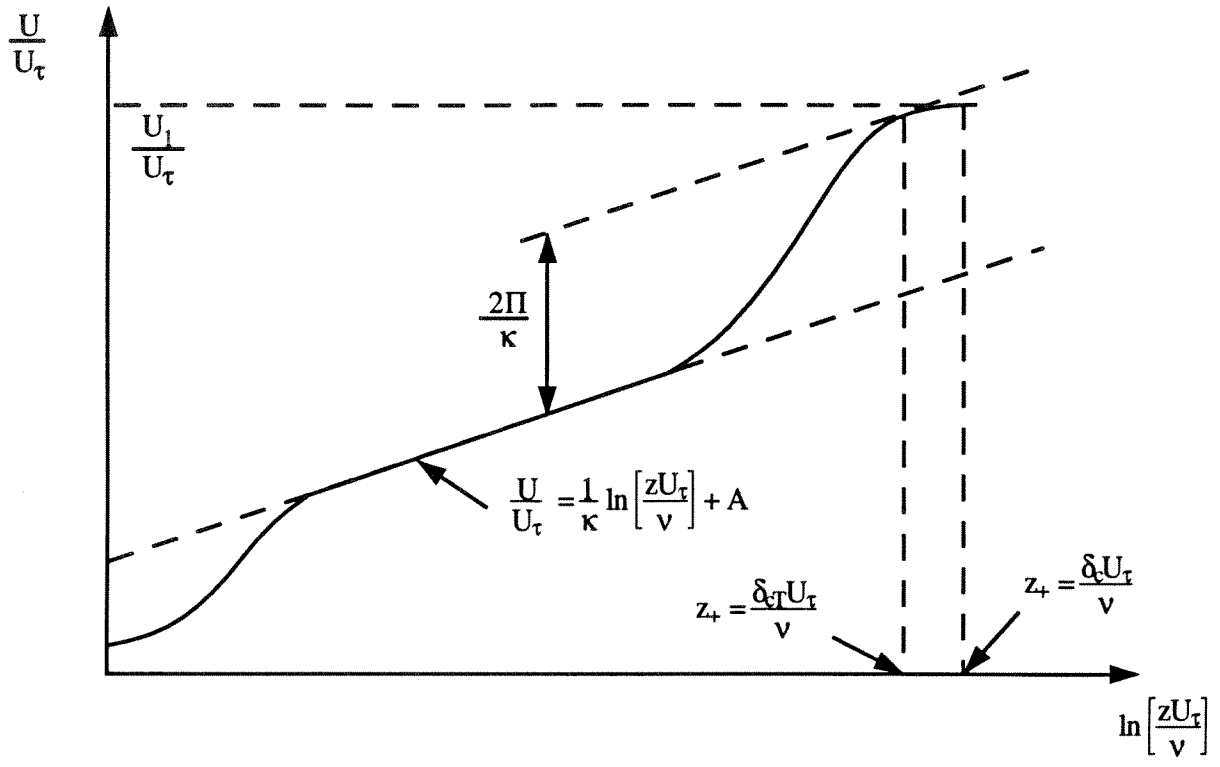

Figure 1: Details of how various wake parameters are defined.

and Li (1990,1991) and Marusic (1991) and is of the form

$$W_c[\eta, \Pi] = 1 - \cos[\gamma\pi\eta] \tag{3}$$

where

$$\gamma = \delta_c/\delta_{cT} \qquad \text{and}$$

$$1+\Pi\gamma\pi\sin[\gamma\pi] = 0. \tag{4}$$

Figure 1 shows how δ_c and δ_{cT} are defined.

This trigonometric formulation is unsuitable for low values of Π since for Π less than about 0.2, the solution for γ follows an unrealistic branch. Also the polynomial formula was found to be slightly more convenient for computing shear stress profiles and mean profile parameters.

In this work the velocity defect formulation will be used throughout. That is

$$\begin{aligned}\frac{U_1 - U}{U_\tau} &= f[\eta, \Pi] \\ &= -\frac{1}{\kappa} ln\ \eta + \frac{\Pi}{\kappa} W_c[1, \Pi] - \frac{\Pi}{\kappa} W_c[\eta, \Pi]\end{aligned} \tag{5}$$

where U_1 is the local freestream velocity.

The mean continuity equation is

$$\frac{\partial U}{\partial x} + \frac{\partial W}{\partial z} = 0 \tag{6}$$

where W is the mean velocity component normal to the wall. Note that two-dimensional mean flow is being assumed.

The mean momentum equation is

$$U\frac{\partial U}{\partial x} + W\frac{\partial U}{\partial z} = -\frac{1}{\rho}\frac{dp}{dx} + \frac{1}{\rho}\frac{\partial \tau}{\partial z} \tag{7}$$

where p is the freestream static pressure and τ is the local shear stress. It should be noted that streamwise gradients of turbulence normal stresses are zero. Later the relationship

$$\frac{\tau}{\rho} = -\overline{u'w'} + \nu\frac{\partial U}{\partial z} \tag{8}$$

will be used. Here $\nu \partial U/\partial z$ is the viscous contribution and $-\overline{u'w'}$ is the Reynolds (kinematic) shear stress where u' and w' are the fluctuating components of velocity in the x and z directions respectively and the overscore denotes a time average. For the region of flow where $zU_\tau/\nu > 50$, the viscous contribution is negligible. Perry (1968), who considered equilibrium layers found that the inclusion of the buffer zone and viscous sublayer in the formulation had negliglible effect on the overall momentum balance and shear stress distribution for practical ranges of Reynolds number and it is assumed here that it is quite safe for the purpose of momentum balances and shear stress profiles to take the logarithmic law profile all the way to the boundary.

Substituting (5) and (6) into (7) and integrating we obtain, after much algebra

$$\begin{aligned}\frac{\tau}{\tau_0} &= 1 + A_1X_1 + A_2X_2 + A_3X_3 + A_4X_4 \\ \text{where} \quad A_i &= A_i[\eta, \Pi, S]\end{aligned} \tag{9}$$

Also

$$\left.\begin{aligned} X_1 &= \frac{d\delta_c}{dx} \\ X_2 &= \frac{\delta_c}{S}\frac{dS}{dx} \\ X_3 &= \delta_c \frac{d\Pi}{dx} \\ X_4 &= \frac{\delta_c}{U_1}\frac{dU_1}{dx} \end{aligned}\right\} \tag{10}$$

where

$$S = \frac{U_1}{U_\tau} = \sqrt{2/C_f'} \tag{11}$$

and

$$C_f' = \frac{\tau_0}{\frac{1}{2}\rho U_1^2} \tag{12}$$

and is the local skin friction coefficient. The A_i's are given by

$$\left.\begin{aligned} A_1 &= \psi_3 + S\psi_4 \\ A_2 &= -\psi_1 - S\psi_2 \\ A_3 &= \psi_6 + S\psi_7 \\ A_4 &= S\psi_5 + \psi_1 + S\psi_2 \end{aligned}\right\} \tag{13}$$

where

$$\left.\begin{aligned} \psi_1 &= 2e_2 - e_3 \\ \psi_2 &= -e_1 \\ \psi_3 &= e_2 - e_3 \\ \psi_4 &= e_4 - e_1 \\ \psi_5 &= e_4 - 2e_1 \\ \psi_6 &= e_6 - e_7 \\ \psi_7 &= -e_5 \end{aligned}\right\} \tag{14}$$

where

$$\left.\begin{aligned} e_1 &= \int_0^\eta f d\eta \\ e_2 &= \int_0^\eta f^2 d\eta \\ e_3 &= f \int_0^\eta f d\eta \\ e_4 &= \eta f \\ e_5 &= \frac{d}{d\Pi} \int_0^\eta f d\eta \\ e_6 &= \frac{d}{d\Pi} \int_0^\eta f^2 d\eta \\ e_7 &= f \frac{d}{d\Pi} \int_0^\eta f d\eta \end{aligned}\right\} \tag{15}$$

This is the form arrived at by Perry and Li (1991) and in an equivalent form by Marusic (1991). Now relationships can be established between the X_i's as follows. From the law of the wall and law of the wake

$$X_2 = E_1(X_1 + NX_3 + X_4) \tag{16}$$

where

$$E_1 = \frac{1}{\kappa S + 1} \tag{17}$$

and

$$N = W_c[1, \Pi] + \Pi \frac{dW[1, \Pi]}{d\Pi} \tag{18}$$

From the outer boundary condition $\tau/\tau_0 = 0$ at $\eta = 1$

$$\left.\begin{aligned} 0 &= 1 + B_1 X_1 + B_2 X_2 + B_3 X_3 + B_4 X_4 \\ \text{where} \quad B_i &= A_i[1, \Pi] \end{aligned}\right\} \tag{19}$$

This can also be derived from the momentum integral equation (see equation (21) later). From equations (16) through to (19) X_1 and X_2 can be expressed in terms of X_3 and X_4 to give

$$\frac{\tau}{\tau_0} = f_1[\eta, \Pi, S] + f_2[\eta, \Pi, S]\delta_c \frac{d\Pi}{dx} + f_3[\eta, \Pi, S] \frac{\delta_c}{U_1} \frac{dU_1}{dx}. \tag{20}$$

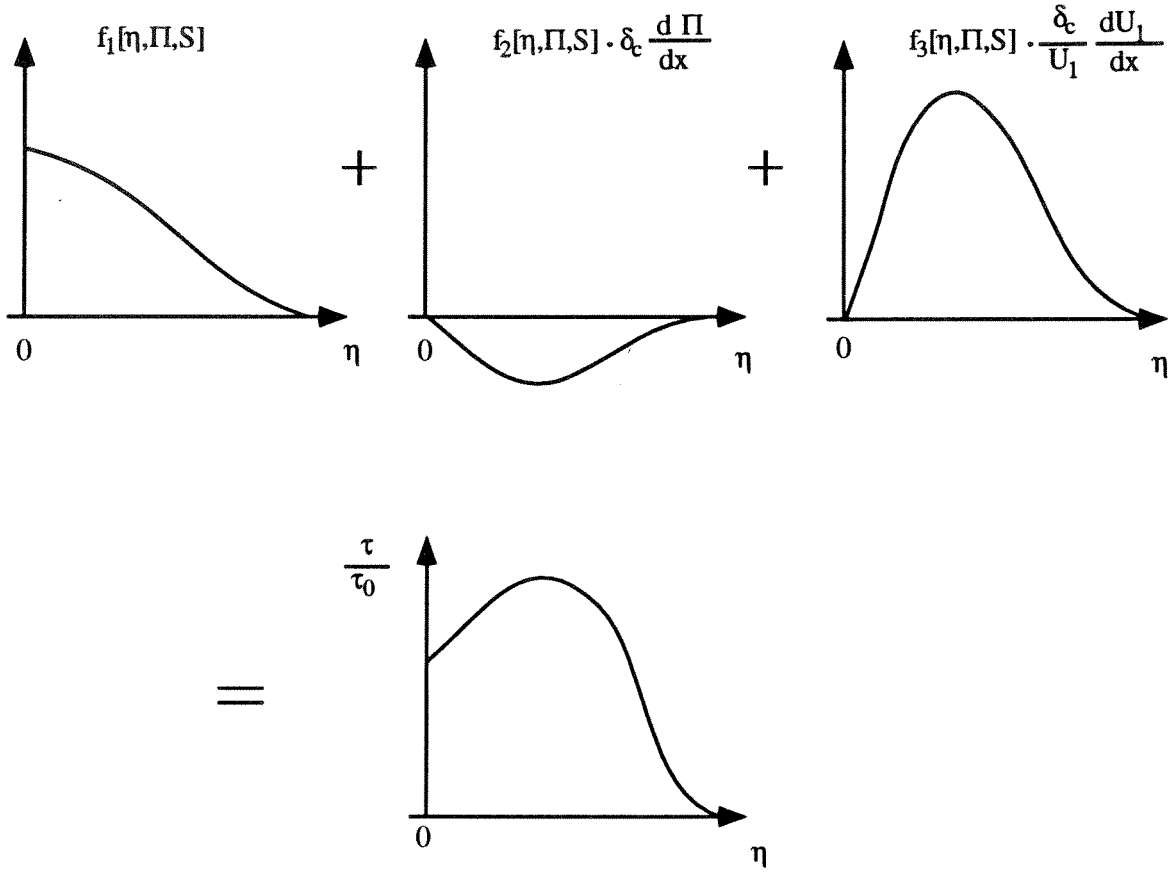

Figure 2: Components of equation (20) for a typical adverse pressure gradient case.

This is the simplest and most convenient form so far derived and it can be seen that there are three components of stress given in (20) and these are shown diagramatically in figure 2 for a typical adverse pressure gradient boundary layer. The first term gives a shear stress distribution which resembles a zero pressure gradient layer. The third term adds a curve with a positive maximum but the second term is negative. A positive $\delta_c d\Pi/dx$ causes a reduction in the stress distribution. In the case of favorable pressure gradients to be considered later with numerical examples, the signs of the second and third terms are opposite to that of adverse pressure gradients.

In an equilibrium layer, the second term in (20) is zero and for adverse pressure gradients, the nondimensional shear stress reaches the highest possible maximum value. This is an interesting property of equilibrium boundary layers.

Figure 3 shows some experimental data of Marusic (1991) for a nonequilibrium layer

compared with equation (20). Here $\delta_c d\Pi/dx$, $(\delta_c/U_1)dU_1/dx$ and S were obtained from experiment and fed into (20) and the agreement is very satisfactory. Figure 4, shows results which the author interpolated from the data of East et al (1979) who carried out a series of experiments a on family of equilibrium layers (i.e. $\delta_c d\Pi/dx$ was approximately zero). The interpolation gives the same values of Π as for Marusic's data and the results are plotted to the same scale. It can be seen that the effect of $\delta_c d\Pi/dx$ is very large in the case of Marusic's data and the maximum nondimensional shear stress is considerably lower than the East et al data. It can be seen that there is no one to one correspondence between the nondimensional velocity defect profile (characterized by Π) and the nondimensional shear stress profiles as is implied in theories which use universal distributions of eddy viscosity or mixing length. From what follows later, such theories would come to grief if $\delta_c d\Pi/dx$ effects are significant.

Equation (20) has been rigorously derived and so is an excellent tool for testing experimental data. Perry and Li (1991) applied (20) (which was in the form of (9)) to the Reynolds shear stress data of many workers. Departures indicate either a lack of two-dimensionality or poor hot-wire techniques.

3. Evolution Equations for Equilibrium Boundary Layers

The equations which govern the streamwise evolution of turbulent boundary layers will be given. Our attention for the moment will be confined to equilibrium layers and hence $\delta_c d\Pi/dx = 0$. We will use the law of the wall, law of the wake and the momentum integral equation. This later equation is

$$\frac{d\theta}{dx} + \left(\frac{\delta^*}{\theta} + 2\right)\frac{\theta}{U_1}\frac{dU_1}{dx} = \frac{1}{S^2} \tag{21}$$

where θ and δ^* are the momentum and displacement thicknesses respectively and are given by

$$\frac{\theta}{\delta_c} = \frac{C_1}{S} - \frac{C_2}{S^2} \tag{22}$$

$$\frac{\delta^*}{\delta_c} = \frac{C_1}{S} \tag{23}$$

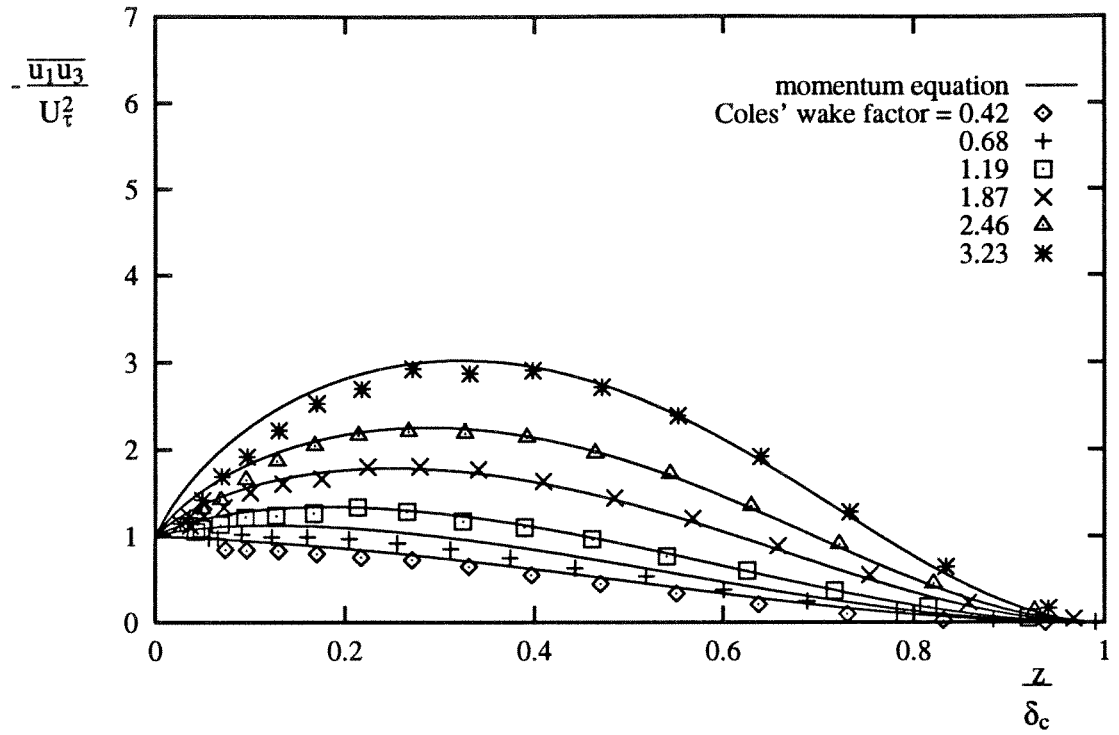

Figure 3: Nonequilibrium flow data of Marusic (1991). Solid lines are obtained using equation (20).

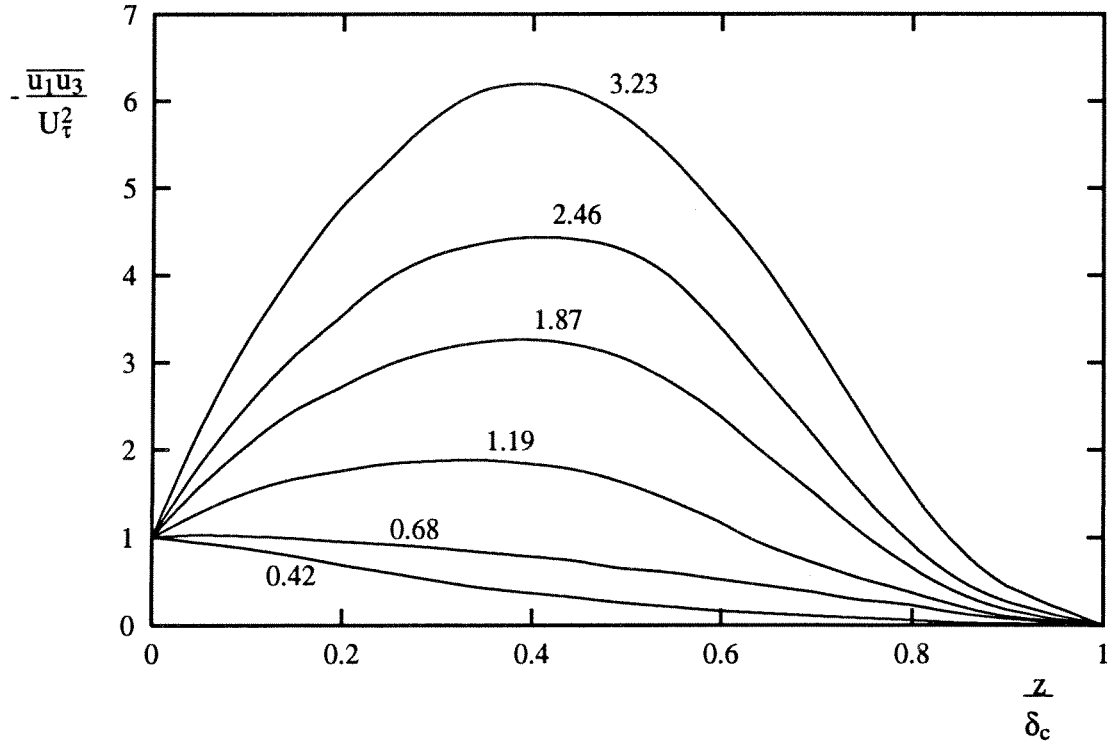

Figure 4: Author interpolated data for the same values of Π as shown in figure 3 for the approximate equilibrium flows of East et al (1979).

where

$$C_1[\Pi] = \int_0^1 f[\eta, \Pi] d\eta = \int_0^\infty \frac{U_1 - U}{U_\tau} d\eta \tag{24}$$

and

$$C_2[\Pi] = \int_0^1 f^2[\eta, \Pi] d\eta = \int_0^\infty (\frac{U_1 - U}{U_\tau})^2 d\eta \tag{25}$$

The analysis which follows makes use of the following definitions and identities

$$\frac{\delta_c}{S}\frac{dS}{dx} = \frac{\delta_c}{U_1}\frac{dU_1}{dx} - \frac{\delta_c}{U_\tau}\frac{dU_\tau}{dx} \tag{26}$$

from the product rule and

$$\frac{\delta^*}{U_1}\frac{dU_1}{dx} = -\frac{\beta}{S^2} \tag{27},$$

$$\frac{\delta_c}{U_1}\frac{dU_1}{dx} = -\frac{\beta}{C_1 S} \tag{28},$$

and

$$\frac{\delta_c}{U_\tau}\frac{dU_1}{dx} = -\frac{\beta}{C_1} \tag{29}$$

where

$$\beta = \frac{\delta^*}{\tau_0}\frac{dp}{dx} \tag{30}$$

where β is the Clauser (1956) pressure gradient parameter.

From the law of the wall and law of the wake

$$\frac{\delta_c U_\tau}{\nu} = K_\tau = E[\Pi] \exp[\kappa S] \tag{31}$$

Here K_τ will be referred to as the Kármán number. $E[\Pi]$ is given by

$$E[\Pi] = \exp[-\kappa(A + \frac{\Pi}{\kappa} W_c[1, \Pi])] \tag{32}$$

Also a frequently occurring function is

$$\Phi = \frac{d\ln U_\tau}{d\ln \delta_c} = \frac{1}{U_\tau}\frac{dU_\tau}{dx}\left(\frac{1}{\delta_c}\frac{d\delta_c}{dx}\right)^{-1} = -\left(\frac{\kappa\beta}{C_1}\left(\frac{d\delta_c}{dx}\right)^{-1} + 1\right)/(\kappa S + 1) \tag{33}.$$

From the law of the wall and law of the wake, an expression for $d\theta/dx$ can be found thus

$$\begin{aligned}\frac{d\theta}{dx} = \{&\frac{d\delta_c}{dx}\left[S(C_1\kappa S^2 - C_2\kappa S + C_2)\right] \\ &- [-C_1 S + 2C_2]\frac{\beta}{C_1}\}/(S^3(\kappa S + 1))\end{aligned} \tag{34}$$

From the momentum integral equation $d\theta/dx$ is given by

$$\frac{d\theta}{dx} = \frac{1}{S^2} + (3SC_1 - 2C_2)\frac{\beta}{S^3 C_1} \tag{35}$$

Equating (34) and (35) gives

$$\frac{d\delta_c}{dx} = \frac{(\kappa S + 1) + (3\kappa C_1 S - 2\kappa C_2 + 2C_1)\beta/C_1}{(C_1\kappa S^2 - C_2\kappa S + C_2)} \tag{36}$$

From equations (26), (29) and (33) it can be shown that

$$\delta_c \frac{dS}{dx} = -\frac{\beta}{C_1} - S\Phi\frac{d\delta_c}{dx} = R[S, \beta, \Pi] \tag{37}$$

and after a considerable amount of algebra, it can be shown that R is given by

$$R = \frac{2C_1\beta S + C_1 S - \beta C_2}{C_1\{\kappa C_1 S^2 - C_2\kappa S + C_2\}} = 0 \tag{38}$$

From equation (31) δ_c on the LHS of (37) can be replaced to give

$$SE\exp[\kappa S]\frac{1}{U_1}\frac{dS}{dx^*} = R[S, \beta, \Pi] \tag{39}$$

which is an evolution equation which effectively comes from the law of the wall, law of the wake and the momentum integral integral equation. Here $x^* = x/\nu$.

From equations (28) and (31) we have

$$S^2 E\exp[\kappa S]\frac{1}{U_1^2}\frac{dU_1}{dx^*} = -\frac{\beta}{C_1} \tag{40}$$

This is a second evolution equation and effectively comes entirely from the law of the wall and law of the wake without reference to momentum balances.

Equations (39) and (40) are a pair of coupled equations which in principle can be solved for S and all other profile parameters as a function of x^*. Also the free stream velocity U_1 in terms of x^* can be found which will yield an equilibrium layer for a fixed and chosen Π. One must keep in mind that E, C_1, and C_2 are all functions of Π alone and hence are invariant with x^* for equilibrium flow. However, a third equation is necessary to obtain closure. We need to know the functional form

$$\beta = \beta[\Pi, S] \tag{41}$$

There have been several theories for this. One comes from Clauser (1954, 1956) where

$$\Pi = F[\beta] \tag{42}$$

i.e., Π is a function of β alone. However, Coles (1957) contends that

$$\left.\begin{aligned} \Pi &= F[D] \\ \text{where} \quad D &= \frac{d\ \ln U_1}{d\ \ln U_\tau} \end{aligned}\right\} \tag{43}$$

and using this actually enables the functional form (41) to be found once we know the value of D for a fixed Π.

Another theory can be constructed from the work of Perry, Bell and Joubert (1966) where

$$\left.\begin{aligned} \Pi &= F[\psi] \\ \text{and} \quad \psi &= \frac{\delta_c}{\tau_0}\frac{dp}{dx} \end{aligned}\right\} \tag{44}$$

i.e., Π is a function only of ψ, i.e., if ψ is fixed so also is Π. Again, using this, a relationship (41) can be obtained. It should also be noted that the form of the F's in (42) (43) and (44) can be found only by experiment and an example for equation (42) will be given later.

It can be shown that no matter what closure assumption is made equations (39) and (40) can be reduced to one second order autonomous *o.d.e.* of the form

$$\frac{d^2S}{dx^{*2}} + f[S,\beta]\left(\frac{dS}{dx^*}\right)^2 = 0 \tag{45}$$

This may be integrated readily once to give

$$\frac{dS}{dx^*} = \left(\frac{dS}{dx^*}\right)_0 \exp\left[-\int_{S_0}^{S} f[S,\beta]ds\right] \tag{46}$$

where the suffix 0 denotes initial values at $x^* = 0$. The solution may be displayed on a phase plane with ordinates dS/dx^* versus S and figure 5 shows a typical phase plane portrait. All solutions collapse if dS/dx^* is appropriately scaled and a number of critical points occur along the S axis. The function $f[S,\beta]$ is a ratio of two polynomials in S and these critical points correspond with the poles and zeros of $f[S,\beta]$. An examination and classification of such critical points is a major study in itself. However, the author has

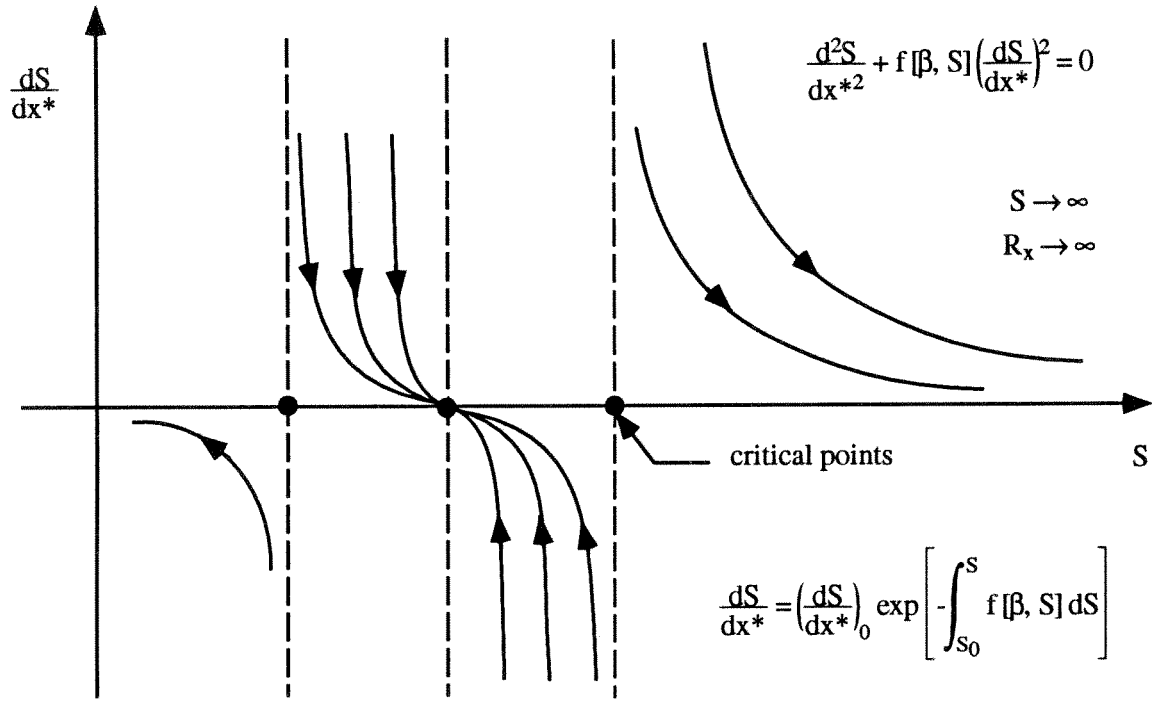

Figure 5: Typical phase plane potrait for (46). Sketch only.

not found so far from data considered in this work any critical points of interest in the practical ranges of S. Of great importance is that as x^* increases indefinitely so also does S as shown at the right hand end of figure 5.

Using equation (39), $(dS/dx^*)_0$ can be found given $S = S_0$ at $x^* = 0$. Also $U_1 = U_0$ at $x^* = 0$. Substituting this into (46) we obtain

$$\frac{dS}{dR_x} = \frac{R[S_0, \beta[\Pi, S_0]]}{S_0 E \exp[\kappa S]} \exp\left[-\int_{S_0}^{S} f[S, \beta] dS\right] \tag{47}$$

Here

$$R_x = \frac{xU_0}{\nu} \tag{48}$$

and represents the most practical of streamwise Reynolds numbers since the variables x, U_0 and ν are known and specified by the user. Taking the case of the Clauser hypothesis, according to (42) a fixed Π corresponds to a fixed β and $f[S, \beta]$ is given by

$$f[S, \beta] = \left(\frac{1}{S} + \kappa - \frac{1}{R}\frac{dR}{dS} + \frac{\beta}{SC_1 R}\right) \tag{49}$$

With (47) the solution using the Clauser hypothesis is

$$\frac{dS}{dR_x} = \frac{R[S,\beta]}{E \cdot S} \exp[-\kappa S] \exp\left[-\int_{S_0}^{S} \frac{\beta}{C_1 R S} dS\right] \tag{50}$$

where R is given by (38). By integrating once more we obtain S as a function of R_x and from this we can calculate all other velocity profile parameters. From equation (40) we can calculate U_1/U_0 as a function of R_x which is the free-stream velocity distribution needed for producing the required equilibrium flow. Unlike usual calculations, here U_1/U_0 versus R_x is a solution rather than a specified input. This is referred to as the "inverse problem". Later we will consider the "direct problem" where U_1/U_0 versus R_x is specified and in general a nonequilibrium flow is produced.

For the case of a zero pressure gradient layer ($\beta = 0$)

$$\frac{dS}{dR_x} = \frac{\exp[-\kappa S]}{E(C_1 \kappa S^2 - C_2 \kappa S + C_2)} \tag{51}.$$

This is usually considered to be an equilibrium layer since β = constant and so also is Π (usually taken to be 0.55).

If we assume that $C_1 \kappa S^2$ dominates the denominator in (51) then

$$\sqrt{\frac{2}{C_f'}} = a_1 \log[R_x \cdot C_f'] + a_2 \tag{52}$$

where a_1 and a_2 are constants. This is the well known von Kármán law of skin friction and represents the only analytical solution so far found for the evolution of a turbulent boundary layer. It can be seen that the work of this report has the potential for producing further analytical solutions.

Similar analytical expressions can be derived using the other hypotheses e.g., closure equations (43) and (44) or hypotheses yet to be derived. The question as to which hypothesis is correct must be decided by investigating the shear stress profile behavior. As mentioned in the introduction, it is expected that the conditions most likely to succeed in giving equilibrium flow (i.e., Π = constant) are those which give self similar shear stress profiles.

4. Comparison of the Various Hypotheses

The performance of the various hypotheses as regards to self similarity of the shear-stress profiles for fixed Π are shown in figures 6 to 13 inclusive.

In figure 6 the results of a zero pressure gradient are shown. Here it is assumed that $\Pi = 0.55$ and all hypotheses so far considered i.e., (42) through (44) give this result. Figures 7 through 9 give the results for the hypotheses given by (42) (Clauser 1956), figures 10 and 11, the hypothesis given by (43) (Coles 1957) and figures 11 and 12 for the hypothesis given by (44) (Perry et al 1966). All numerical values chosen are those of Perry (1968) which were based partly on Coles' (1957) values attributed to the flow cases of Clauser (1954). The flow case $\Pi = 10$ used β given by equation (56) in §5.

For the hypotheses (43) and (44) the asymptotic form for the shear stress profiles is completely different from the profiles at finite S and so these hypotheses do not look very promising.

The Clauser hypothesis performs the best but in the author's view it is still far from satisfactory.

5. Conditions for improved self-similarity of shear stress profiles for fixed Π

It can be seen that the hypotheses considered so far do not produce satisfactory self-similarity of the shear stress distribution for a fixed Π. It is well known from the work of Rotta (1962) that precise self similarity is not possible on a smooth surface except for equilibrium sink flow. This flow case will be dealt with later. However, a better approximate self similarity should be possible than those produced by either (42),(43) or (44).

Since for equilibrium flow $d\Pi/dx = 0$, (20) becomes with the aid of (28)

$$\frac{\tau}{\tau_0} = f_1[\eta, \Pi, S] - f_3[\eta, \Pi, S]\frac{\beta}{C_1 S}. \tag{53}$$

Although it is not possible to collapse τ/τ_0 for all η at a fixed Π, let us seek conditions necessary for forcing the profiles to match at $\eta = m$ where m will be chosen to give

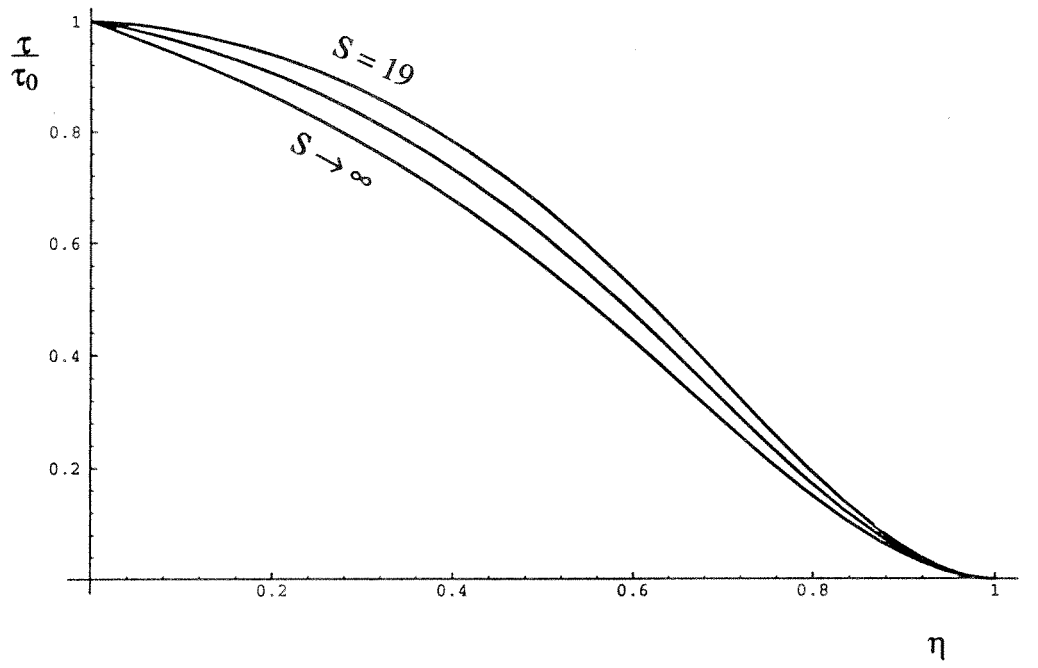

Figure 6: Clauser development (42) for zero pressure gradient flow; $\Pi = 0.55$, $\beta = 0 =$ constant.

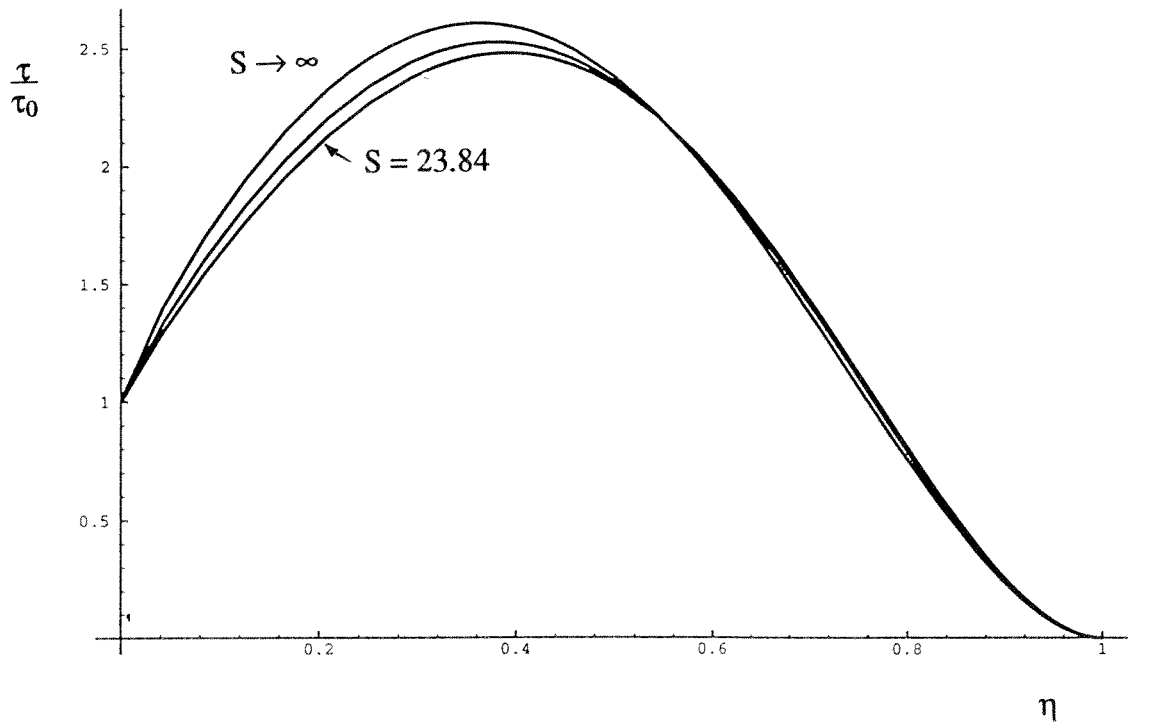

Figure 7: Clauser development (42) for $\Pi = 1.54$, $\beta = 2 =$ constant.

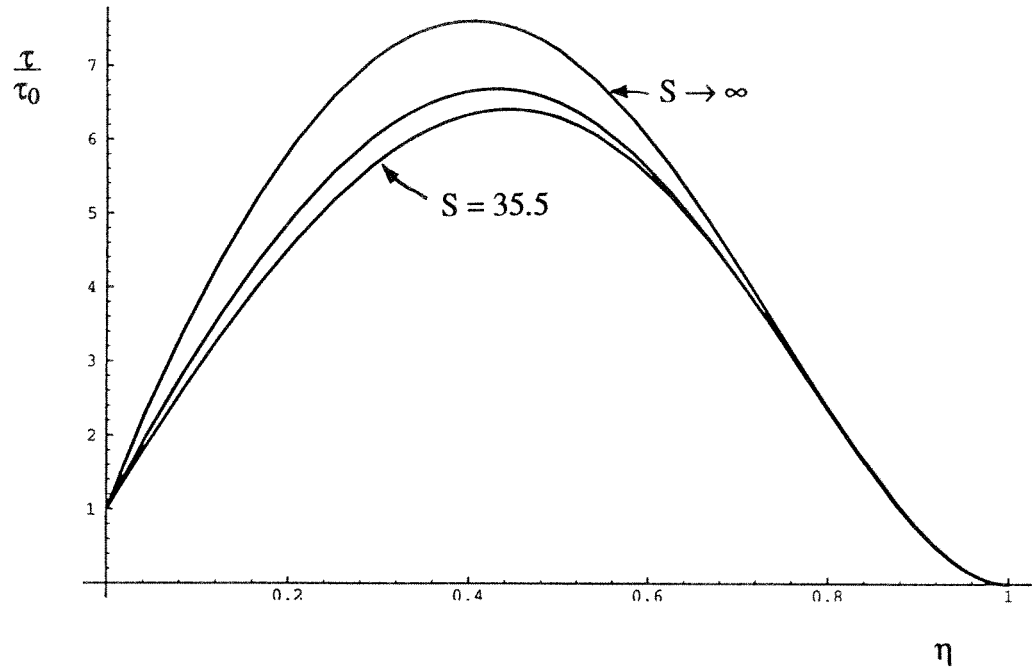

Figure 8: Clauser development (42) for $\Pi = 3.93$, $\beta = 7 = \text{constant}$.

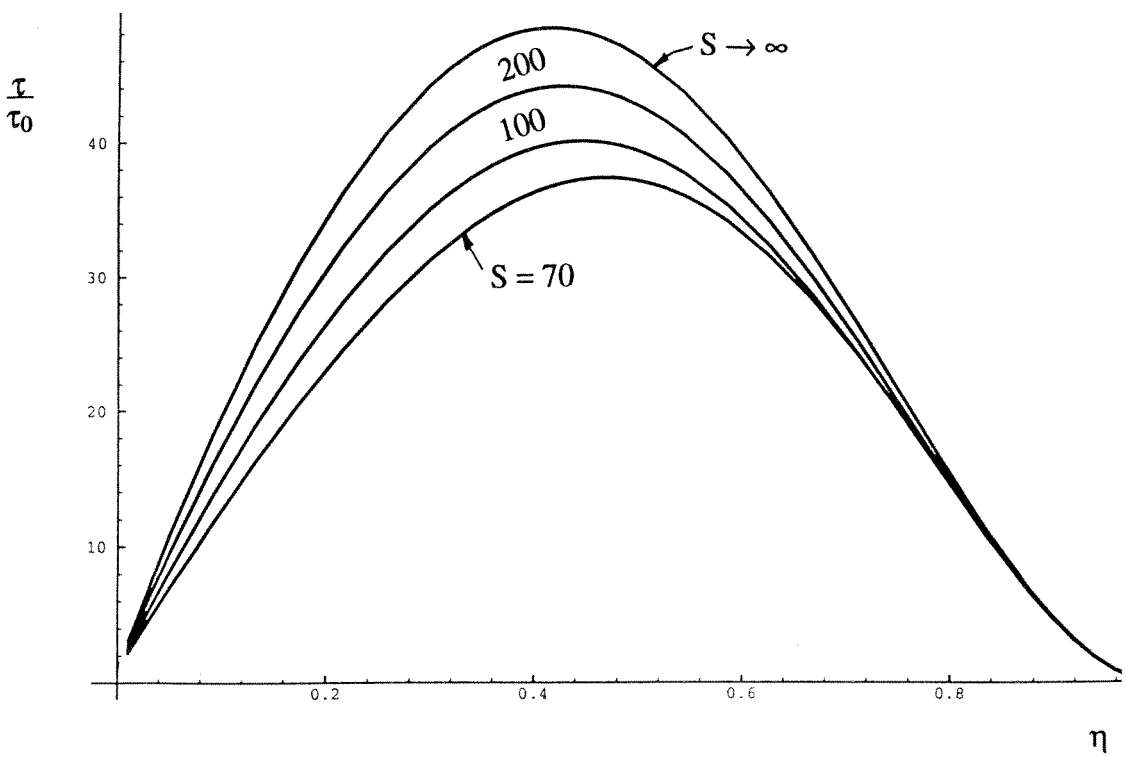

Figure 9: Clauser development (42) for $\Pi = 10$, $\beta = 47 = \text{constant}$.

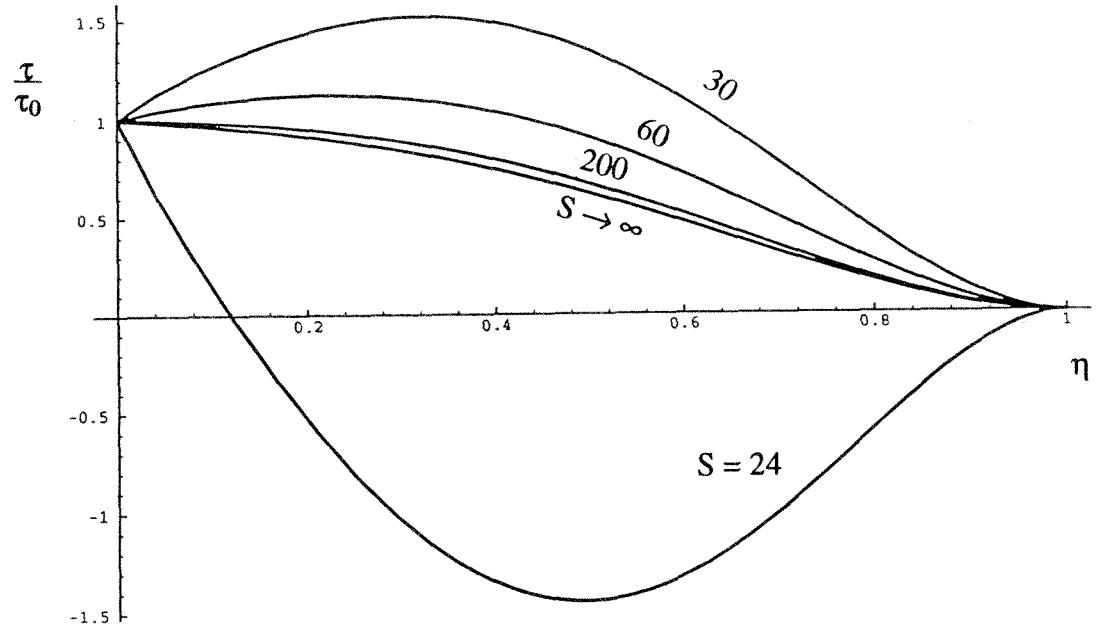

Figure 10: Coles development (43) for $\Pi = 1.54$, $D = 0.795$.

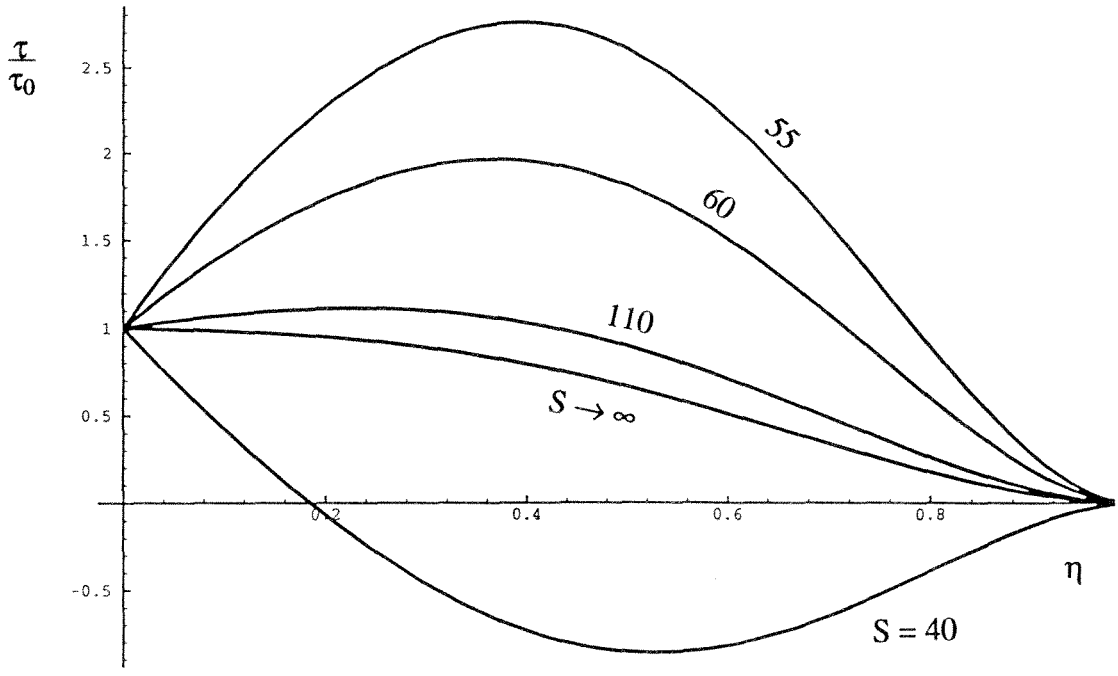

Figure 11: Coles development (43) for $\Pi = 3.93$, $D = 0.863$.

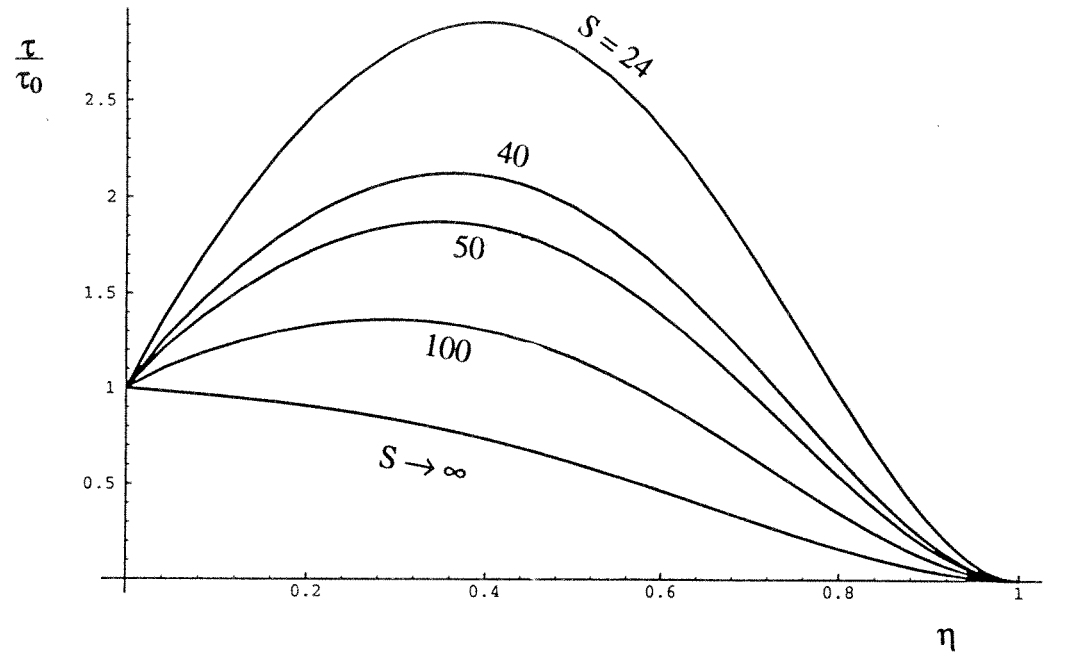

Figure 12: Perry, Bell & Joubert development (44) for $\Pi = 1.54$, $\psi = 9.85$.

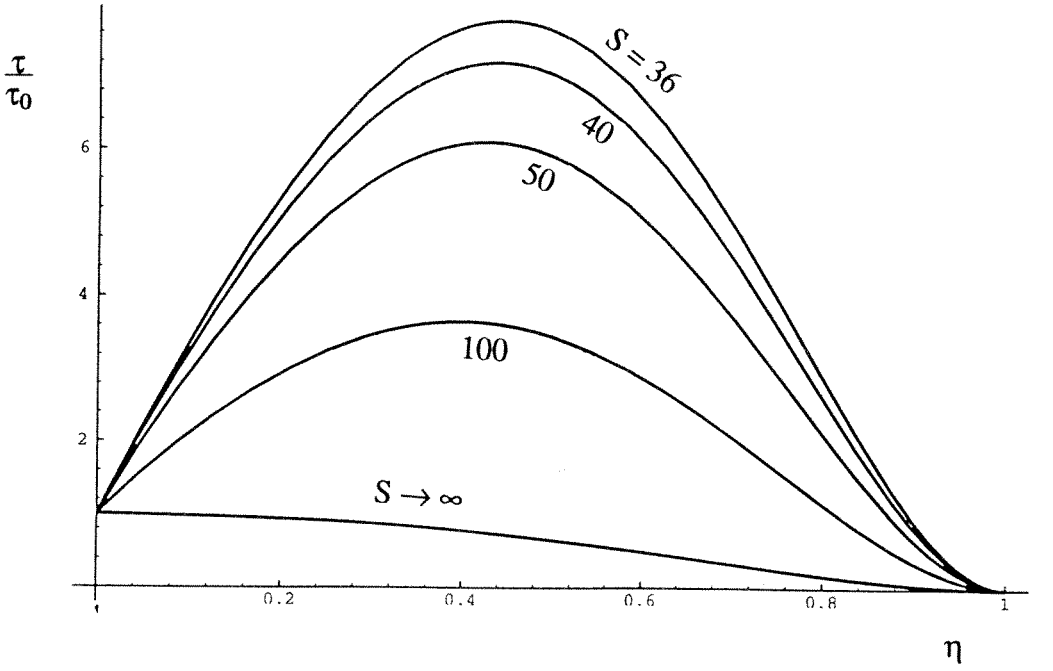

Figure 13: Perry, Bell & Joubert development (44) for $\Pi = 3.93$, $\psi = 26$.

reasonable collapse for most of the profile. In other words

$$\left(\frac{\tau}{\tau_0}\right)_{\eta=m} = f_1[m,\Pi,S] - f_3[m,\Pi,S]\frac{\beta}{C_1 S} = \mathcal{L}[\Pi,m] \tag{54}$$

where in (54) β and S will be varied for fixed Π in such a way as to produce a fixed $\mathcal{L}$. It will be shown shortly that $m = 0.4$ appears to be close to an optimum choice for close to precise self similarity for a wide range of Π and for all S. It turns out that $f_1[m,\Pi,S]$ is a ratio of two polynormals in S of the same order and as $S \to \infty$, f_1 approaches a constant. Also $f_3[m,\Pi,S]/C_1 S$ has similar properties to f_1 and as $S \to \infty$, $f_3/C_1 S$ approaches a constant. The evolution equation based on the hypothesis

$$\mathcal{L} = \mathcal{L}[\Pi] \tag{55}$$

is the same general form as (45) and the critical points on the dS/dx^* versus S phase plane are all at impractically low values of S. Hence again the general behavior of $S \to \infty$ as $R_x \to \infty$ applies. From (54) it can be seen that β must approach an asymptotic value $\beta_g[\Pi]$ which is a function of Π alone. In order to obtain closure, it is necessary to know the function $\beta_g[\Pi]$. East et al (1979) carried out a series of experiments on a family of equilibrium layers and assumed that β was a function only of Π and data seems to fit a relationship proposed by Green et al (1973) which is

$$\beta_g[\Pi] = \left(0.024\left(\frac{C_2[\Pi]}{C_1[\Pi]}\right)^2 - 1\right)/0.8 \tag{56}$$

This is shown in figures 14 and 15 using the Lewkowicz (1982) formulation. Here the suffix g denotes Green et al (1973).

Although East et al's experiments were not carried out with $S \to \infty$ for the purpose of this preliminary investigation it will be assumed that β_g corresponds with the asymptotic value of β for fixed $\mathcal{L}$. This is a temporary assumption just to develop the mathematics and numerical schemes. When and if a more accurate version of (56) is found it will be replaced.

Let β variations for a fixed $\mathcal{L}$ and a given asymptotic value of β_g be denoted by

$$\beta = \beta_{\ell g}[\Pi, S] \tag{57}$$

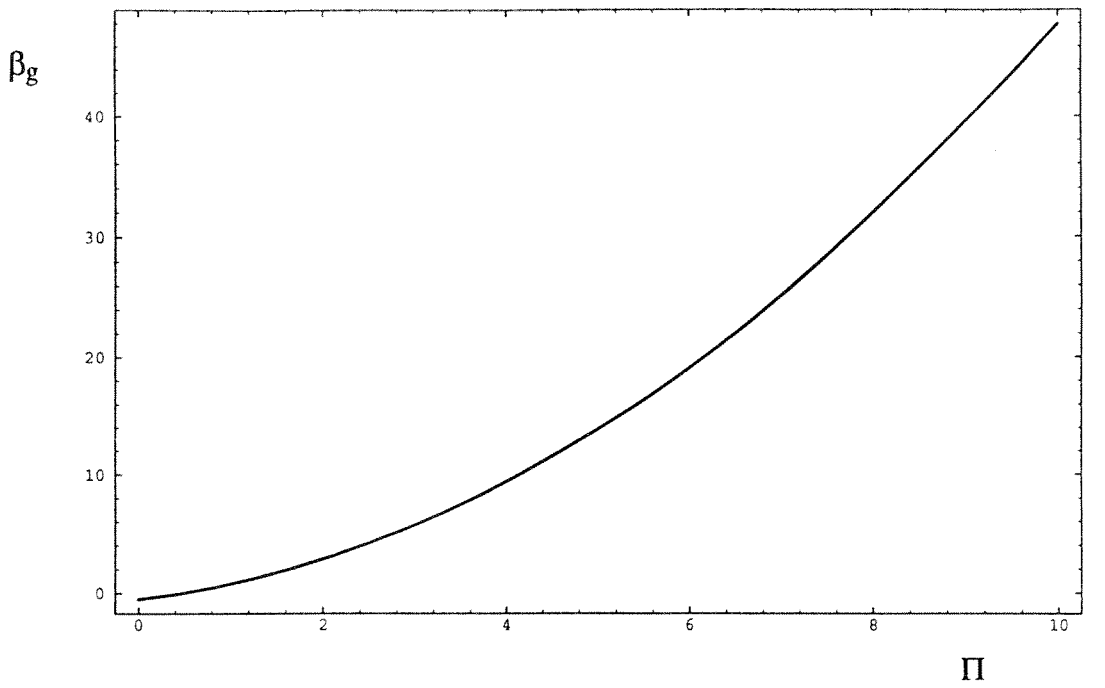

Figure 14: Green et al function (56) ($0 < \Pi < 10$).

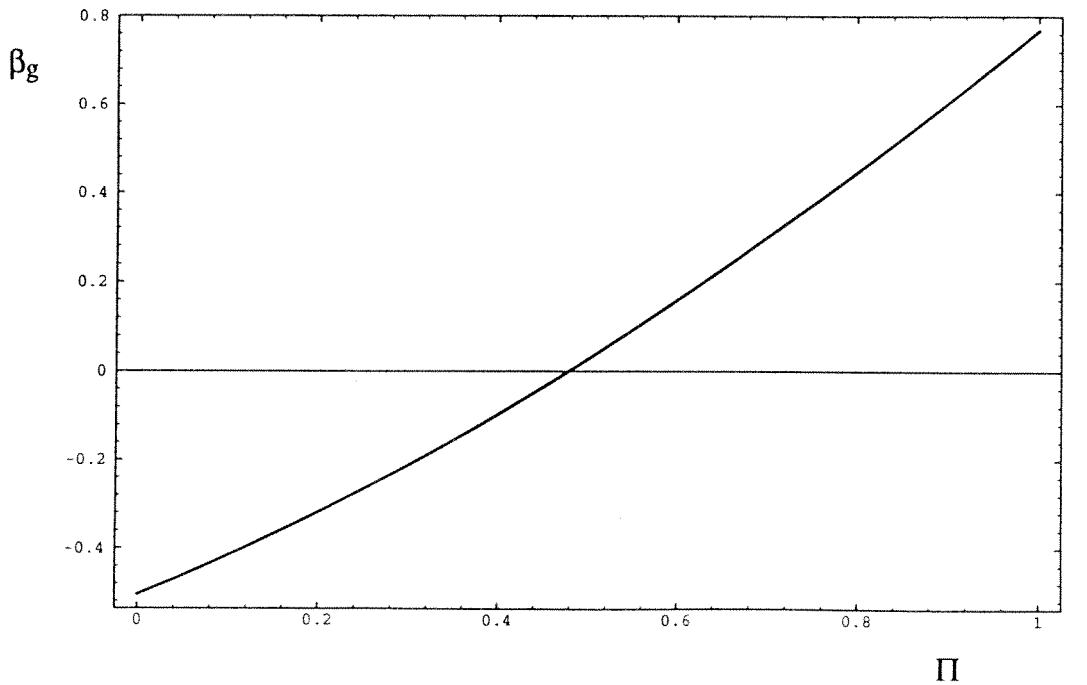

Figure 15: Green et al function (56) ($0 < \Pi < 1$).

and

$$\beta_g = \beta_{\ell g}[\Pi, \infty] \tag{58}$$

and it is understood that $m = 0.4$.

Equation (54) can be written as

$$\beta_{\ell g}[\Pi, S] = \frac{C_1[\Pi]S}{f_3[0.4, \Pi, S]} \left\{ f_1[0.4, \Pi, S] - f_1[0.4, \Pi, \infty] \cdot \lim_{S \to \infty} \left\{ \frac{f_3[0.4, \Pi, S]}{C_1[\Pi]S} \right\} \beta_g[\Pi] \right\} \tag{59}$$

Equation (59) gives a known analytical function for (57).

Figures 16 through 22 show the shear stress profiles according to equations (53), (56) and (59) where S is taken through the lowest practical value to $S \to \infty$. The lowest values of S were calculated to give a Kármán number as defined in (31) to be of order 100. Any value lower than this would be regarded as laminar or transitional flow. Probably a more realistic value would be 300 but 100 was used. Figure 23 shows $m = 0.5$ rather than 0.4 and the later seems to give better self similarity for $\eta < 0.5$. The value of $\Pi = 10$ is deemed to be the close to $\Pi \to \infty$ and probably the concept of a finite S and the existence of the law of the wall becomes irrelevant. $\Pi > 10$ will be considered the subject of another study.

Figures 24 through to 29 show plots of $\triangle\beta$ versus S for different Π's. Here $\triangle\beta$ is defined as

$$\beta_{\ell g}[m, \Pi, S] = \triangle\beta[m, \Pi, S] + \beta_g[\Pi] \tag{60}$$

and results for different values of m are shown. It is interesting to note that for $\Pi < 0.45$ the resulting $\triangle\beta[m, \Pi, S]$ is very insensitive to the choice of m but $m = 0.4$ has been chosen here. Probably the choice of m could be varied with Π for optimum shear stress profile collapse but this will be left for later refinements. It should be noted that according to (56), $\Pi = 0.45$ corresponds with $\beta_g = 0$ whereas $\Pi = 0.55$ is usually taken to be the appropriate value for zero pressure gradient layers. This difference can be resolved by accepting the possibility that a zero pressure gradient boundary layer is not an equilibrium layer and at low but practical values of S, $\Pi = 0.55$ but diminishes slowly to 0.45 for $S \to \infty$. More comments on this will be made later.

Thus we have established new conditions necessary to give an improved self similarity of the shear stress profiles for equilibrium flow. Although the relationships are complex

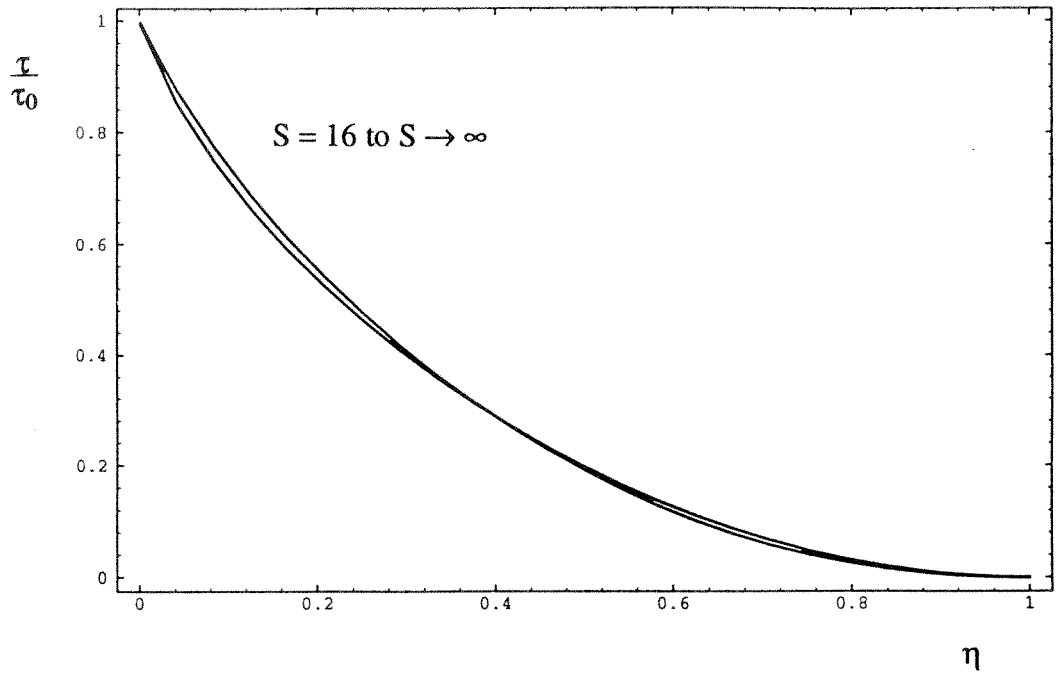

Figure 16: Shear stress profiles using equation (53) with (56) and (59) ($m = 0.4$). $\Pi = 0.1$, $\beta_g = -0.4168$.

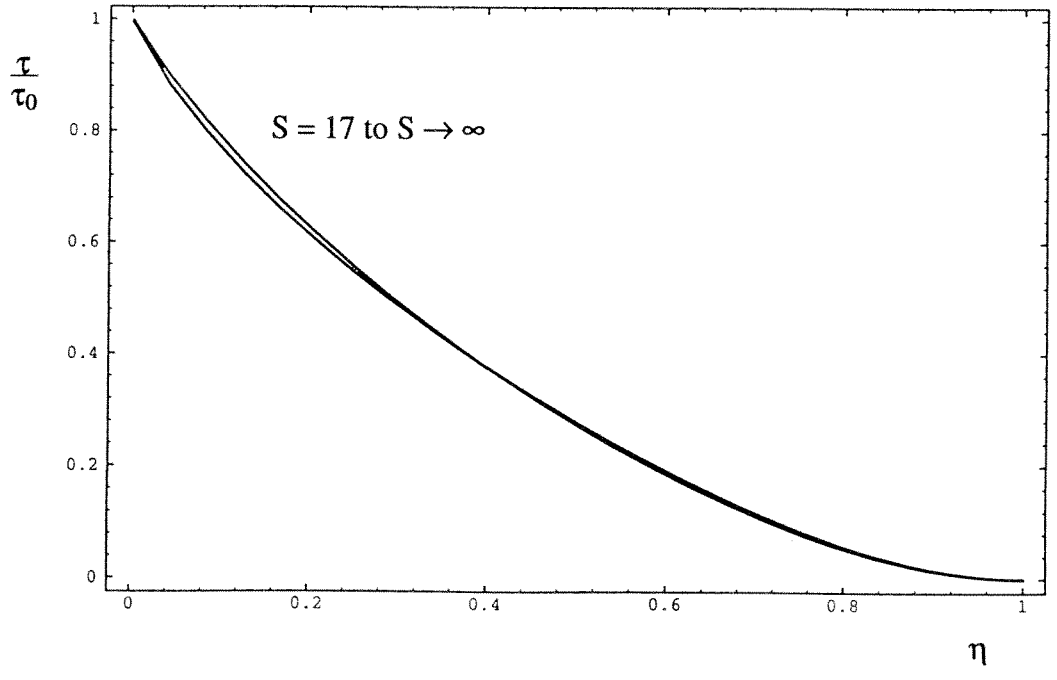

Figure 17: (Caption as in figure 16) $\Pi = 0.2$, $\beta_g = 0.3185$.

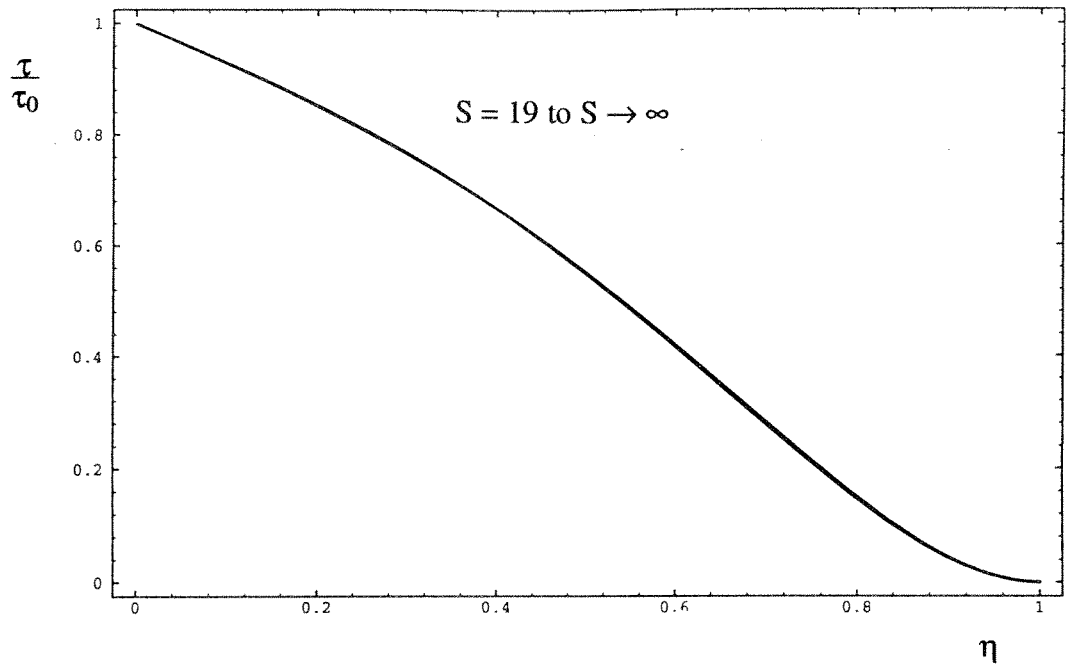

Figure 18: (Caption as in figure 16) $\Pi = 0.45$, $\beta_g = 0$.

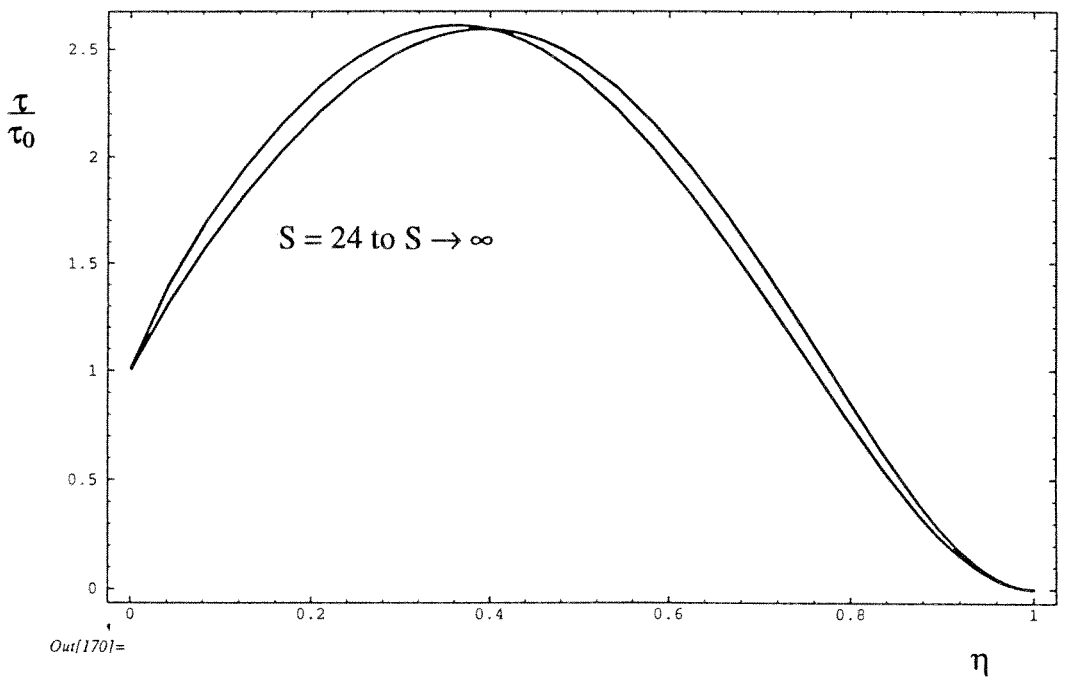

Figure 19: (Caption as in figure 16) $\Pi = 1.54$, $\beta_g = 2$.

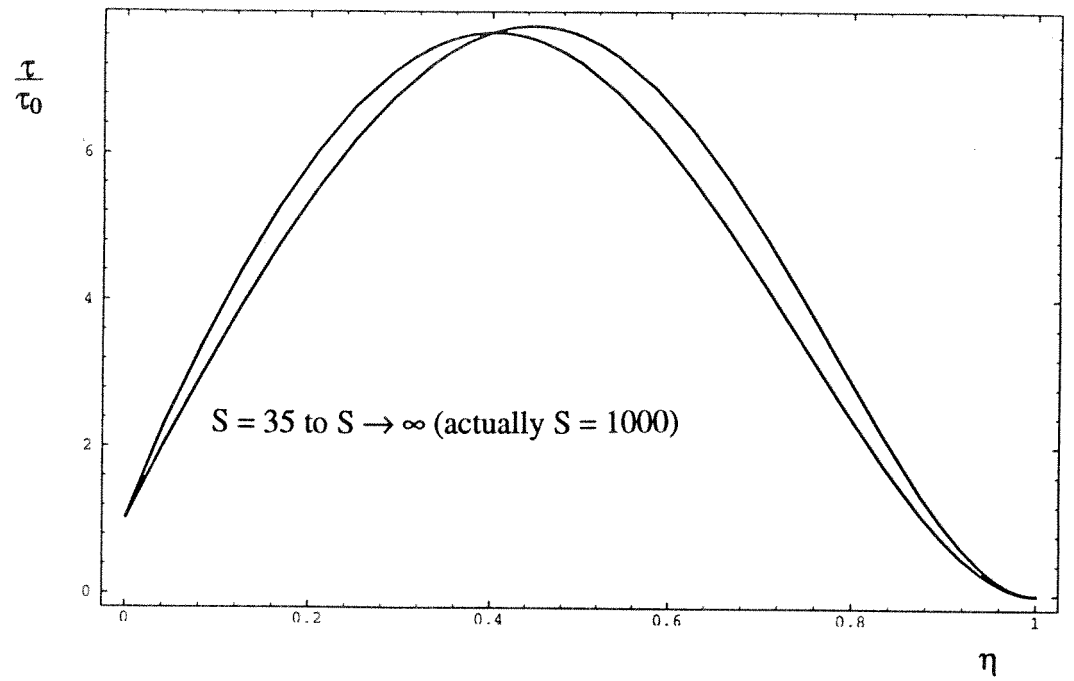

Figure 20: (Caption as in figure 16) $\Pi = 3.93$, $\beta_g = 7$.

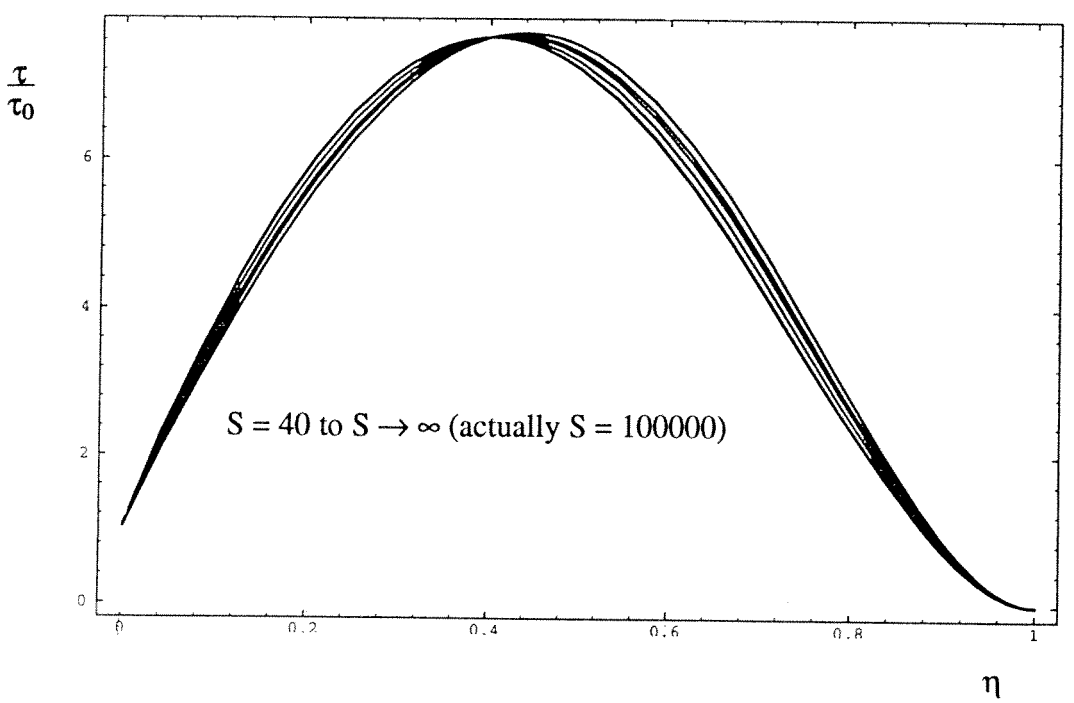

Figure 21: Same as figure 20 but with more values of S.

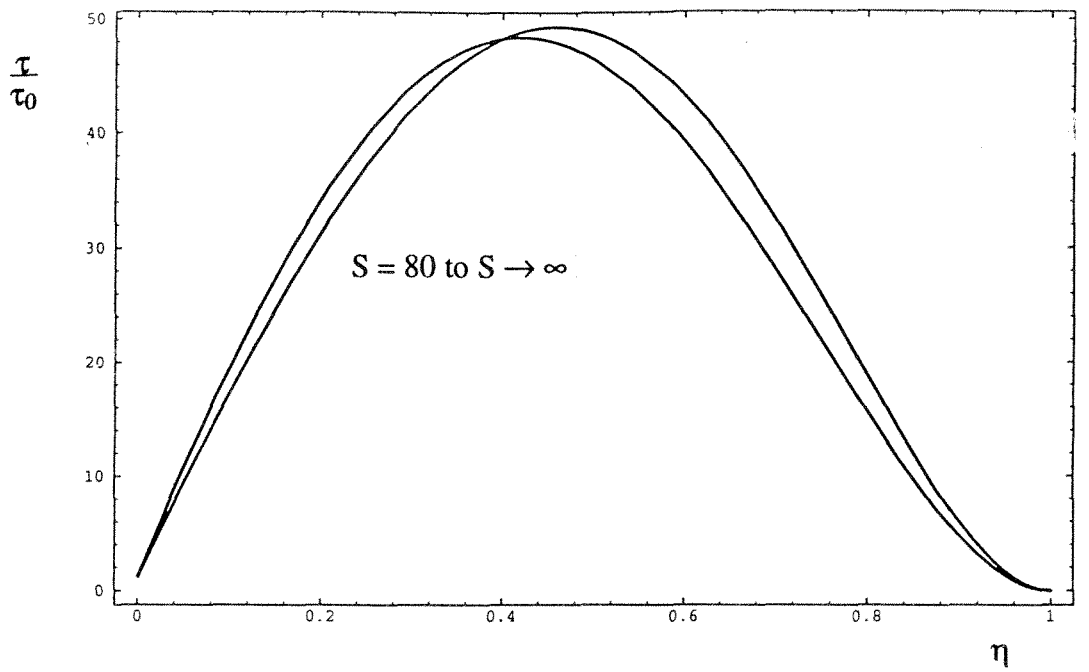

Figure 22: (Caption as in figure 16) $\Pi = 10$, $\beta_g = 47$.

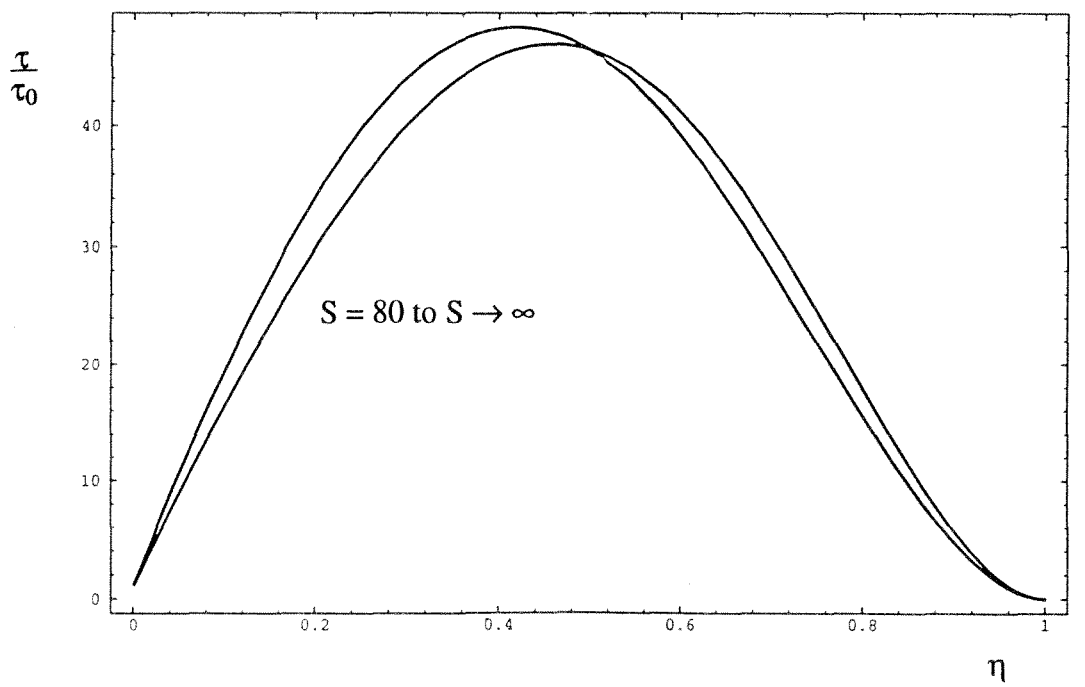

Figure 23: Case as in figure 22, except $m = 0.5$ instead of $m = 0.4$.

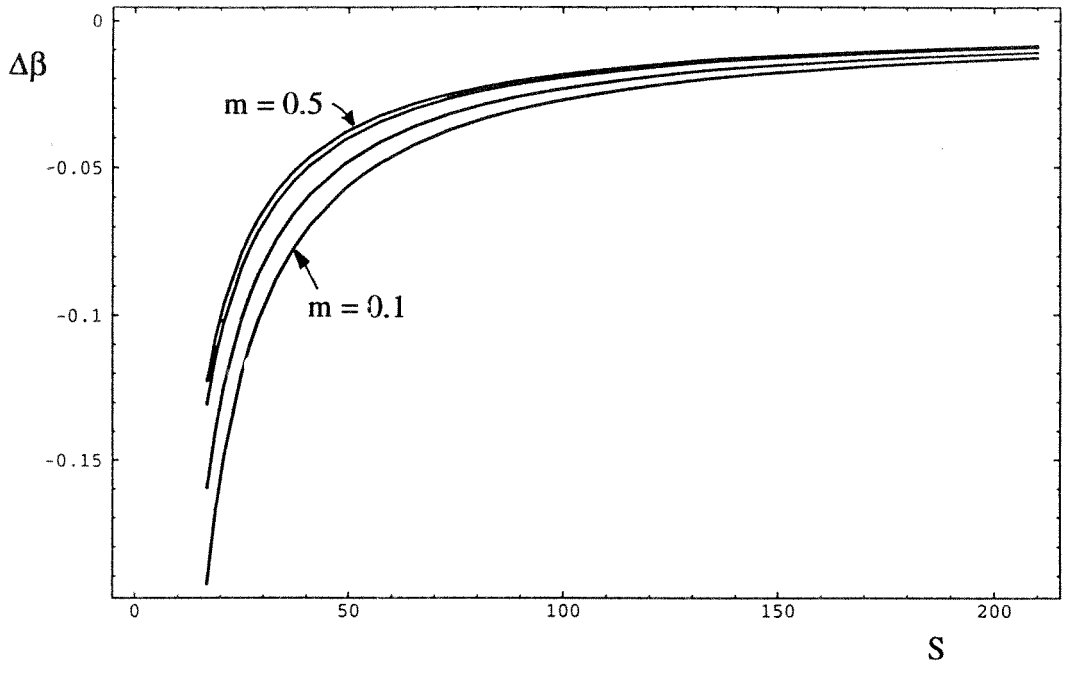

Figure 24: $\triangle\beta$ versus S for $\Pi = 0.1$, $\beta_g = -0.4168$.

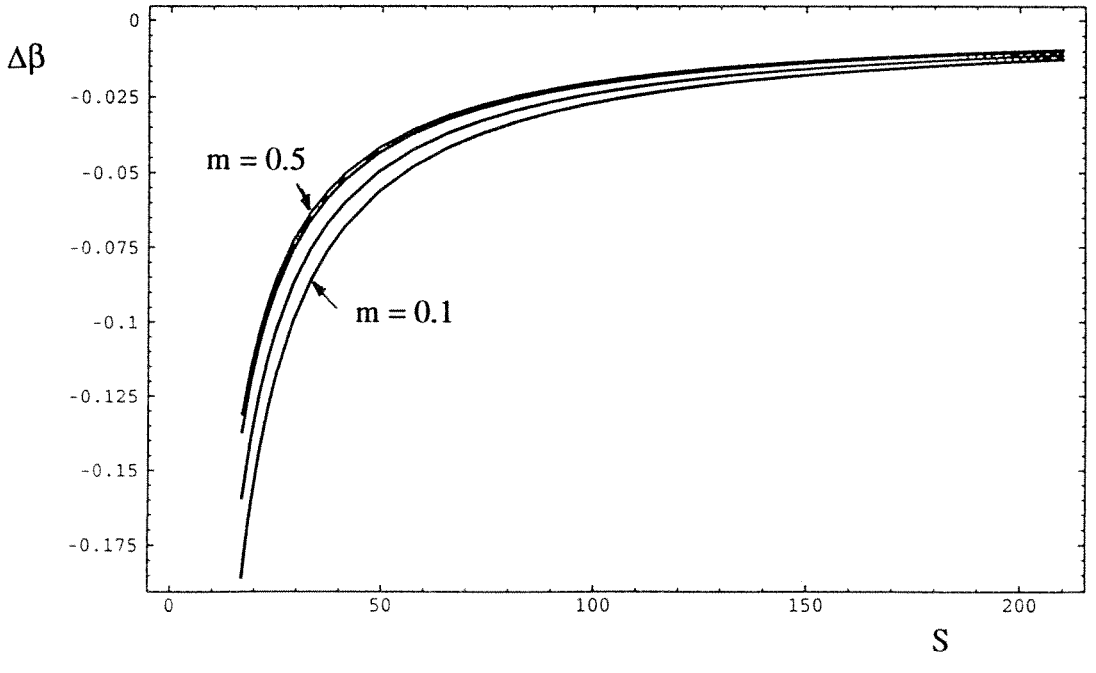

Figure 25: $\triangle\beta$ versus S for $\Pi = 0.2$, $\beta_g = -0.3185$.

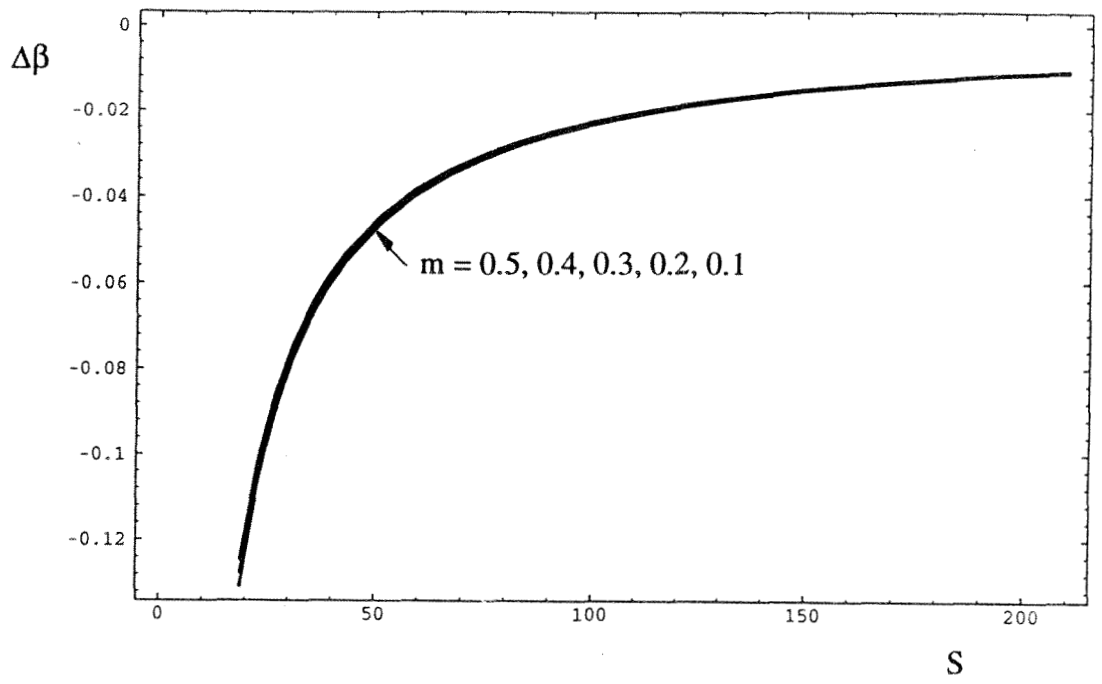

Figure 26: $\triangle\beta$ versus S for $\Pi = 0.45$, $\beta_g = 0$.

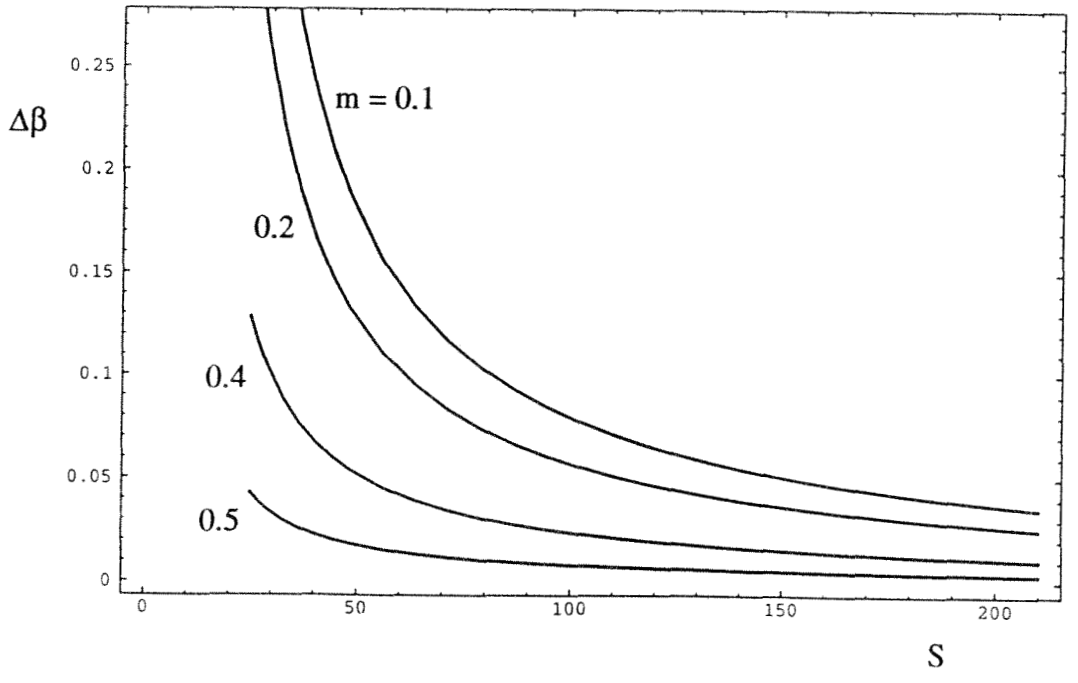

Figure 27: $\triangle\beta$ versus S for $\Pi = 1.54$, $\beta_g = 2$.

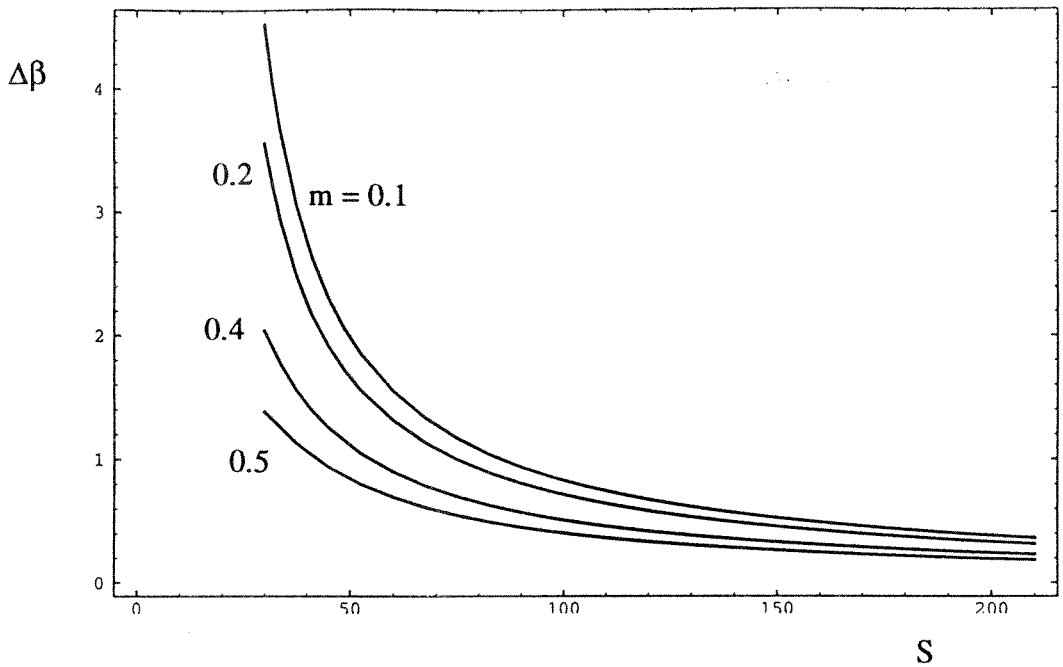

Figure 28: $\triangle\beta$ versus S for $\Pi = 3.93$, $\beta_g = 7$.

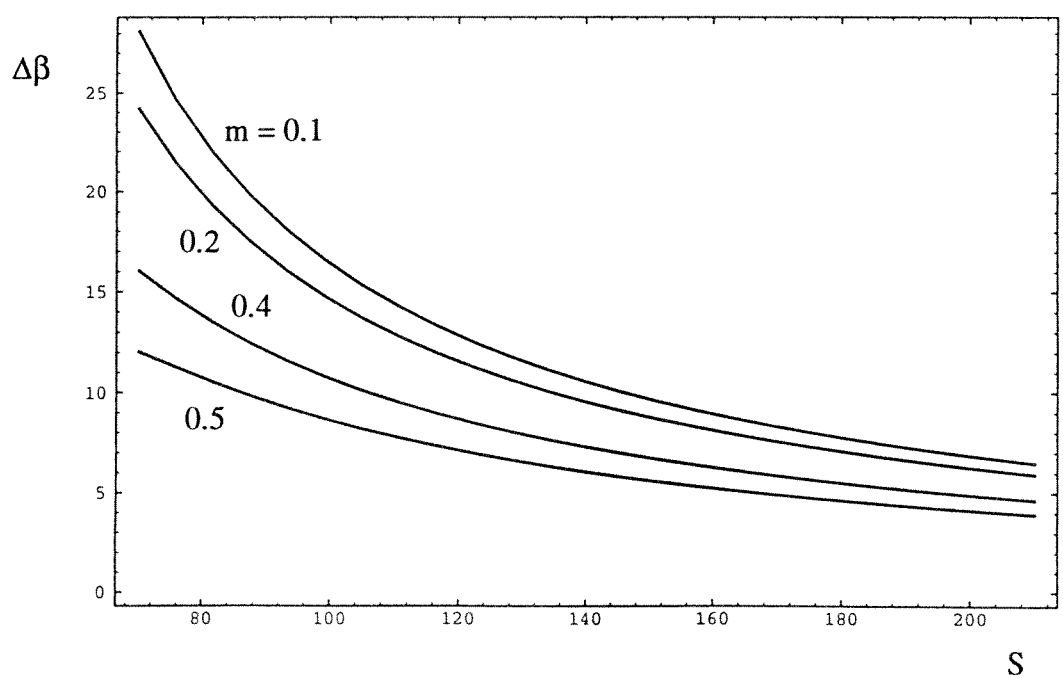

Figure 29: $\triangle\beta$ versus S for $\Pi = 10$, $\beta_g = 47$.

they can be computed readily provided we have a closure relationship for equation (58). Using the equivalent of equation (45), the inverse problem can be solved and the required U_1/U_0 versus R_x can be established for a given Π. The author has done this but because of space and time restrictions, this will have to be the subject of a more complete report. An interesting point about D and ψ considered earlier in §3 is that if the shear stress profiles are forced to have self similarity as above, then as $S \to \infty$, $D \to 1$ and $\psi \to 0$. Thus these quantities do not appear to be suitable to express as a function of Π.

6. The Quasi Equilibrium Hypothesis

Let us rewrite (39) and (40) as

$$SE[\Pi]\exp[\kappa S]\frac{1}{\chi}\frac{dS}{dR_x} = R[S, \beta_{\ell g}, \Pi] \tag{61}$$

$$\text{and} \qquad S^2E[\Pi]\exp[\kappa S]\frac{1}{\chi^2}\frac{d\chi}{dR_x} = -\frac{\beta_{\ell g}}{C_1[\Pi]} \tag{62}$$

$$\text{where} \qquad \chi = \frac{U_1}{U_0} = \sqrt{1 - C_p} \tag{63}$$

where C_p is the pressure coefficient.

Let us now assume that these equations can be applied to *non equilibrium* boundary layers provided that $\delta_c d\Pi/dx$ is sufficiently small and that local values of Π for a given R_x can be used in (61) and (62). Such layers will be referred to as quasi equilibrium layers. One measure for sufficient smallness of $\delta_c d\Pi/dx$ can be derived from the shear stress equation (20) i.e.,

$$\frac{f_2[m, \Pi, S]\delta_c d\Pi/dx}{f_1[m, \Pi, S] + f_3[m, \Pi, S](\delta_c/U_1)(dU_1/dx)} \ll 1 \tag{64}$$

Given then condition (64), equations (61) and (62) will be applied to some interesting non equilibrium flow cases. So as to keep the study as analytical as possible, streamwise pressure distributions will be chosen which can be characterized by one single parameter. Such flows are sink and source flows.

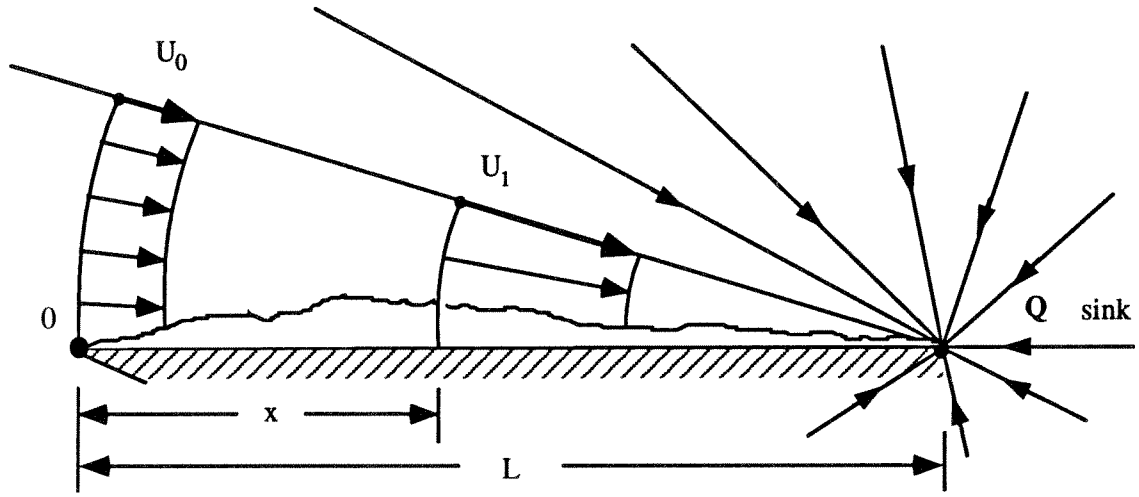

Figure 30: Sink flow.

6.1 Favorable Pressure Gradients

Let us consider sink flows. These are shown diagramatically in figure 30 and if boundary layer displacement effects are neglected, continuity gives

$$\left.\begin{aligned} \frac{U_1}{U_0} = \chi = \frac{1}{1 - KR_x} \\ \text{where} \qquad K = \frac{\nu}{LU_0} \end{aligned}\right\} \tag{65}$$

and K is often referred to as the acceleration parameter. In fact K is related to the sink strength, thus

$$K = \frac{2\pi\nu}{Q} \tag{66}$$

It is easy to show that

$$\frac{1}{\chi^2}\frac{d\chi}{dR_x} = K \tag{67}$$

Hence we can now set about solving the direct problem where χ is known. Equation (62) can be written as

$$\left.\begin{aligned} KC_1[\Pi]S^2E[\Pi]\exp[\kappa S] - \beta_{\ell g}[S,\Pi] = 0 \\ \text{i.e.} \quad F[K,\Pi,S] = 0 \end{aligned}\right\} \tag{68}$$

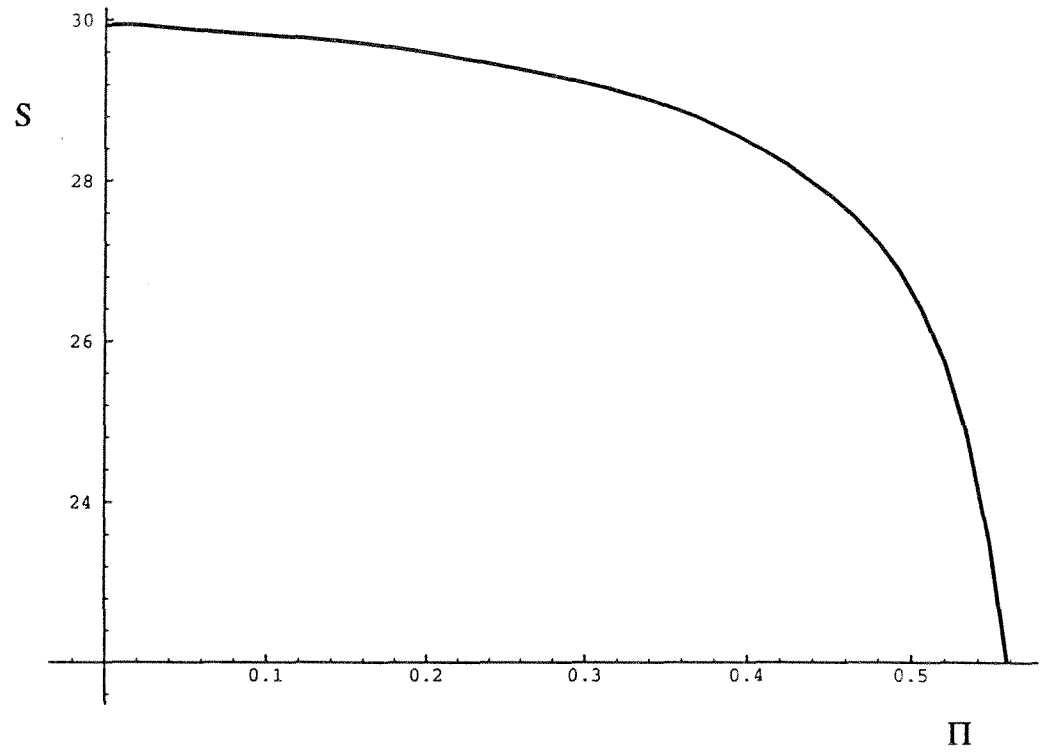

Figure 31: S versus Π for sink flow, from solution of (68). $K = 10^{-8}$.

Now $\beta_{\ell g}$ is known analytically from (59) and equation (68) can be solved for Π at fixed K and S numerically. This gives a typical plot shown in figure 31.

Equation (65) and the results of (68) are substituted into (61) to give

$$R_x = \frac{1}{K}\left\{1 - \exp\left[K\int_{S_0}^{S} H[S]ds\right]\right\} \tag{69}$$

where

$$H[S] = \frac{SE[\Pi[S]]\exp[\kappa S]}{R[S, \beta_{\ell g}[\Pi[S], S], \Pi[S]]} \tag{70}$$

Here S_0 is the initial value of S and has been chosen such that K_τ in (31) is of order 100. It is expected that this would be appropriate for a boundary layer which has been freshly tripped. If however, one is interested only in values of R_x which are high, the results should be insensitive to the precise value of S_0 chosen. Once R_x versus S has been found, all other profile parameters can be displayed by using parametric plots (Mathematica) using the following relations.

$$K_\tau = E[\Pi[S]]\exp[\kappa S] \tag{71}$$

$$\frac{\delta_c U_0}{\nu} = \frac{U_0}{U_1} SE[\Pi[S]] \exp[\kappa S] \tag{72}$$

$$R_\theta = \frac{\theta U_1}{\nu} = E[\Pi[S]] \exp[\kappa S]\{C_1[\Pi[S]]S - C_2[\Pi[S]]\}/S \tag{73}$$

Figures 32 through to 37 show results for $K = 10^{-8}$. Of particular interest is figure 32 which shows the layer initially thickening and then thinning linearly to zero thickness when $R_x = 10^8$. From the other figures it appears that S, R_θ and K_τ asymptote to constant values invariant with R_x and thus satisfy the Rotta (1962) conditions for precise equilibrium flow. Figures (38a - h) show shear stress profiles given by equation (20) . Since the quasi equilibrium results give Π versus R_x, the quantity $\delta_c d\Pi/dx$ can be calculated and the shear stress profiles can be calculated with the $\delta_c d\Pi/dx$ effect included and with it excluded. If it is included, the shear stress profiles are higher since $\delta_c d\Pi/dx$ is negative. Both sets of profiles have been calculated and the discrepancy can be seen in the profiles for the region where the boundary layer is growing. Thus the method has a built in alarm which warns the user if the assumption of quasi equilibrium is breaking down. Unfortunately we do not yet know how serious the discrepancy is for the results shown. The author repeated all of these calculations for $K = 10^{-6}$ and although the Reynolds number for $\delta_c U_0/\nu$, R_θ and K_τ were one to two orders of magnitude lower, the general behavior was much the same and the flow asymptotes to a condition of precise equilibrium sink flow.

6.1.1 Precise Equilibrium Flow

Let us seek solutions to (61) such that $dS/dR_x = 0$. This yields

$$R = \frac{2C_1\beta S + C_1 S - \beta C_2}{C_1\{\kappa C_1 S^2 - C_2\kappa S + C_2\}} = 0 \tag{74}$$

and this is possible only if

$$2C_1\beta S + C_1 S - \beta C_2 = 0 \tag{75}$$

From (62)

$$K = -\frac{\beta}{C_1 S^2 E \exp[\kappa S]} \tag{76}$$

$$S \to \infty \text{ as } K \to 0 \text{ i.e. as } \frac{U_0 L}{\nu} \to \infty$$

Hence (75) gives

$$\left.\begin{aligned} 2C_1\beta S + C_1 S = 0 \\ \text{or} \quad \beta = -\frac{1}{2} \end{aligned}\right\} \tag{77}$$

From the numerical examples with $\beta = \beta_{\ell g}$, it appears that for finite S, Π approaches a constant value slightly larger than zero, and $\beta_{\ell g}$ approaches a value smaller than $-\frac{1}{2}$. However, for $S \to \infty$, $\Pi \to 0$ and $\beta_{\ell g} \to \beta_g$ which is close to $-\frac{1}{2}$. Relation (76) and other associated relations have a similar behavior to the analysis of Jones and Launder (1972). It should be noted that $H[S]$ in (69) must have a singularity $(-\infty)$ at a certain value of S corresponding to $x = L$. In this way (69) reduces to $R_x = 1/K$ for $x = L$.

6.2 Zero Pressure Gradient Flows

Here we put $K = 0$ in equations (61) and (62) and with the aid of (65) and (67), (62) gives

$$\left.\begin{aligned} \beta_{\ell g}[S, \Pi] = 0 \\ \text{and so} \quad \Pi = \Pi[S] \end{aligned}\right\} \tag{78}$$

can be found using (59) and (61) gives

$$R_x = \int_{S_0}^{S} \frac{SE[\Pi[S]] \exp[\kappa S]}{R[S, 0, \Pi[S]]} dS \tag{79}.$$

Relationship (78) is shown plotted in figure 39 and in figure 40 Π versus R_x is plotted. With this formulation one can see that a zero pressure gradient layer is not an equilibrium layer at least for finite S since Π varies with R_x. Figures 41 to 45 show other calculated variations. In figure 46, a plot of Π versus R_θ is shown. It can be seen that Π drops monotonically with increasing R_θ. According to the formulation of given by (56), Π should asymptote to a value of 0.45, but the fall off with R_θ is extremely slow. Also it has been shown by Coles (1962) that at Reynolds numbers of R_θ less than 5000 Π increases with R_θ. This variation with R_θ is a Reynolds number effect which cannot be explained by the present theory, nor as far as the author is aware can it be adequately explained by any other theory. Cebeci and Smith (1974) have proposed a curve fit to the data collected by Coles for Π versus R_θ. This curve fit shows Π rising with R_θ and levels to a constant value for R_θ smaller than approximately 5000. A correction factor which corrects the author's calculations for

$R_\theta < 5000$ and asymptotes to 1 rapidly for $R_\theta \geq 5000$ has been applied. The result is shown in figure 47. One can see that variation of Π shows a peak close to $R_\theta = 5000$ a slow fall off. Figures 48(a) and 48(b) show the Coles (1962) correlation. It should be noted that $\Delta\overline{U}/U_\tau = 2\Pi/\kappa$ and 48(b) shows a peaking of Π at about $R_\theta = 5000$ with a slow fall off to a value of $\Pi = 0.41$. This fall off is much more rapid than the author's calculation and could be due to compressibility effects as suggested by Coles (1962). Figures 49(a-f) shows the calculated shear stress profiles with and without the effect of $\delta_c d\Pi/dx$ included. It can be seen that $\delta_c d\Pi/dx$ has no effect and although the shear stress profiles do vary with R_x, they are in true quasi-equilibrium.

At the moment there is no clear way of incorporating the Coles low Reynolds number effect into the theory here and would need to be the subject of another study. For the moment, if we confine ourselves to high Reynolds numbers, this low Reynolds number effect should become unimportant for the subsequent evolution downstream. It would cause only a slight fractional change in the effective origin for R_x.

6.3 Adverse Pressure Gradient Flows

For adverse pressure gradients being produced by a source, the analysis is the same as for favorable pressure gradients except $K = -(x_0 U_0/\nu)^{-1}$ where x_0 and U_0 are defined in figure 50. Figures 51 through 56 show how the profile parameters vary for $K = -7.5 \times 10^{-8}$ and figures 57(a-h) show the calculated shear stress profiles with and without the effect of $\delta_c d\Pi/dx$. The effect of $\delta_c d\Pi/dx$ does not appear to be particularly strong and so perhaps this represents a case of quasi equilibrium flow.

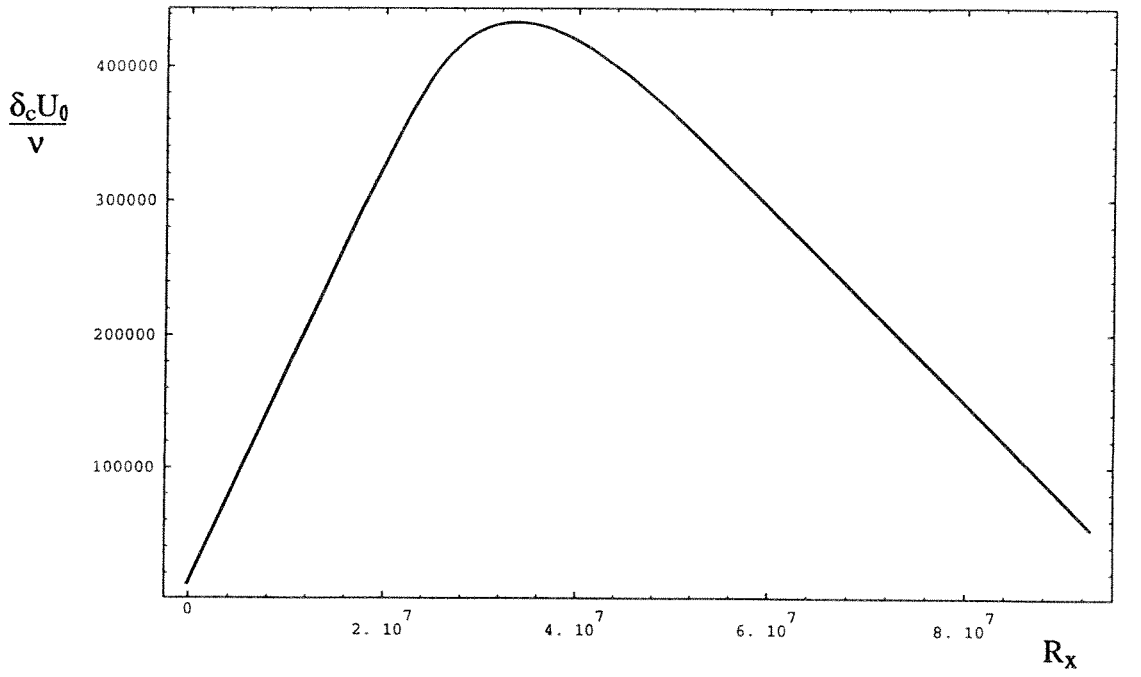

Figure 32: Sink flow boundary layer growth with R_x. $K = 10^{-8}$.

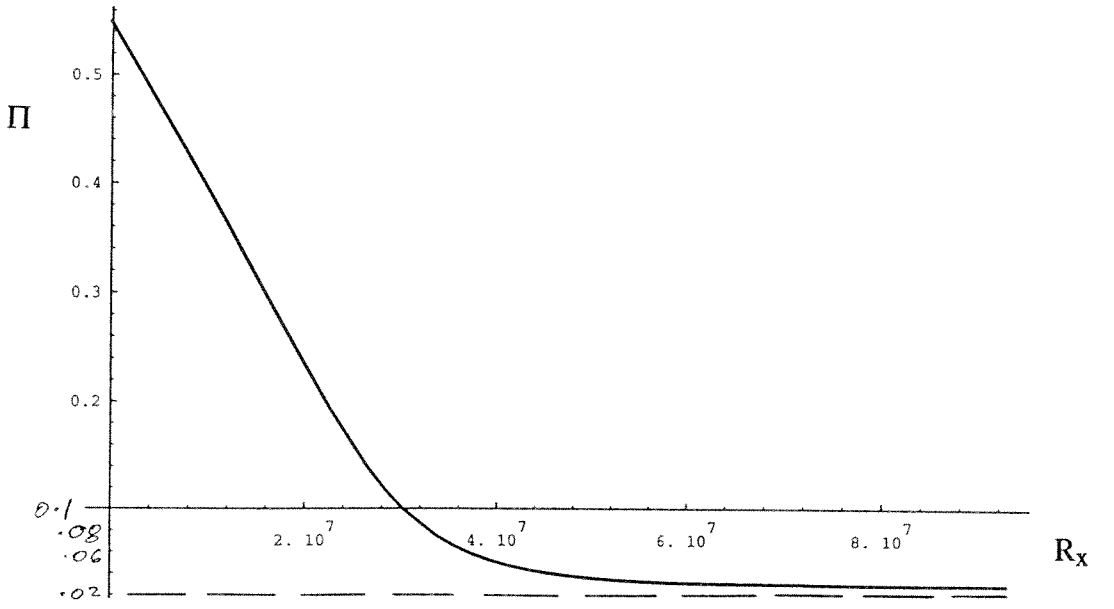

Figure 33: Π versus R_x for sink flow. $K = 10^{-8}$.

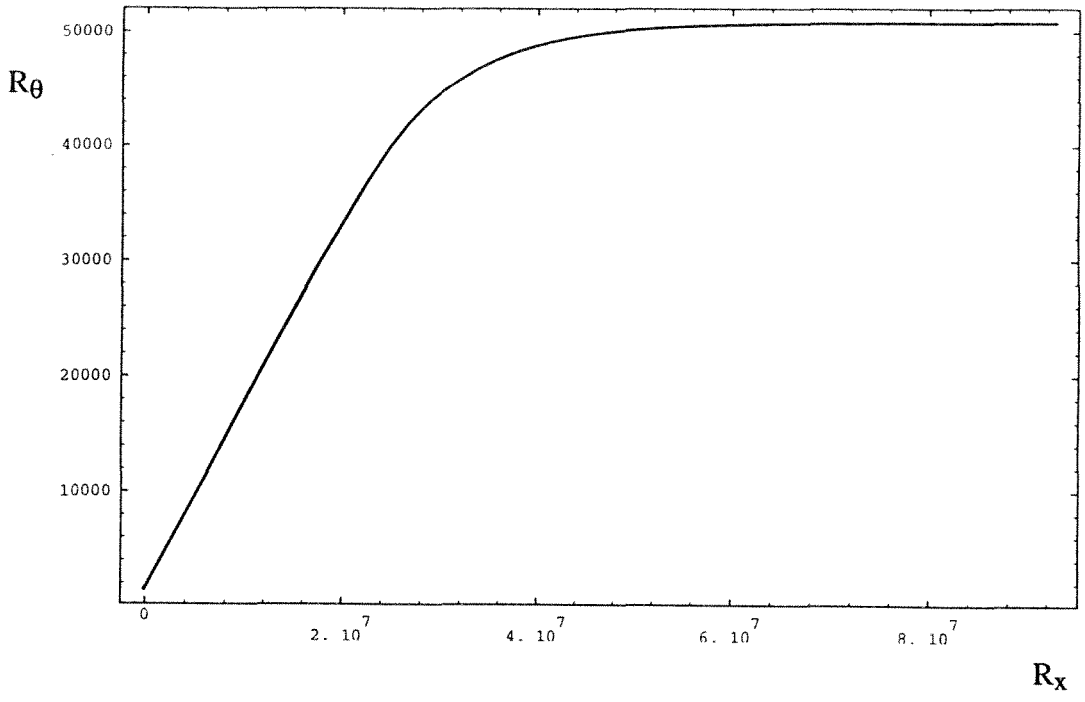

Figure 34: R_θ versus R_x for sink flow. $K = 10^{-8}$.

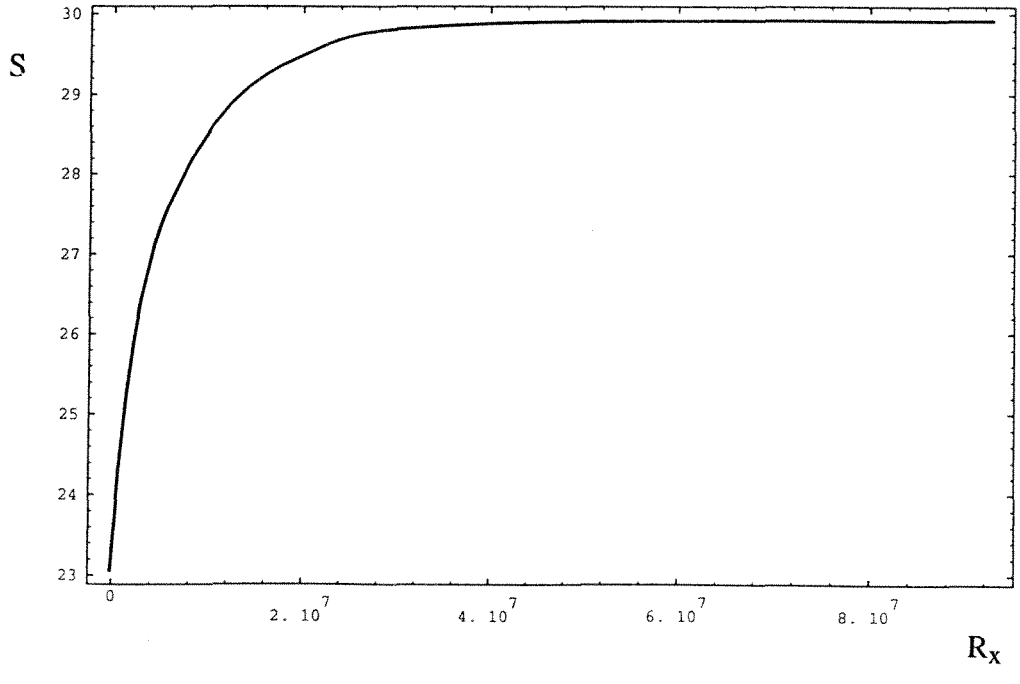

Figure 35: S versus R_x for sink flow. $K = 10^{-8}$.

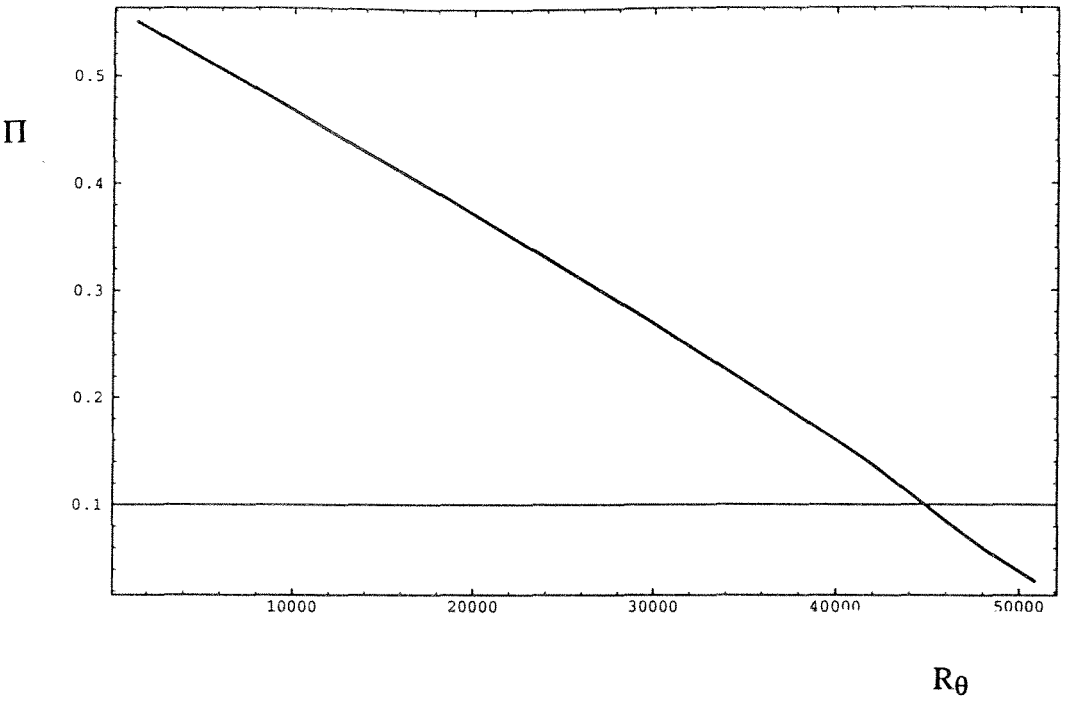

Figure 36: Π versus R_θ for sink flow. $K = 10^{-8}$.

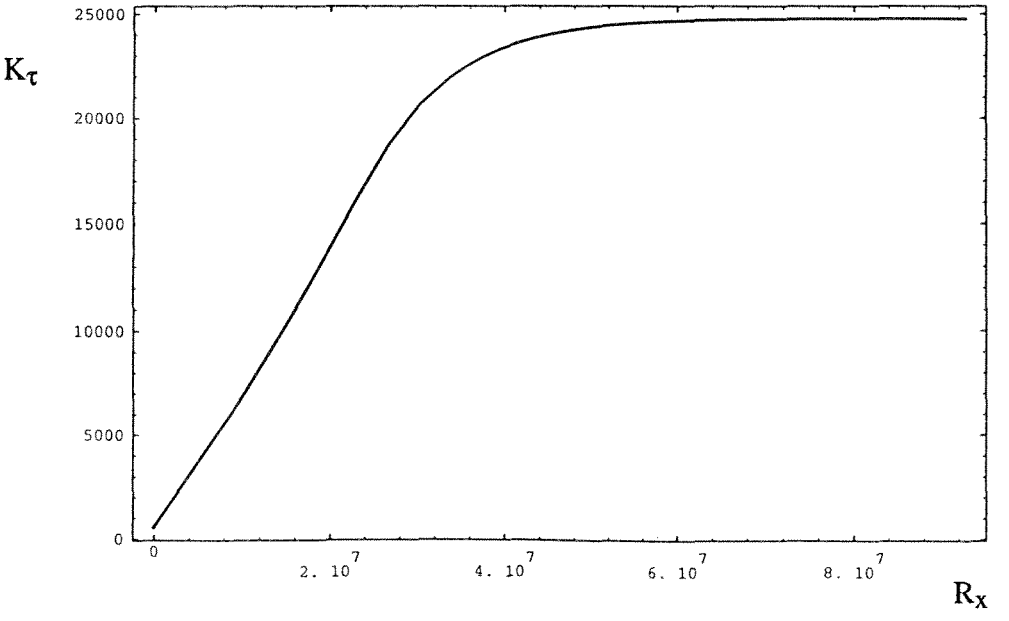

Figure 37: Kármán number K_τ versus R_x for sink flow. $K = 10^{-8}$.

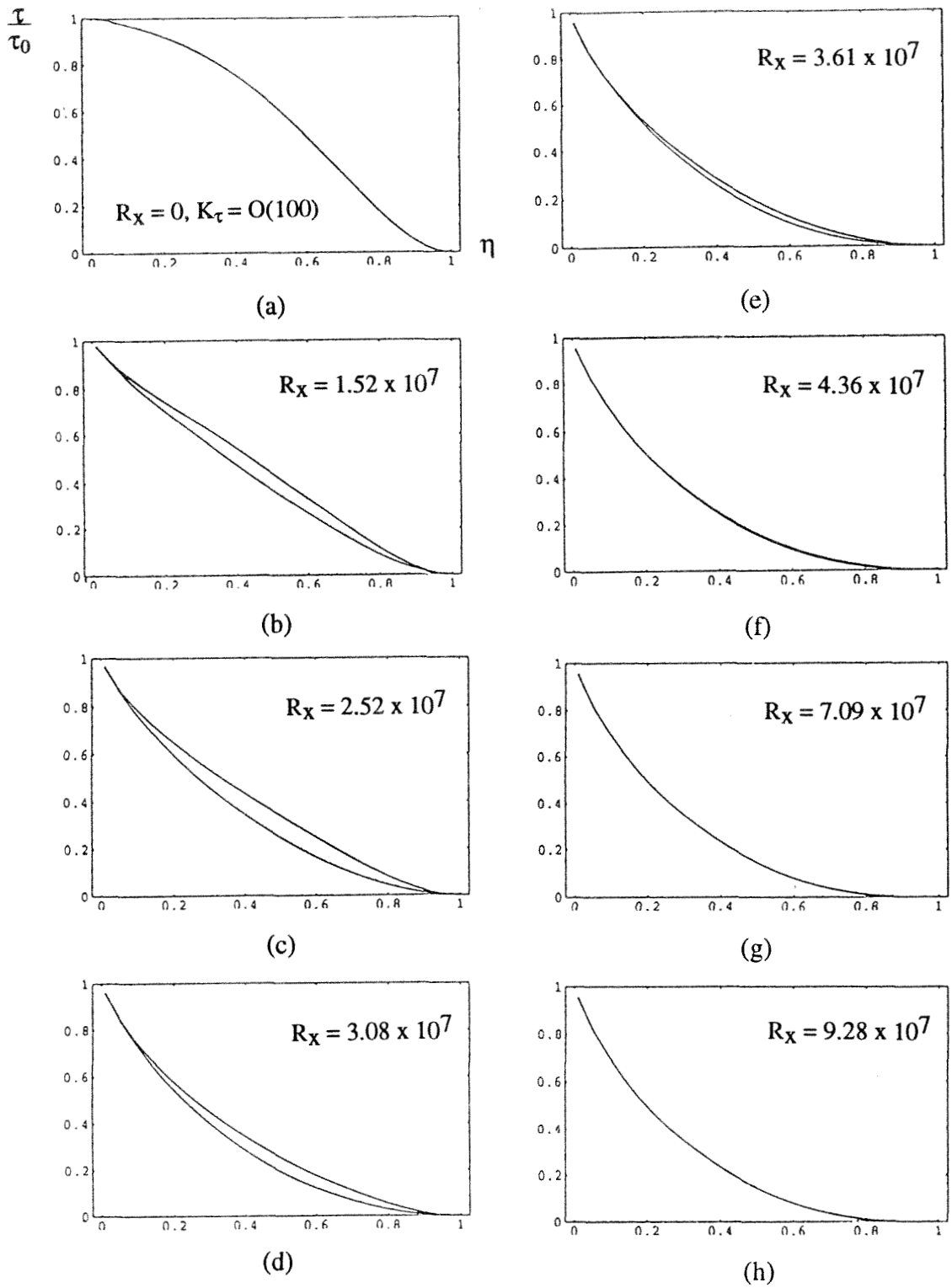

Figure 38: Sink flow shear stress profiles given by equation (20) with and without the inclusion of the $\delta_c d\Pi/dx$ term. In all cases, $K = 10^{-8}$.

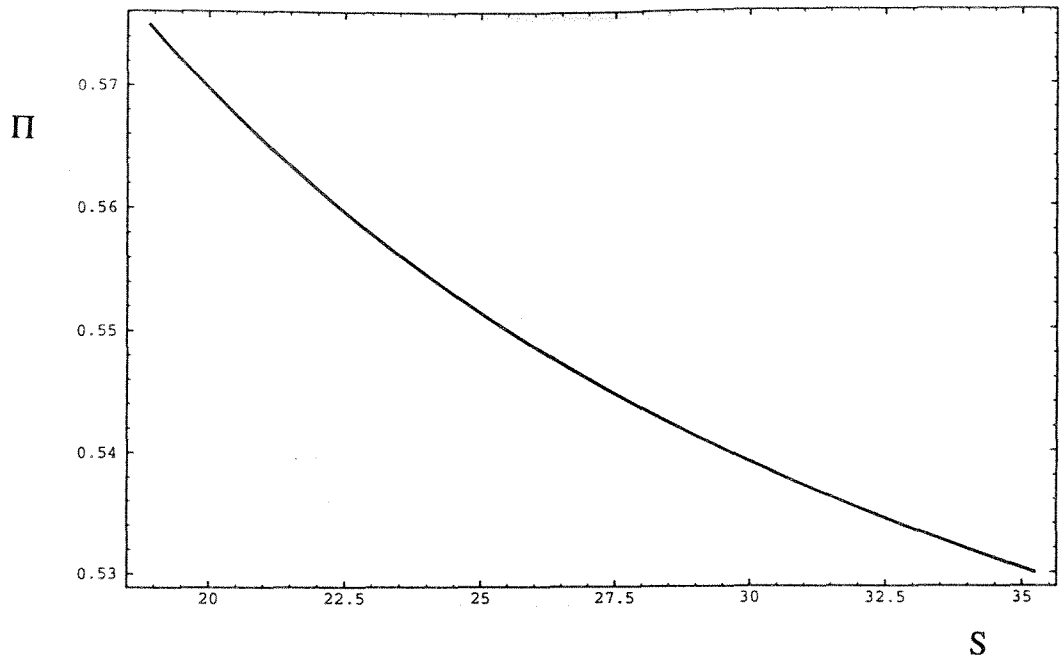

Figure 39: Π versus S for zero pressure gradient flow ($K = 0$) using (78).

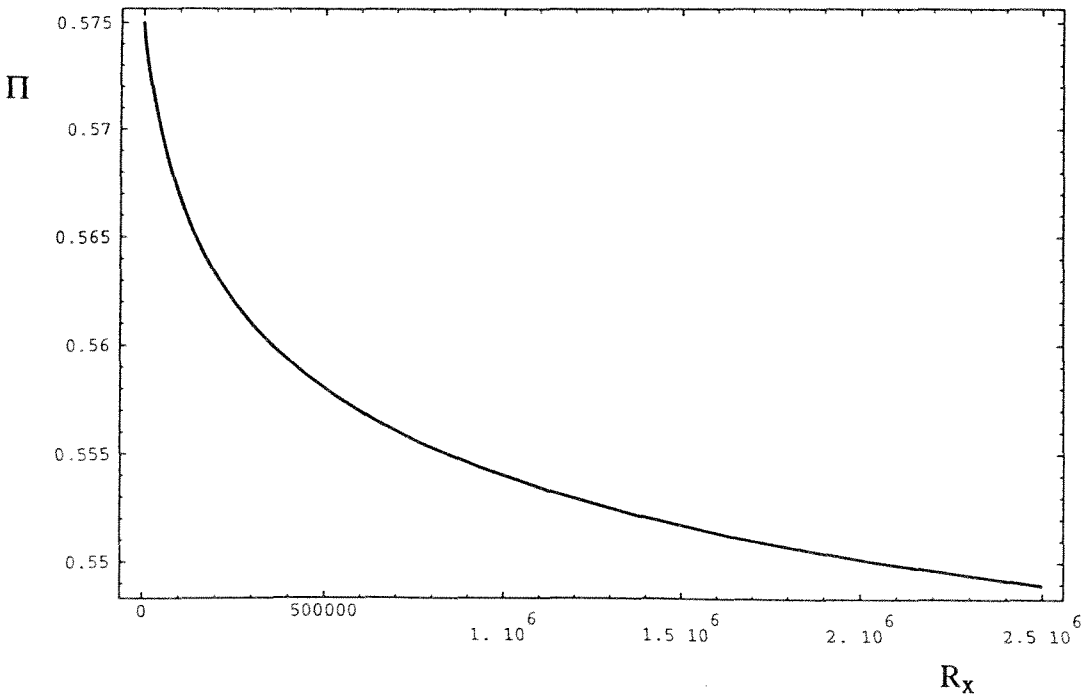

Figure 40: Π versus R_x for zero pressure gradient flow ($K = 0$) using formulations (78) and (79).

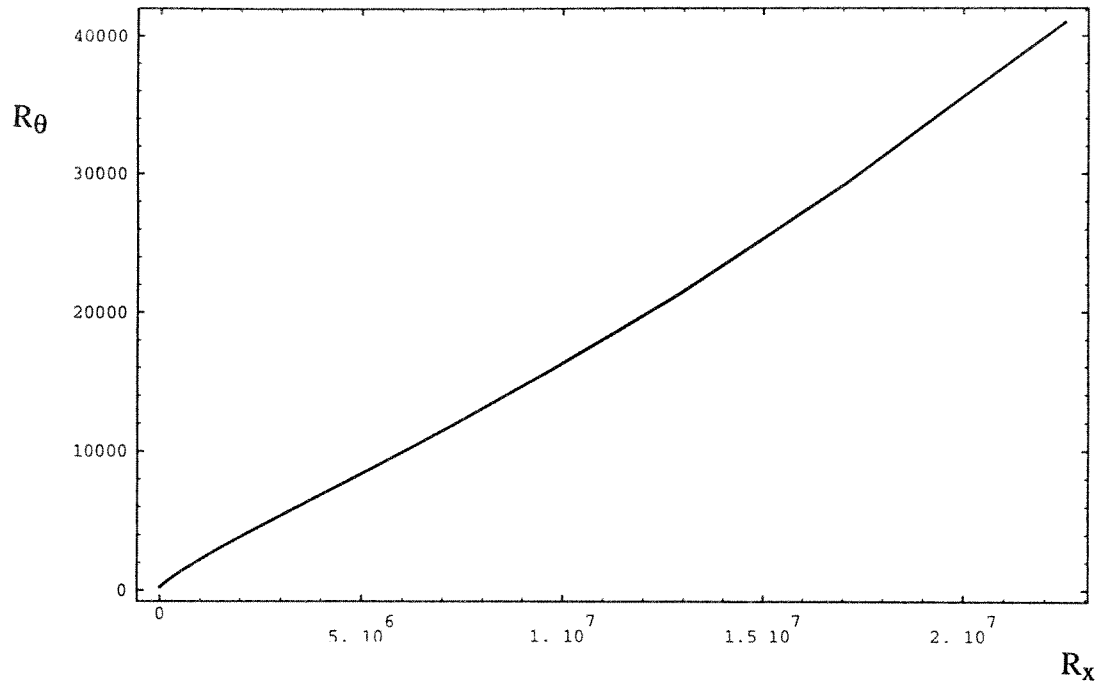

Figure 41: R_θ versus R_x for zero pressure gradient flow ($K = 0$) using formulations (78) and (79).

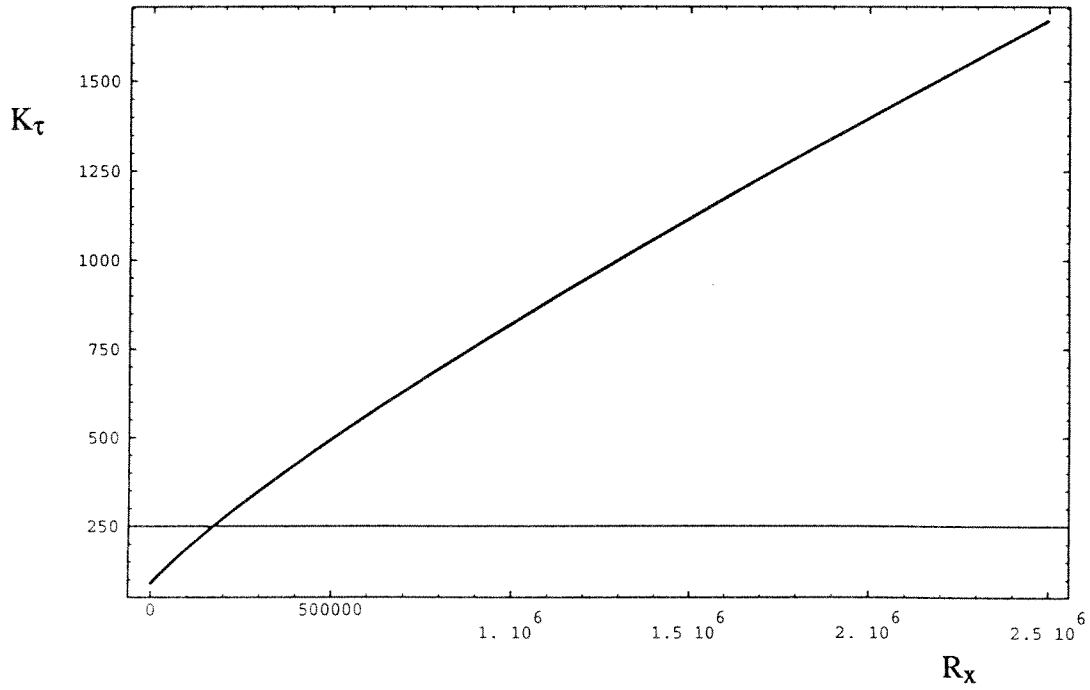

Figure 42: Kármán number K_τ versus R_x for zero pressure gradient flow ($K = 0$) using formulations (78) and (79).

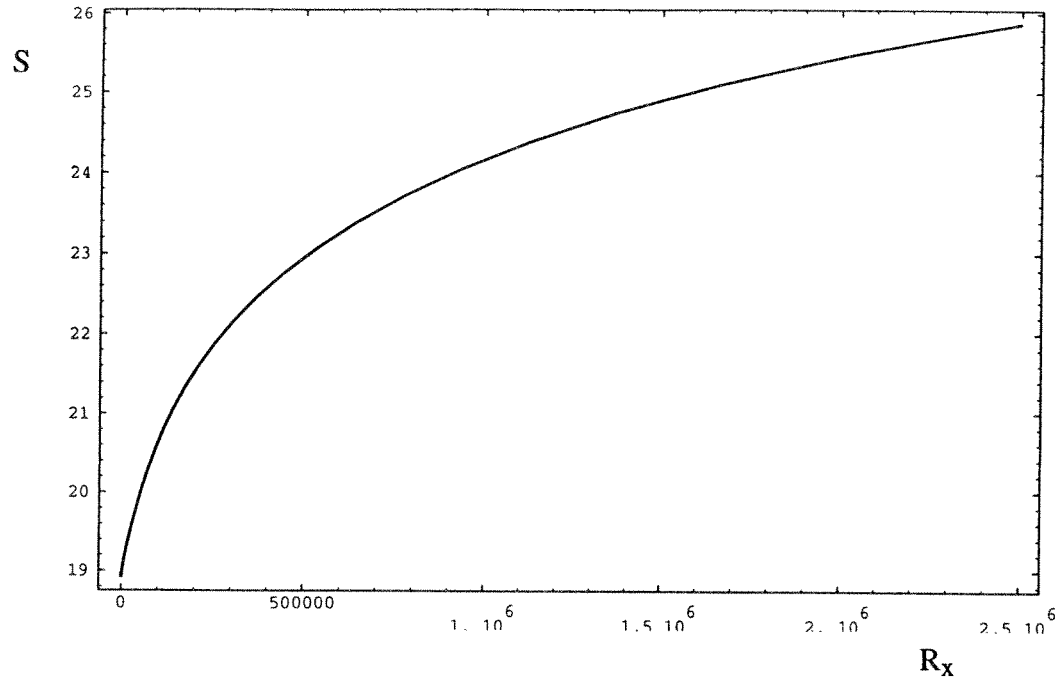

Figure 43: S versus R_x for zero pressure gradient flow ($K = 0$) using formulations (78) and (79).

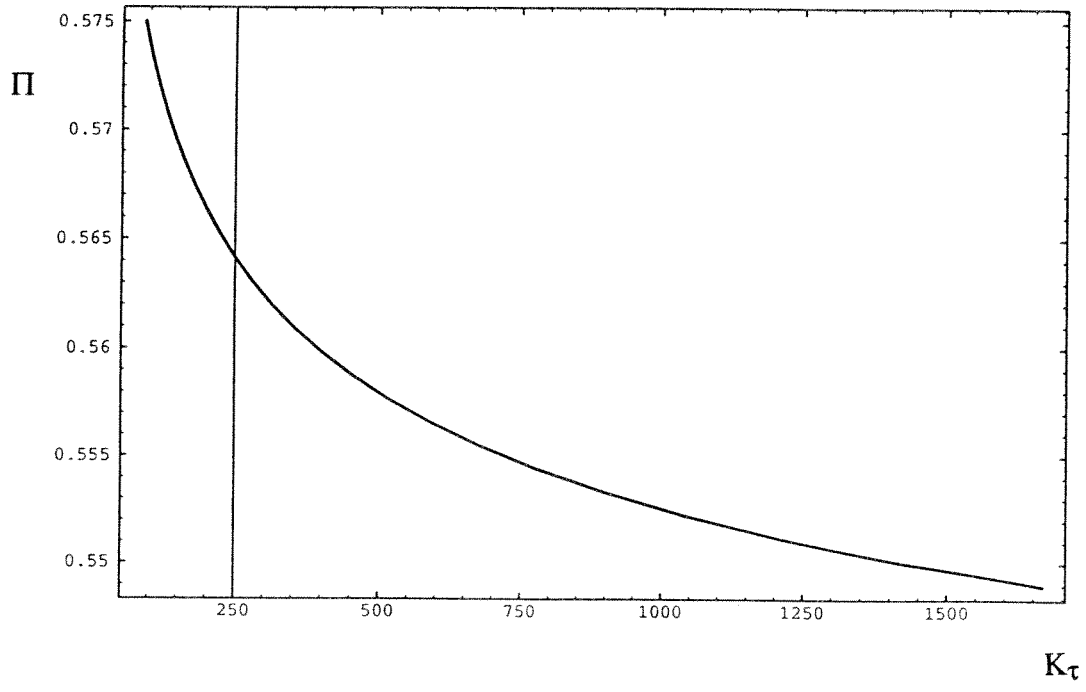

Figure 44: Π versus K_τ for zero pressure gradient flow ($K = 0$) using formulations (78) and (79).

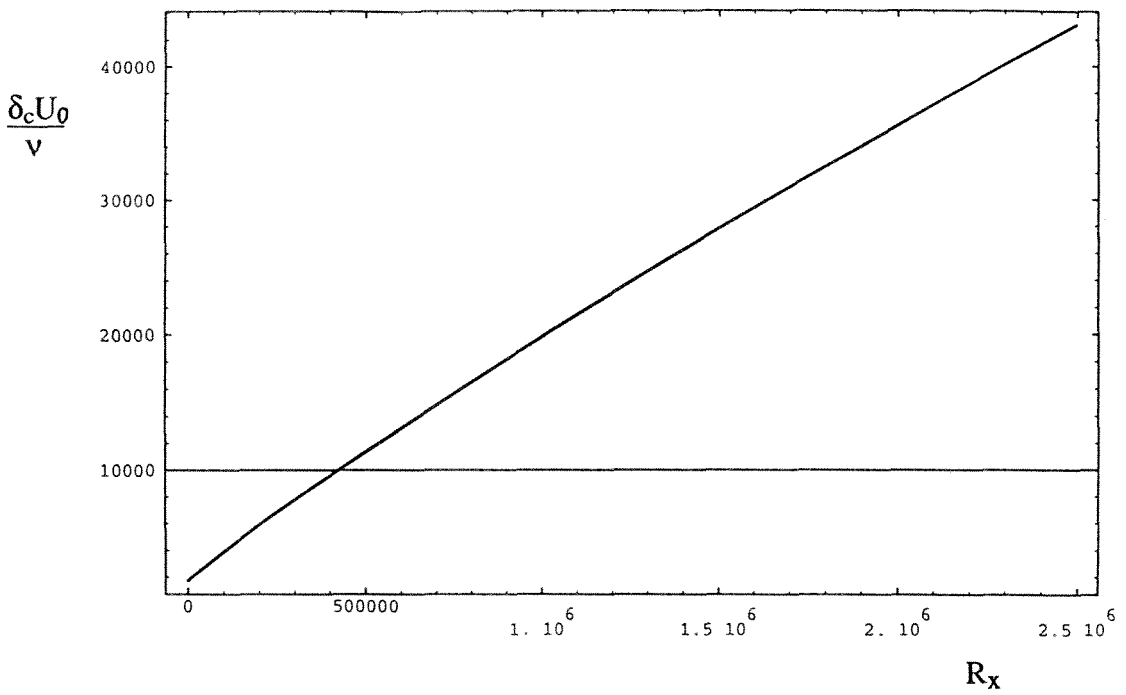

Figure 45: Zero pressure gradient flow boundary layer growth with R_x from formulations (78) and (79).

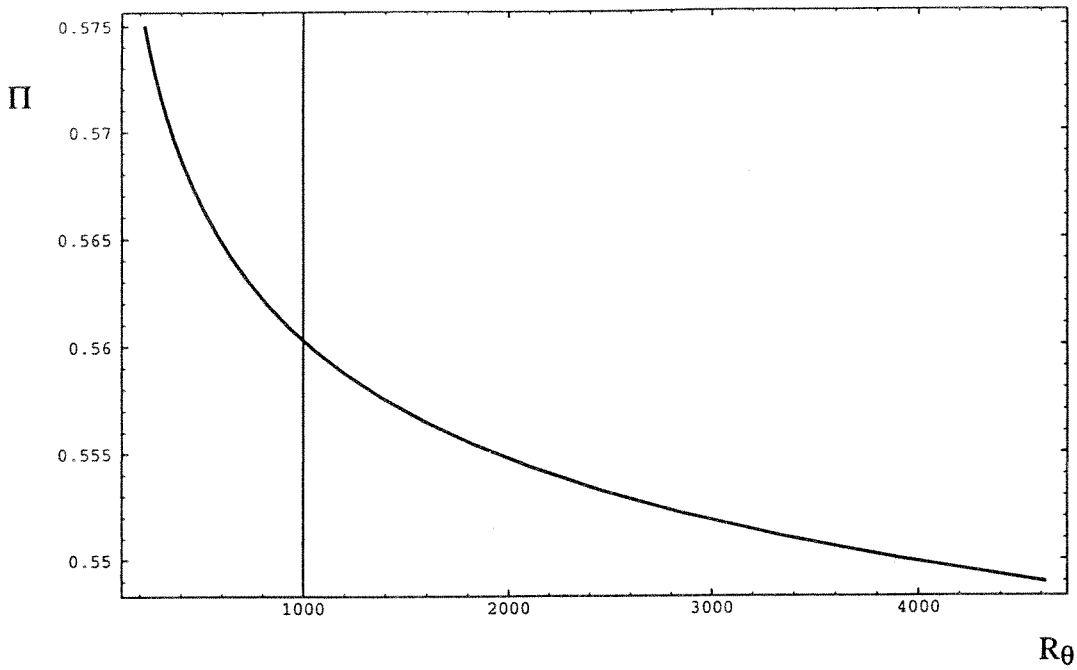

Figure 46: Π versus R_θ for zero pressure gradient flow ($K = 0$) using formulations (78) and (79).

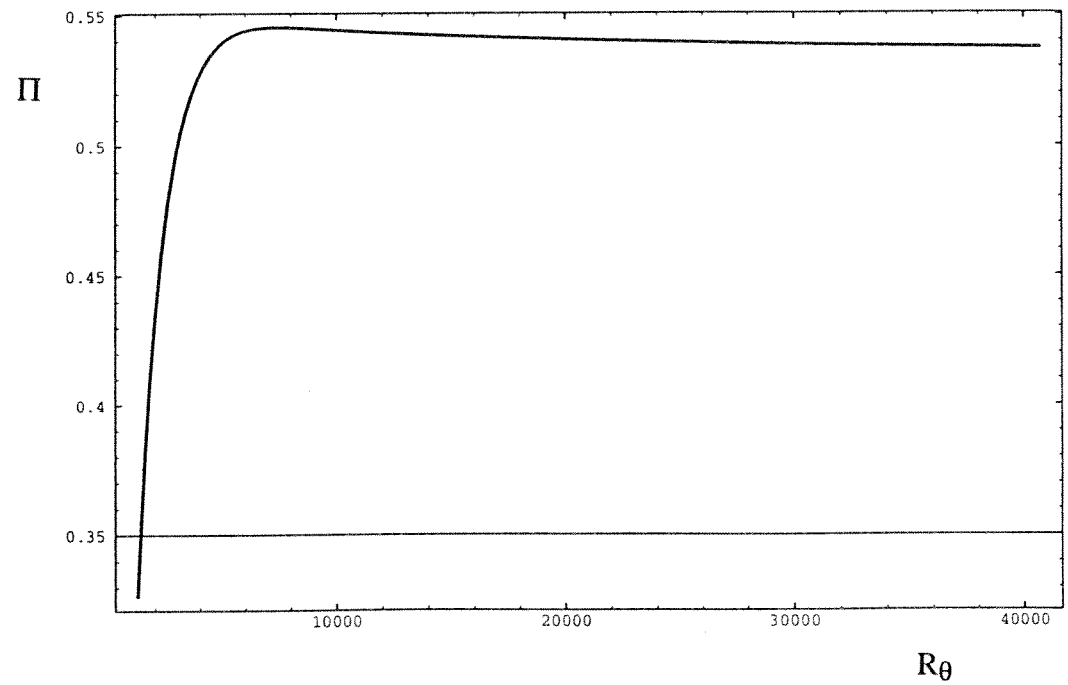

Figure 47: Π versus R_θ for zero pressure gradient flow with correction factor applied (see text).

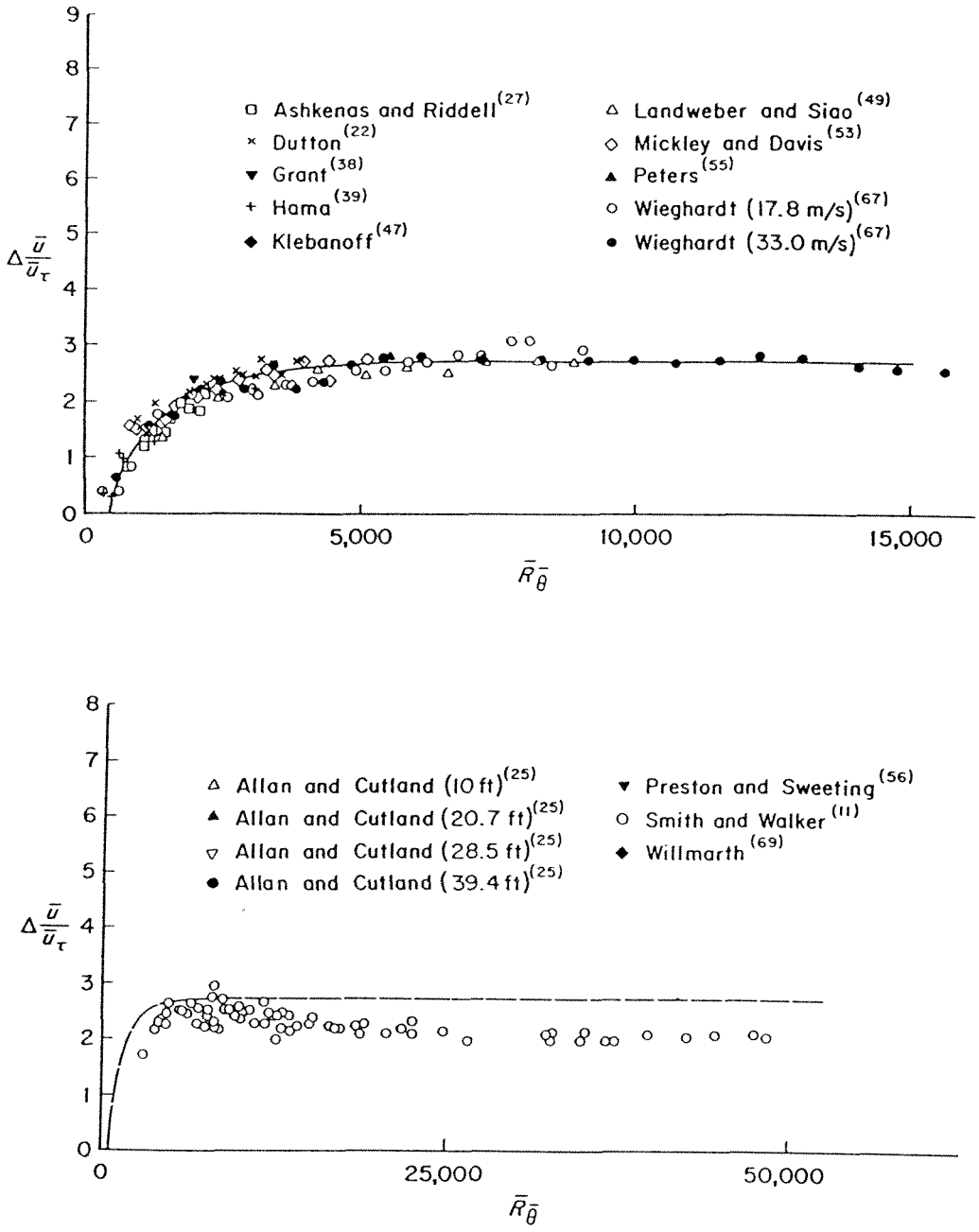

Figure 48: Π versus R_θ correlation taken from Coles (1962). Note that: $\Delta\overline{U}/U_\tau = 2\Pi/\kappa$.

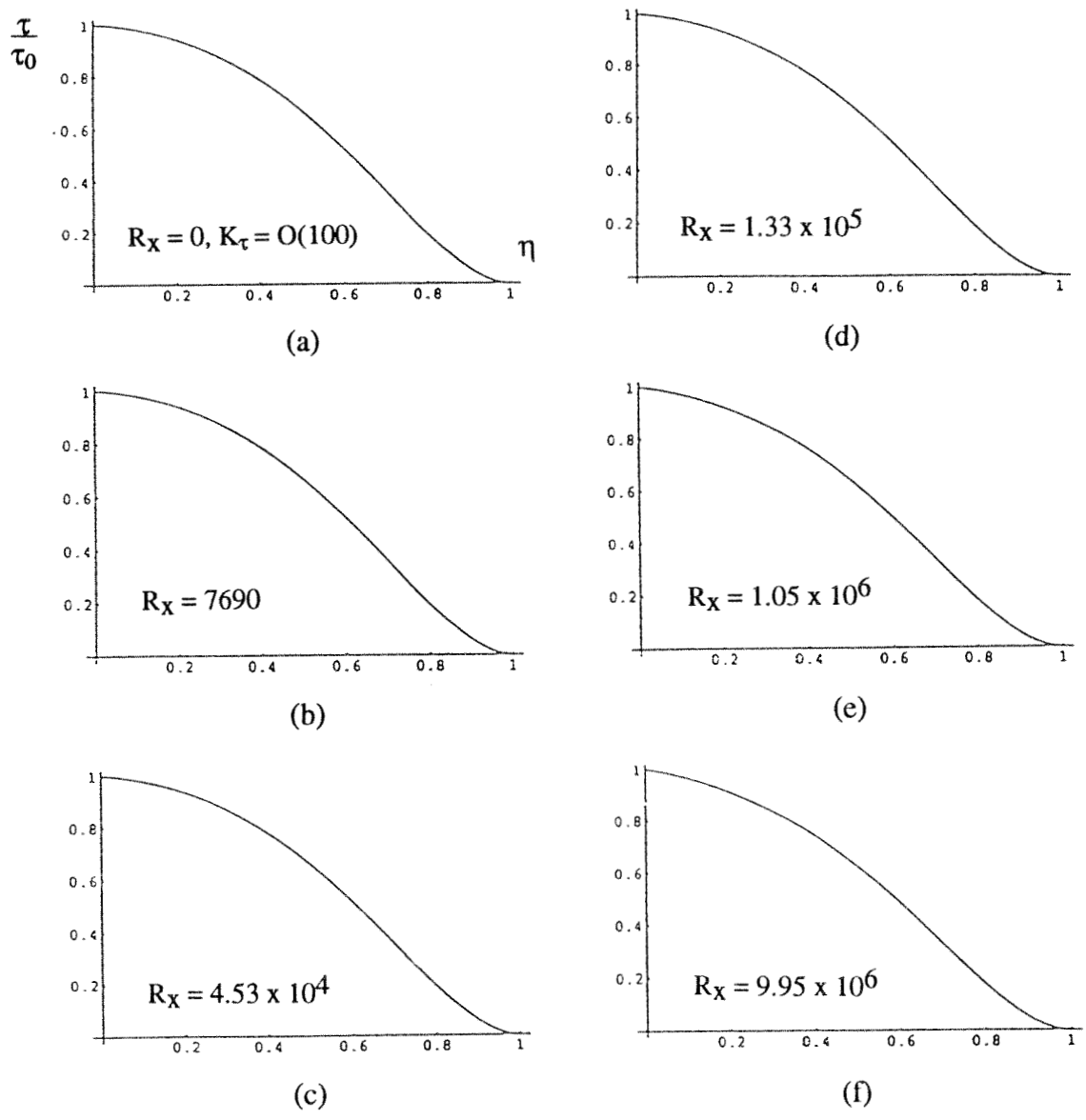

Figure 49: Zero pressure gradient flow ($K = 0$) shear stress profiles given by equation (20) with and without the inclusion of the $\delta_c d\Pi/dx$ term.

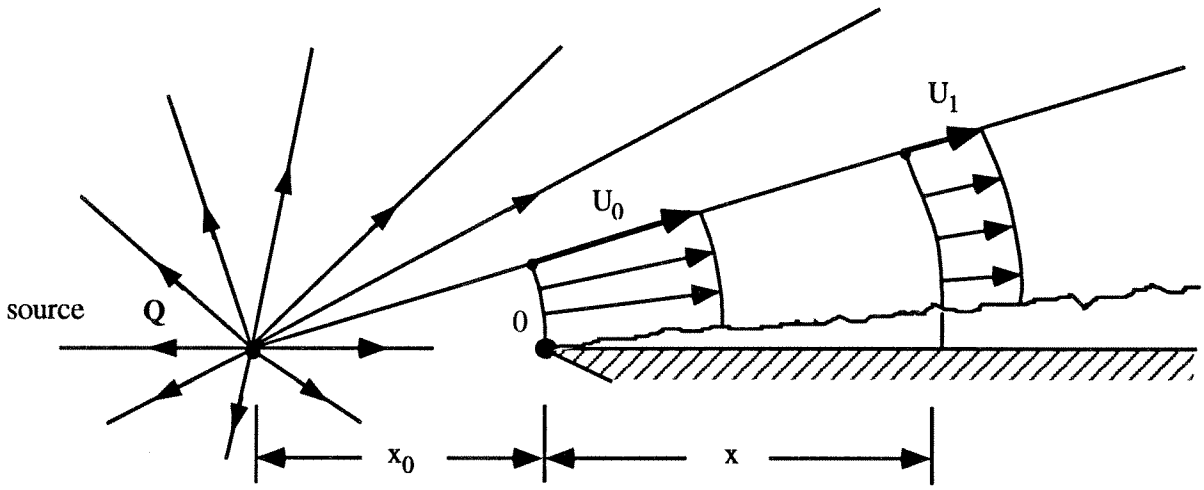

Figure 50: Source flow.

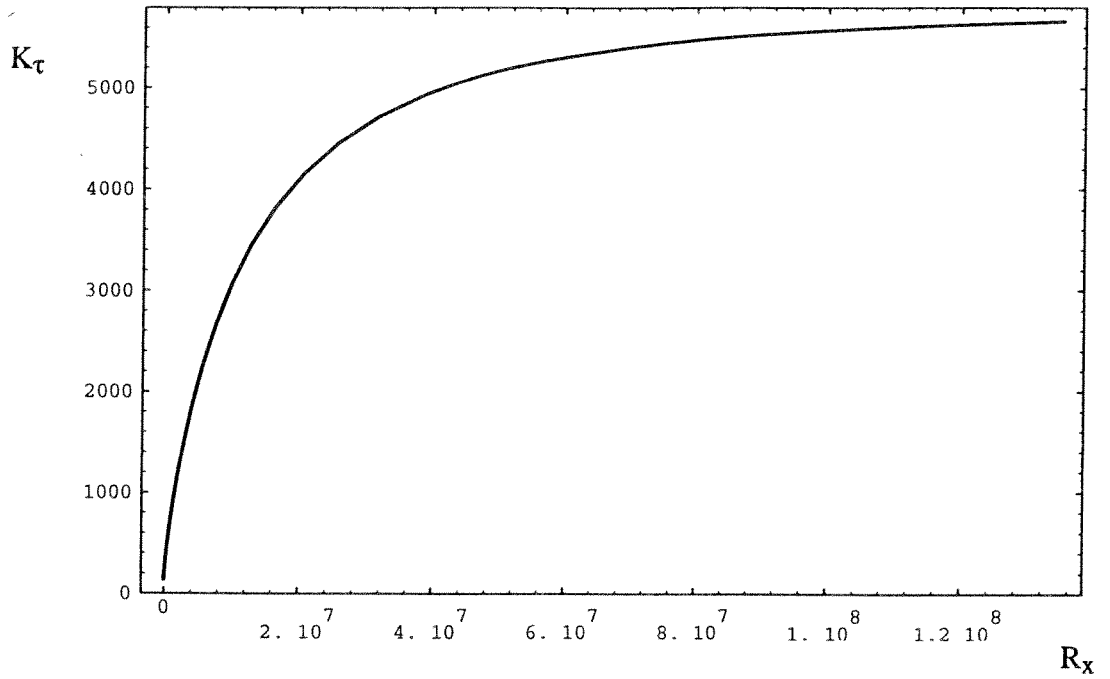

Figure 51: Kármán number K_τ versus R_x for source flow, $K = -7.5 \times 10^{-8}$.

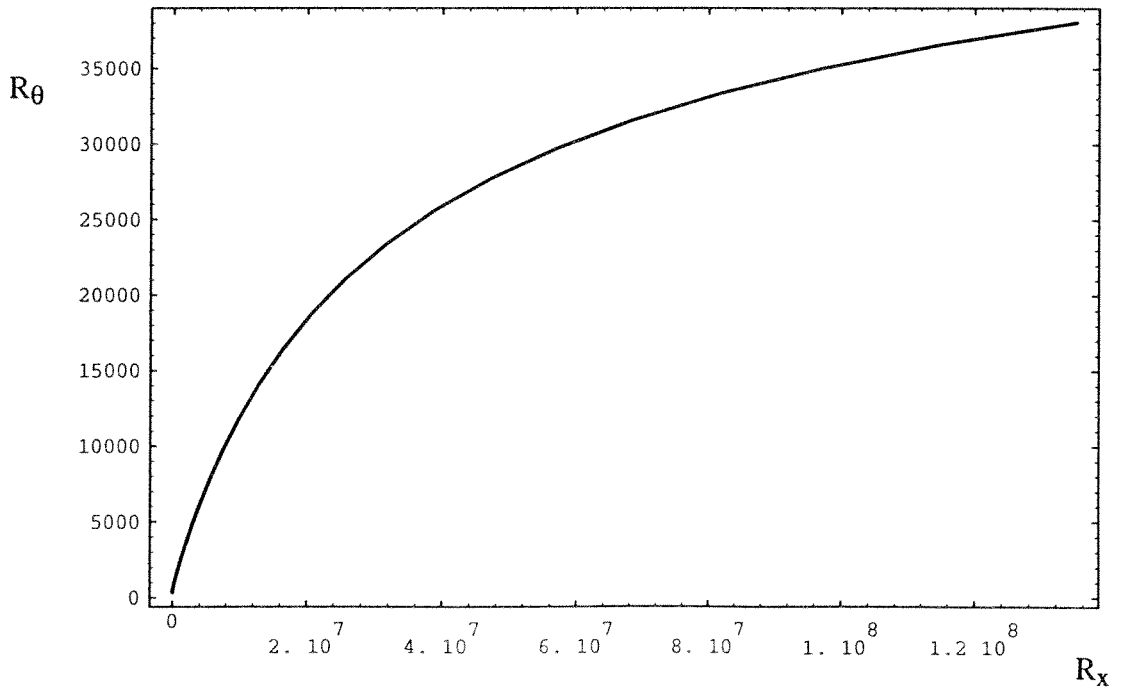

Figure 52: R_θ versus R_x for source flow, $K = -7.5 \times 10^{-8}$.

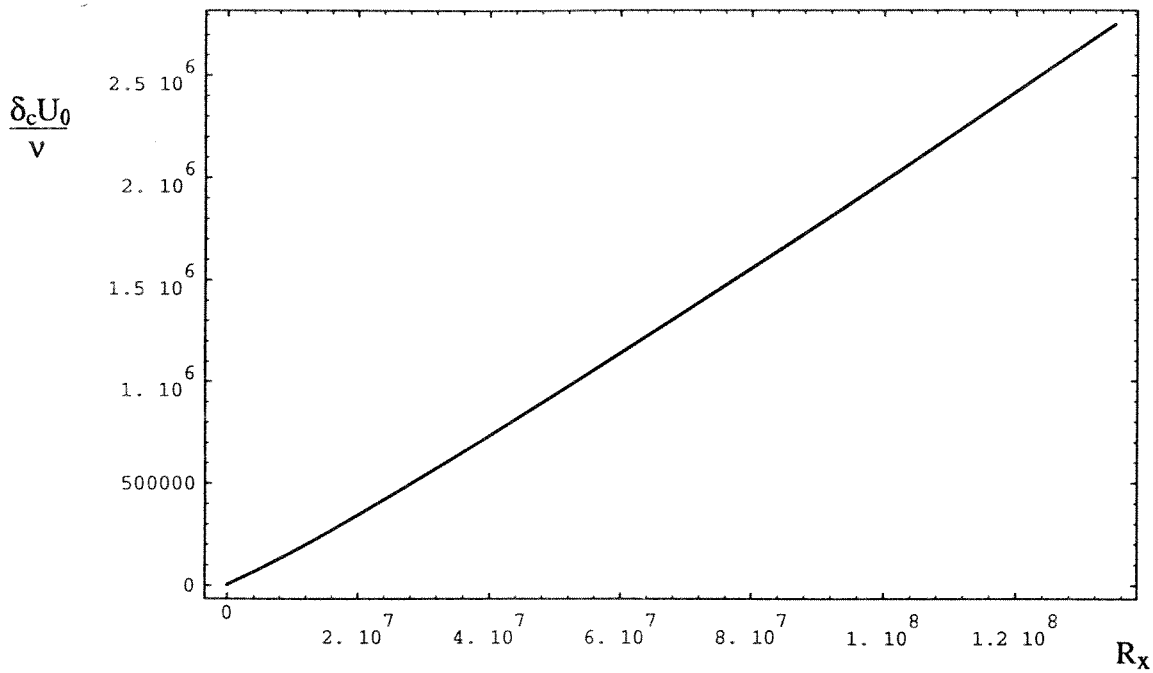

Figure 53: Source flow boundary layer growth versus R_x. $K = -7.5 \times 10^{-8}$.

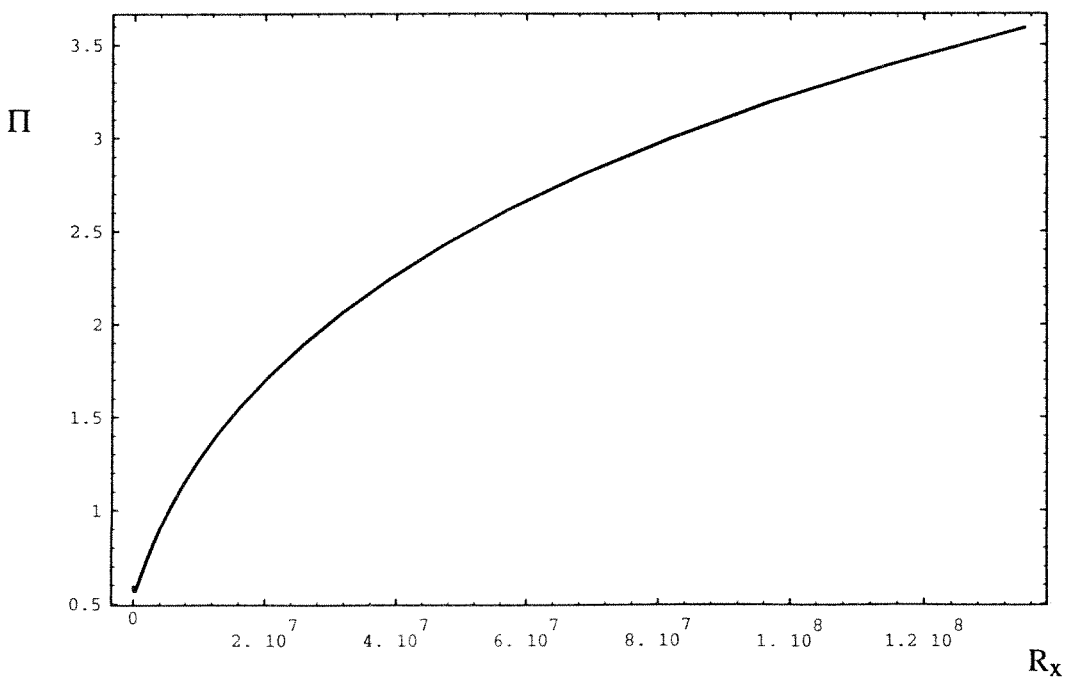

Figure 54: Π versus R_x for source flow, $K = -7.5 \times 10^{-8}$.

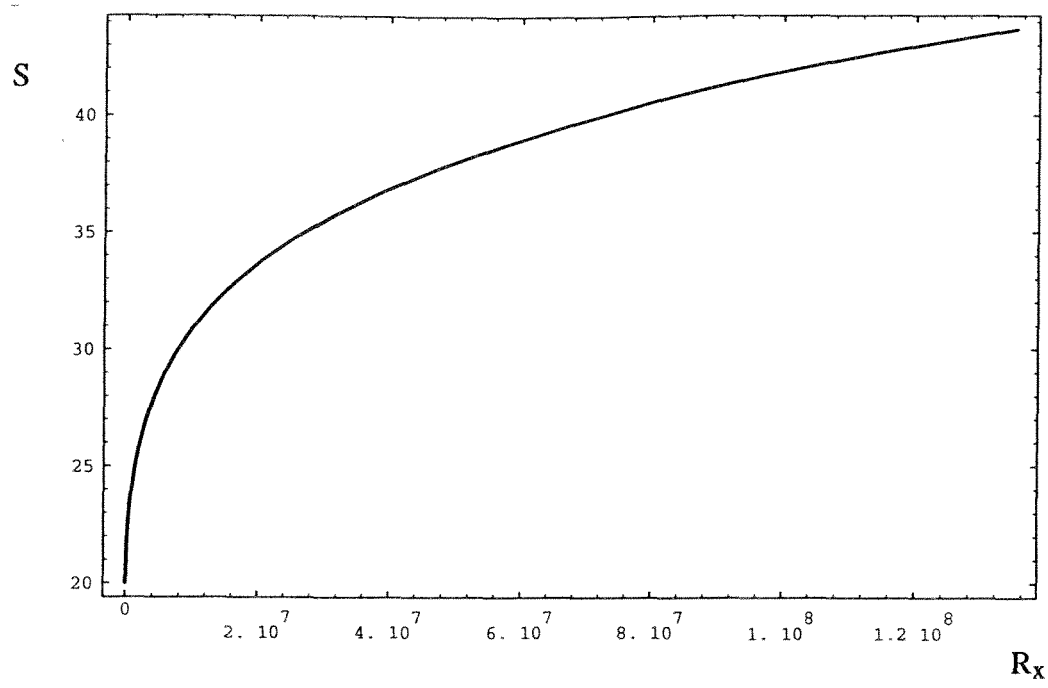

Figure 55: S versus R_x for source flow, $K = -7.5 \times 10^{-8}$.

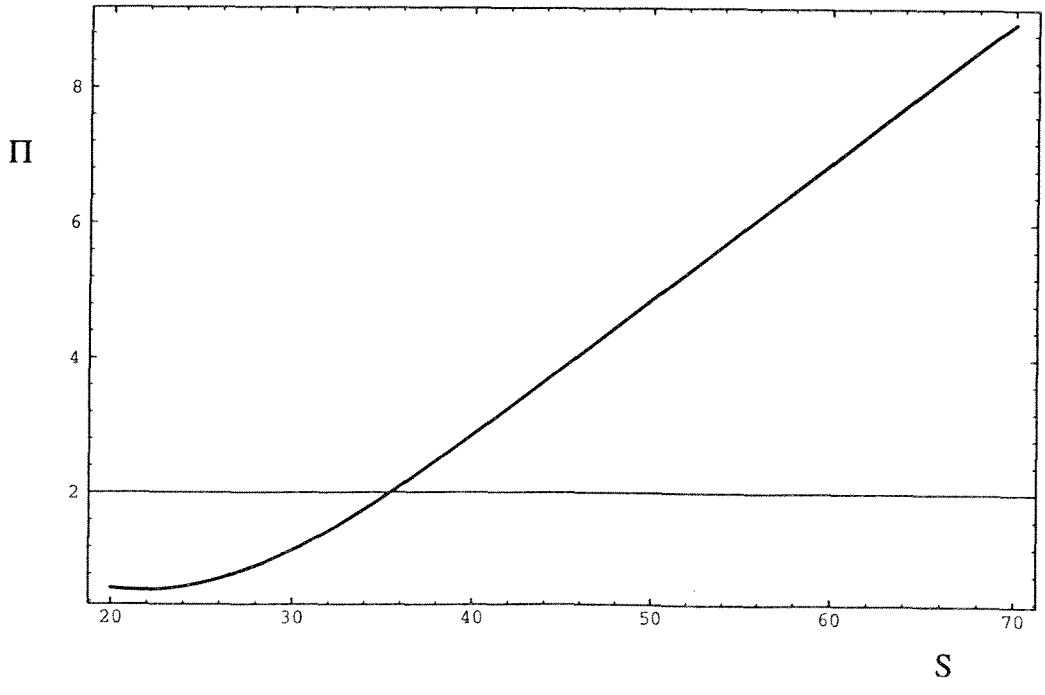

Figure 56: Π versus S for source flow, $K = -7.5 \times 10^{-8}$.

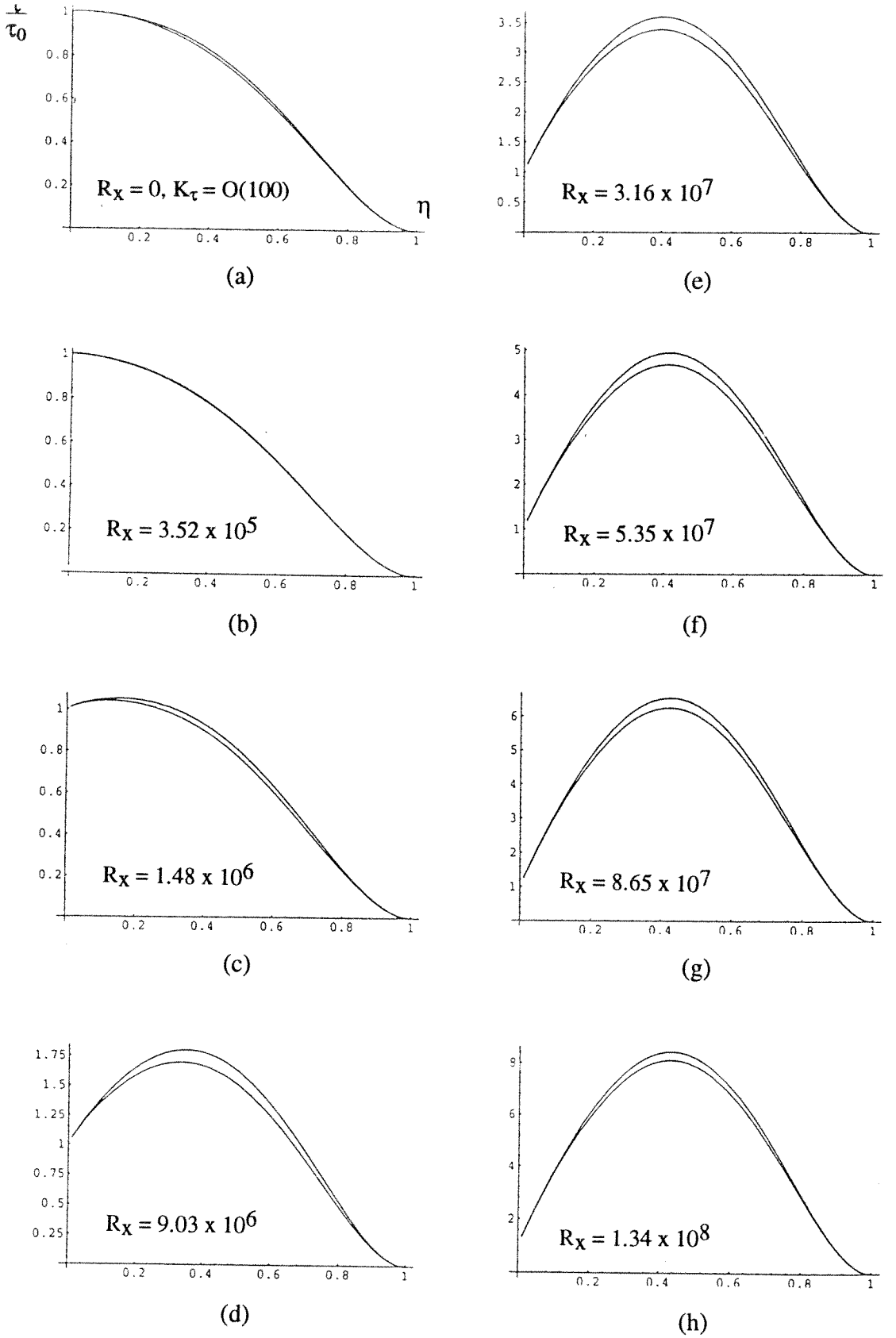

Figure 57: Source flow shear stress profiles given by equation (20) with and without the inclusion of the $\delta_c d\Pi/dx$ term. In all cases, $K = -7.5 \times 10^{-8}$.

7. Non-quasi Equilibrium Flow

It is quite obvious that for more general flow cases evolution equations need to be derived with an account made for the effects of $\delta_c d\Pi/dx$. This will give rise to differential equations involving $\delta_c d\Pi/dx$. Furthermore, a simple relationship between the asymptotic value of β (i.e., β_a say) and Π will no longer suffice for obtaining closure. For quasi equilibrium $\beta_a = \beta_g$ with β_g given by a curve fit like equation (56). However, this would need to be replaced by some sort of multi-dimensional fit and as a first attempt to consider a broader class of layers we could try

$$\beta_a = \beta_a \left[\Pi, \delta_c \frac{d\Pi}{d_x} \right] \tag{80}$$

and that in general

$$\beta = \beta \left[S, \Pi, \delta_c \frac{d\Pi}{d_x} \right] \tag{81}$$

It is conjectured that an analysis similar to that for equilibrium flow can be carried out which will yield (80) by forcing shear stress profiles to be invariant with S. In quasi equilibrium flow it was assumed that if Π is fixed so also is the shear stress distribution (i.e., S is not involved). By analogy, in non-quasi equilibrium flow Π and $\delta_c d\Pi/dx$ fix the shear stress profiles.

From the above philosophy and conjectures it can be seen that for closure we need equation (81). This relationship would probably need to be deduced from experiment. Unfortunately, this relation is for infinite S and experiments are carried out at finite S. Perhaps some sort of extrapolation scheme could be devised for obtaining (81). Whatever is devised it is obvious that a great deal of high quality experiments will be required. Large gaps will exist in the data no matter how extensive or thorough the experimental program is, and some sort of modeling might be needed to curve fit the results for the purposes of extrapolation and interpolation. As in the past, turbulence modeling gives rational tools for curve fitting.

A promising candidate for such modeling is the attached eddy hypothesis.

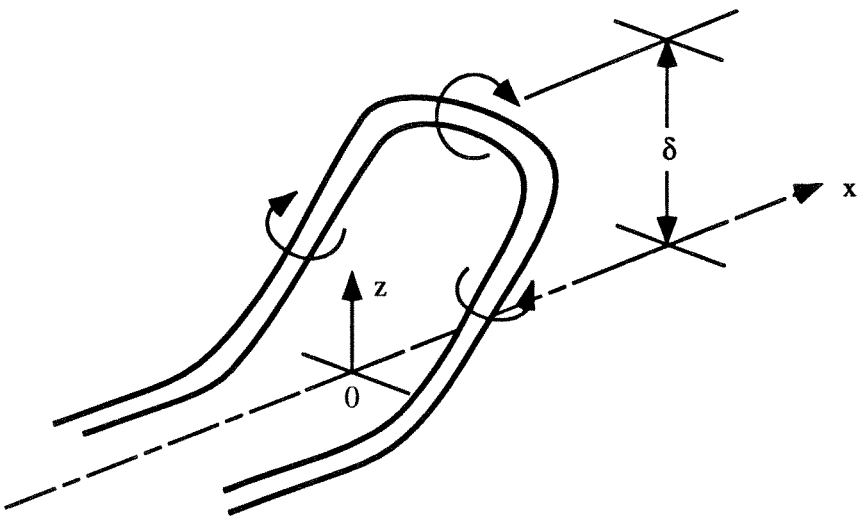

Figure 58: Sketch of attached eddy of length scale δ.

8. Application of the Attached Eddy Hypothesis

Figure 58 shows schematically a representative attached eddy in a turbulent boundary layer. It leans in the streamwise direction at a fixed angle, its height is δ and it can be seen to contribute to a spanwise component of vorticity. If there is a random array of such eddies with an average surface density proportional to $1/\delta^2$, then the contribution from such an array of height δ to the mean vorticity is given by ξ, where

$$\xi = \frac{U_\tau}{\delta} f\left[\frac{z}{\delta}\right] \tag{82}$$

where U_τ is the characteristic velocity scale of the eddy (assumed to be the friction velocity). The function f depends on eddy shape and can be found by finding the mean spanwise component of vorticity on horizontal sectioning planes. See Perry and Chong (1982) and Perry, Henbest and Chong (1986). From the Biot Savart law the contribution to the Reynolds stress $\Delta(\overline{u_i u_j})$ is given by

$$\frac{\Delta(\overline{u_i u_j})}{U_\tau^2} = I_{ij}\left[\frac{z}{\delta}\right] \tag{83}$$

Here u_i are fluctuating components of velocity, i.e. $u_1 = u'$, $u_2 = v'$ and $u_3 = w'$ used earlier. This application of the Biot Savart law need be applied to only one eddy and an image of it in the wall. Again this is outlined in Perry et al (1986). Introducing logarithmic variables

$$\lambda = ln\left[\frac{\delta}{z}\right], \lambda_1 = ln\left[\frac{\delta_1}{z}\right] \text{ and } \lambda_E = ln\left[\frac{\delta_c}{z}\right] \tag{84}$$

then it can be shown, with an array of eddies randomly distributed over the wall, that the gradient of the mean velocity defect $U_D^* = (U_1 - U)/U_\tau$ and the Reynolds stress $\overline{u_i u_j}$ are given by two convolution integrals

$$\frac{dU_D^*}{d\lambda_E} = \int_{-\infty}^{\infty} Mf[\lambda]e^{-\lambda}\omega[\lambda - \lambda_E]T[\lambda - \lambda_E]d\lambda \tag{85}$$

$$\frac{\overline{u_i u_j}}{U_\tau^2} = \int_{-\infty}^{\infty} MI_{ij}[\lambda]\omega[\lambda - \lambda_E]T^2[\lambda - \lambda_E]d\lambda \tag{86}$$

where eddies have scales δ ranging from δ_1 (the scale of the smallest eddy $\approx 100\nu/U_\tau$) to δ_c, the scale of the largest eddy which is equal to the boundary layer thickness. It is assumed that all eddies are geometrically similar.

Equations (85) and (86) were first derived by Perry, Li and Marusic (1991) and are a generalization of Townsend's (1976) attached eddy hypothesis. However, they incorporated a change of eddy shape with scale which the author presently considers to be unnecessary at this stage. Here ω is a weighting function which is a measure of how the *pdf* of eddy scales differ from an inverse power law in δ. T is a weighting function which is a measure of how the velocity scale of eddies of a given scale δ differ from U_τ. The function ω switches to zero when $\lambda < \lambda_1$ and $\lambda > \lambda_E$. This effectively controls the limits of the integration.

The constant M in (85) and (86) is universal and its value depends on how f and I_{ij} are normalized. For $\delta/\delta_c \to 0$ but $\delta > \delta_1$, ω and T are unity and this ensures that we obtain the logarithmic defect law and $-\overline{u_1 u_3}/U_\tau^2 \to 1$ for z/δ_c sufficiently small. It is assumed that $\delta_c/\delta_1 \gg 1$, where this is actually proportional to the Kármán number. The functions $I_{ij}[z/\delta]$ are the Townsend eddy intensity functions and are shown in figure 59. Of particular importance is the behavior of $I_{ij}[z/\delta]$ as $z/\delta \to 0$. This behavior can be derived from Townsend's inviscid boundary condition applied at $z/\delta = 0$. These eddies

are assumed to ride over the boundary with slip. For simplicity we will assume that a representative eddy is a "Π-shaped" eddy, as shown in figure 60.

This gives a Dirac delta function for $f[\lambda]$ and $I_{13}[z/\delta]$ will be assumed to be a triangle. This is not precisely the case but is close. It satisfies the Townsend (1976) inviscid boundary condition and also shows the rapid drop in the far field influence of the eddy for $z > \delta$. The triangle distribution and the delta function are very convenient functions for convolution integrals and although they are approximation they are adequate for demonstration purposes here. Suppose we made ω and T equal to unity for all $\lambda - \lambda_E$ i.e., all δ/δ_c. Equation (85) will give a pure logarithmic defect profile and we know

$$\frac{dU_D^*}{d\lambda_E} = \frac{1}{\kappa} \tag{87}$$

and this sets the value of M and thus the normalizing factor for $f[\lambda]e^{-\lambda}$ is known. Thus $Mf[\lambda]e^{-\lambda}$ is known. Equation (86) gives a linear stress distribution equal to 1 for $z/\delta \to 0$. This boundary condition sets the normalization for $MI_{13}[\lambda]$. This case could represent flow in a duct with parallel walls since we have a logarithmic law in velocity defect from the wall to the centre and τ/τ_0 is linear going from 1 at $z/\delta_c = 0$ to 0 at $z/\delta_c = 1$. This result is completely at variance with standard eddy viscosity or mixing length theories. These would insist on a constant shear stress for a logarithmic profile of velocity whereas here we have a linear stress. Other mean velocity and shear stress profiles can be correctly represented with this formulation by appropriate and plausible variations of T and ω with (δ/δ_c). The formulation fits in very naturally with the law of the wall and law of the wake model and shear stress profiles of the correct shape can be easily generated.

Let us see if we can derive a function $\beta_a = \beta_a[\Pi]$ for quasi equilibrium flow with simple hypotheses. We will use the zero pressure gradient layer as a basic flow and attempt to use only emperical constants belonging to this zero pressure gradient case. For this example we will take $\Pi = 0.55$ (although perhaps with hindsight 0.45 should have been tried).

In equation (85) $dU_D^*/d\lambda_E$ is known since Π is known. $Mf[\lambda]e^{-\lambda}$ is known as was determined above since we are assuming a "Π eddy" shape. If we deconvolve (85) we obtain ωT. Now from the momentum theory for zero pressure gradient it can be shown

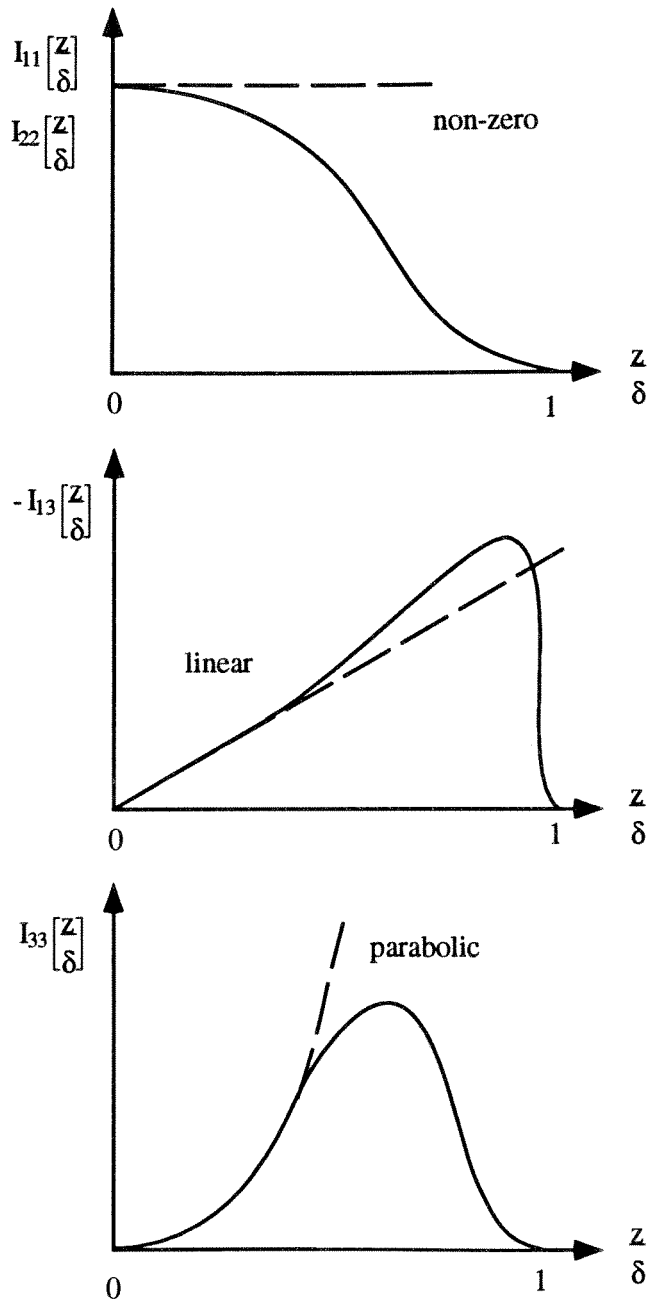

Figure 59: Townsend's eddy intensity functions. Sketch only

from (20) that for $\beta = 0$ and $\delta_c d\Pi/dx = 0$

$$\lim_{S\to\infty} \frac{\tau}{\tau_0} = 1 + \frac{\eta f - \int_0^\eta f d\eta}{C_1} \tag{88}$$

This has the interesting property that

$$\lim_{S\to\infty} \frac{\partial\tau/\tau_0}{\partial\eta} = -\frac{1}{\kappa C_1} \tag{89}$$

Here again we see, this time from momentum, that a logarithmic profile in mean velocity can be consistent with a varying stress distribution. Hence the LHS of (86) is known; $MI_{13}[\lambda]$ is known and by a deconvolution ωT^2 is known. From this and the previous result, ω and T are known separately for the zero pressure gradient case.

Let it now be assumed that

$$\omega = \omega[\lambda - \lambda_E]$$

and

$$T = T[\lambda - \lambda_E, \Pi]$$

i.e. $\omega[\lambda - \lambda_E]$ is universal for equilibrium and quasi equilibrium flow but T, the weighting factor for velocity scales depends on Π as well as $\lambda - \lambda_E$. Let us now apply (85) and (86) to pressure gradient flows. From (85) if we know Π we know the LHS. We know $Mf[\lambda]e^{-\lambda}$ since eddy shape will be assumed to be independent of pressure gradient. Now, $\omega[\lambda - \lambda_E]$ is known since it was obtained from the zero pressure gradient case and is taken to be universal. By a deconvolution of (85) we obtain $T[\lambda - \lambda_E, \Pi]$. We now substitute this into equation (86). We know $MI_{13}[\lambda]$ and $\omega[\lambda - \lambda_E]$ since it is universal and from a convolution of (86) we determine $-\overline{u_1 u_3}/U_\tau^2$.

Now it is known from (20) that for $\delta_c d\Pi/dx = 0$

$$\lim_{S\to\infty} \frac{\tau}{\tau_0} = 1 + \frac{2\beta_a \eta f}{C_1} + \frac{\eta f - \int_0^\eta f d\eta}{C_1} \tag{90}$$

By varying β_a we match (90) to the convolution integral result obtained from (86) above thus establishing a relationship between β_a and Π. In figure 61 the matched τ/τ_0 distributions given by (90) and (86) are shown. The matching was done on a least squares basis.

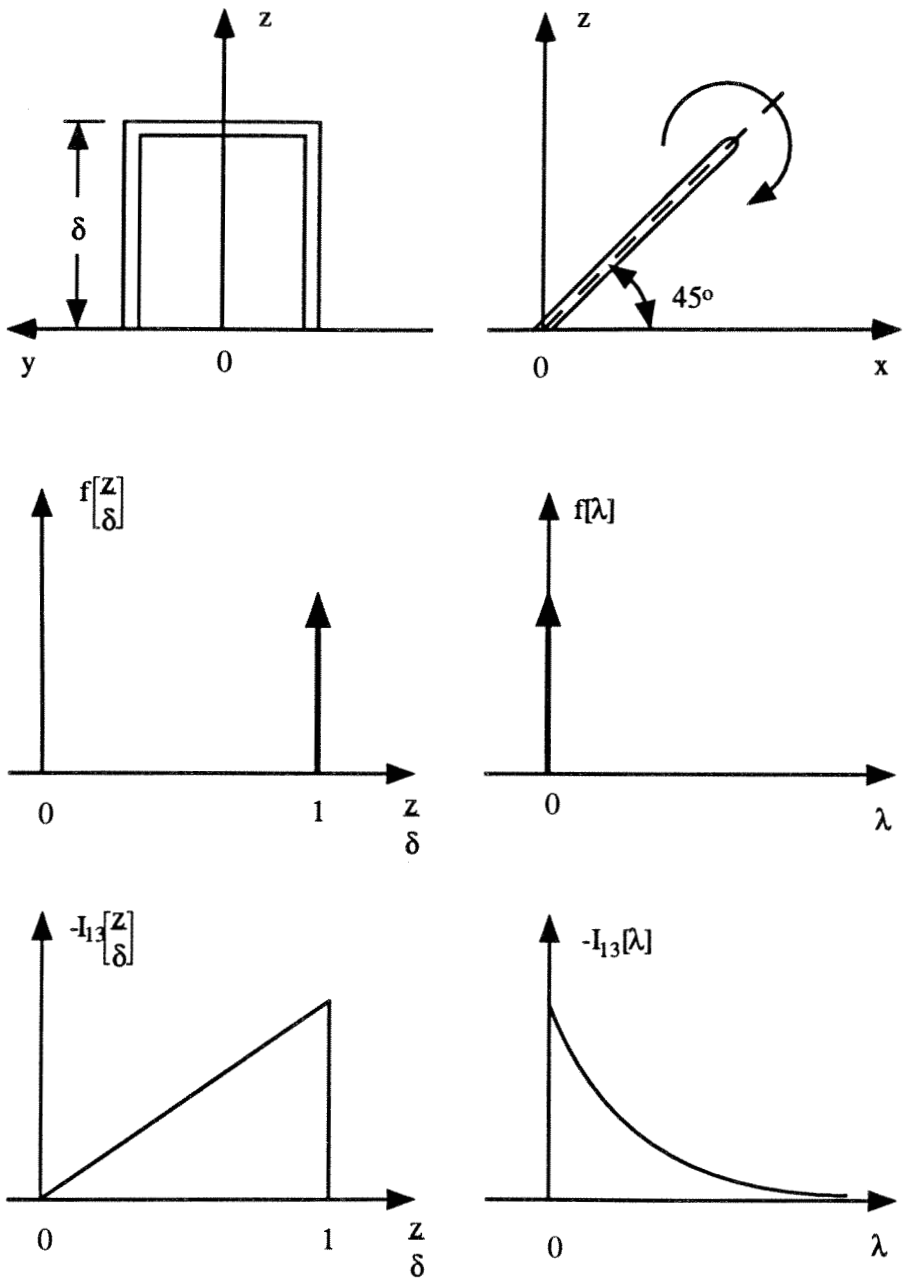

Figure 60: "Π-shaped" eddy details, its vorticity distribution and the assumed triangular eddy intensity distribution.

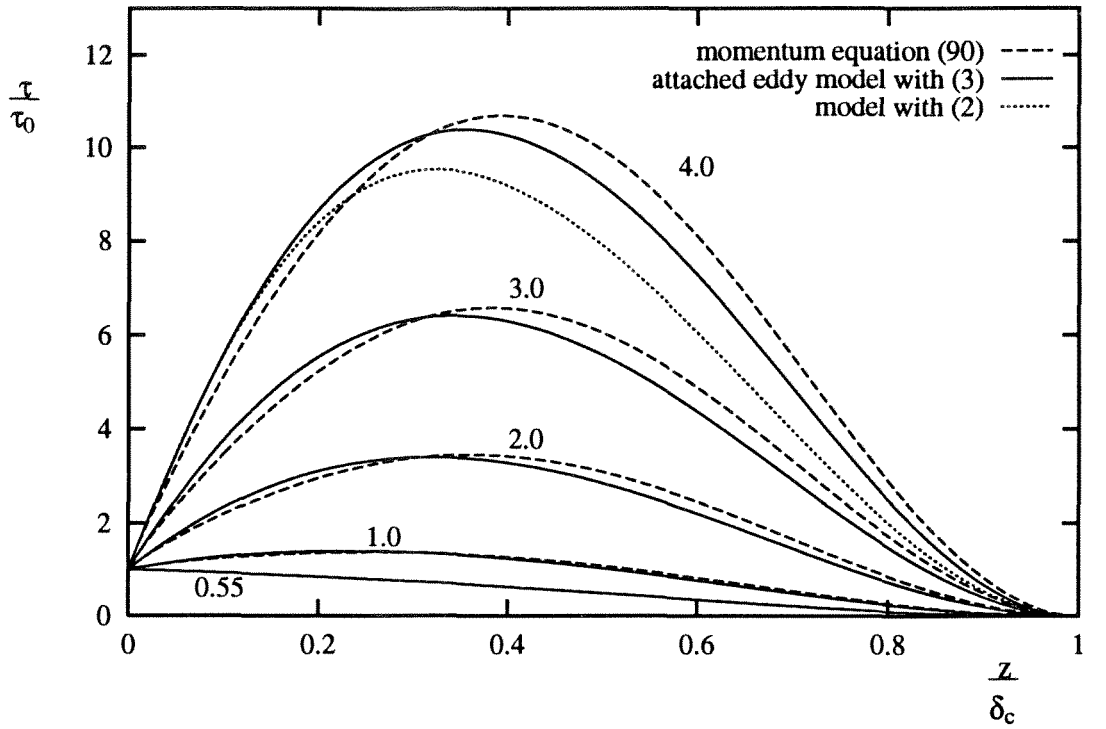

Figure 61: Comparison of the attached eddy model shear stress with the momentum equation (90) result.

For the particular arbitary choices made for f and I_{13}, it is seen that the trigonometric Coles wake function given by (3) works better than the Lewkowicz formulation (2) as seen for the $\Pi = 4$ case. On the other hand, the results from (90) and (56) are insensitive to the choice between these two wake functions. Figure 62(a) and (b) show β_a versus Π. Equation (3) was used for $\Pi > 0.25$ but (2) was used for $\Pi < 0.25$ because of problems with γ mentioned in §2. Considering the present crudity of the model, the results look promising.

Once the correct eddy shape is known the attached eddy hypothesis should give the broadband distributions of $\overline{u_1^2}/U_\tau^2$, $\overline{u_2^2}/U_\tau^2$, $\overline{u_3^2}/U_\tau^2$, $\overline{u_1 u_3}/U_\tau^2$ and all spectral distributions (see Perry, Henbest and Chong (1986) and Perry and Li (1991)). However, additional contributions from the Kolmogorov subrange would also need to be incorporated by further eddy structures additional to the attached eddies.

For the case of non-quasi equilibrium flow both ω and T will probably be functions

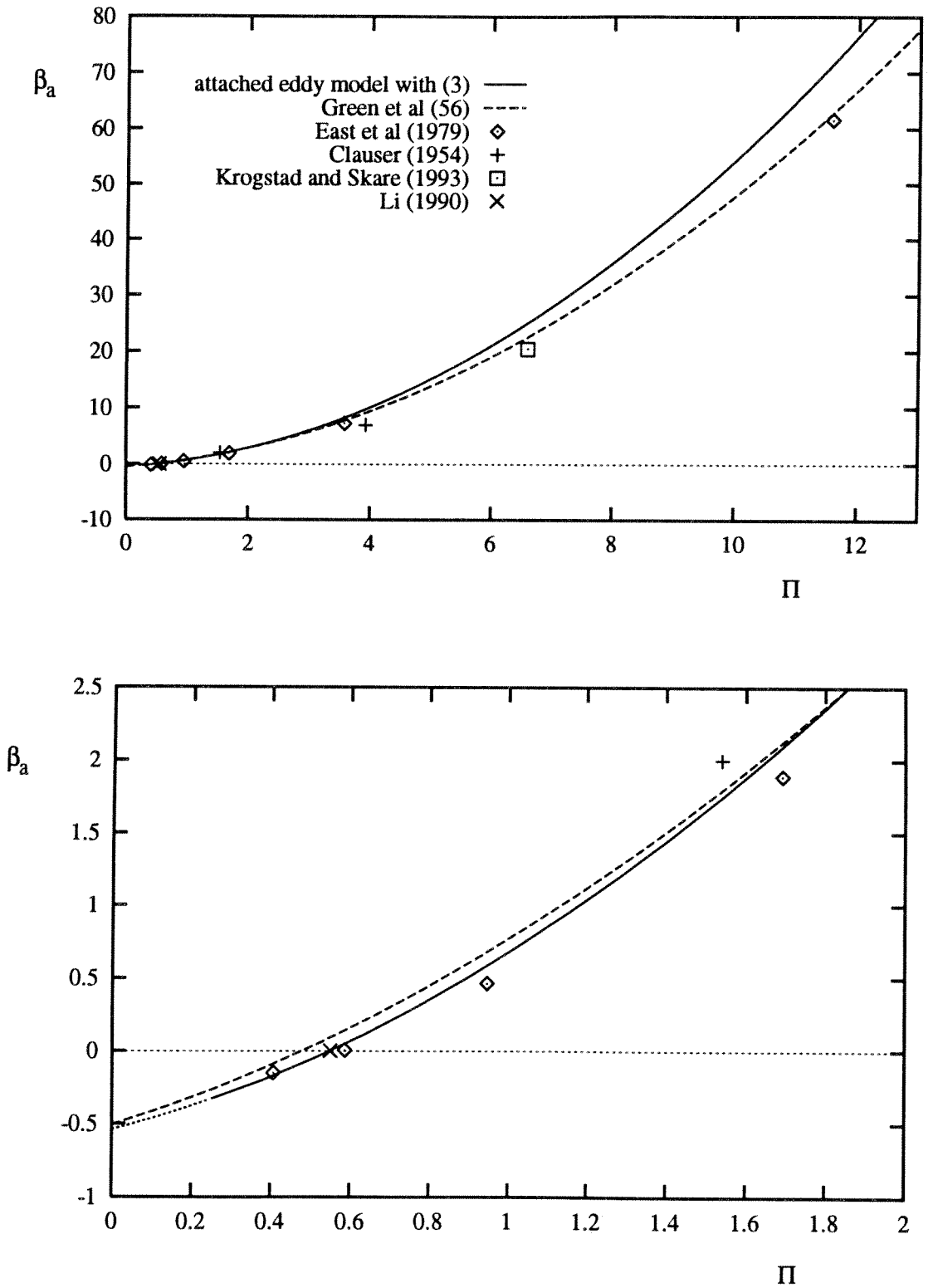

Figure 62: Attached eddy model prediction compared to empirical curve-fit of Green et al (1973) and experimental data. For the model formulation (3) is used for $\Pi > 0.25$ (solid line) and formulation (2) is used for $\Pi < 0.25$ (dotted line).

of both $\lambda - \lambda_E$ and Π. It is hoped that with the aid of experiment and hypotheses, some further valid physical insights into eddy structure will emerge.

9. Conclusions and Discussion

It appears that with the law of the wall and the wall of the wake formulations together with the self preserving flow hypothesis of Rotta (1962), that approximate equilibrium and quasi equilibrium layers have their nondimensional shear stress distributions completely specified once Π is specified. Thus Π specifies completely both the nondimensional velocity defect distribution and shear stress distribution. This is equivalent to having a universal distribution of eddy viscosity given by

$$\frac{\epsilon}{\delta_c U_\tau} = \phi[\eta, \Pi] \tag{91}$$

Such a relationship was first anticipated by Clauser (1956) and later developed in closely related closure schemes by Cebeci and Smith (1974) and Mellor and Gibson (1966). Thus equilibrium and quasi equilibrium conditions imply that equation (91) should be valid. This of course does not mean that there exists a gradient diffusion mechanism at work, it is simply that by default equations of the form of (91) work here. Such equations always work if there is a simultaneous self similarity in velocity defect and shear stress (e.g. plain mixing layers and under some conditions jets and wakes). As soon as $\delta_c d\Pi/dx$ has any effect (as is the case in the Marusic layer) equation (91) would come to grief if used as a closure hypothesis in a standard differential field method. On the other hand, one could say that the method developed here for equilibrium and quasi equilibrium flow is effectively an integral version of a Cebeci and Smith type of method but it has built in a warning which indicates when (91) is breaking down. Furthermore, closure does not come via an equation like (91) but an equation which gives the asymptotic value of β_a in terms of Π i.e.

$$\beta_a = \beta_a[\Pi]$$

This may be obtained experimentally perhaps if we know how to extrapolate to infinite S or with the aid of something like the attached eddy hypothesis. Such an hypothesis with

its convolution integrals used in conjunction with the integral scheme proposed here is consistent with Townsend's (1961) statements about modeling of wall turbulence. Rather than using exchange coefficients related to local flow variables, the layers should be looked at as an "integrated whole" with the transport properties at one point being related to motions in regions remote from the point of interest.

For the more general class of layers the influence of $\delta_c d\Pi/dx$ is appreciable and it is conjectured that we need a relation like

$$\beta_a = \beta_a \left[\Pi, \delta_c \frac{d\Pi}{d_x} \right].$$

The functional form of this could be deduced from systematic experimental data and the attached eddy hypothesis could be a useful curve-fitting device for interpolation and extrapolation. Perhaps by monitoring the behaviour of the weighting functions ω and T in experiments, some clues for further hypotheses may emerge.

Of course, everything treated here depends on the Rotta (1962) hypothesis, that is, given that conditions from continuity and momentum necessary for self similar flow are applied, it does not necessarily mean that this will occur. They are necessary conditions but may not be sufficient. Further systematic experiments are needed to verify this hypothesis.

10. Acknowledgements

The author wishes to acknowledge the great help resulting from many stimulating discussions with Dr D. Coles and Dr H. G. Hornung of G.A.L.C.I.T. Also the author's research fellow Dr Ivan Marusic is acknowledged for his help with the development of the material in §8 and in editing and assisting in the preparation of this report.

The author appreciates the efforts of Karen Cheetham and Georgia Frueh of G.A.L.C.I.T. who typed the first draft of the manuscript.

The Farichild Fellowship Scheme is gratefully acknowledged for enabling the author to spend the calendar year 1992 at G.A.L.C.I.T where he carried out this work. The author also acknowledges the Australian Research Council for the financial support of other aspects of this project being carried out in Australia.

11. References

Cebeci, T. & Smith, A. M. O. (1974). *Analysis of turbulent boundary layers.* Academic Press, New York.

Clauser, F. H. (1954). Turbulent boundary layers in adverse pressure gradients. *J. Aero. Sci.* **21**, 91–108.

Clauser, F. H. (1956). The turbulent boundary layer. *Advances in Mechanics* **4**, 1–51.

Coles, D. E. (1956). The law of the wake in the turbulent boundary layer. *J. Fluid Mech.* **1**, 191–226.

Coles, D. E. (1957). Remarks on the equilibrium turbulent boundary layer. *J. Aero. Sci.* **24**, 459–506.

Coles, D. E. (1962). The turbulent boundary layer in a compressible fluid. *USAF The Rand Cooperation, Rep. R-403-PR*, Appendix A.

East, L. F., Sawyer, W. G., & Nash, C. R. (1979). An investigation of the structure of equilibrium turbulent boundary layers. *R.A.E. Tech Report* 79040.

Green, J. E., Weeks, D. J., & Brooman, J. W. F. (1973). Prediction of turbulent boundary layers and wakes in compressible flow by a lag-entrainment method. *ARC R and M 3791.*

Jones, W. P. & Launder, B. E. (1972). Some properties of sink flow turbulent boundary layers. *J. Fluid Mech.* **56**, 337.

Krogstad, P.-Å. & Skåre, P. E. (1993). An experimental investigation of a turbulent equilibrium boundary layer near separation. In *Proc. Int. Conf. on Near-Wall Turbulent Flows.* Arizona, USA.

Lewkowicz, A. K. (1982). An improved universal wake function for turbulent boundary layers and some of its consequences. *Z. Flugwiss. Weltraumforsch.* **6**, 261–266.

Li, J. D. (1989). *The turbulence structure of wall shear flow.* PhD thesis University of Melbourne.

Marusic, I. (1991). *The structure of zero- and adverse- pressure gradient turbulent boundary layers.* PhD thesis University of Melbourne.

Mellor, G. L. & Gibson, D. M. (1966). Equilibrium turbulent boundary layers. *J. Fluid Mech.* **24**, 225–253.

Perry, A. E. (1968). A theoretical study of equilibrium turbulent boundary layers. (originally unpublised) now: *Rep.* FM-19. 1992 Dept. of Mech. Eng., University of Melbourne.

Perry, A. E., Bell, J. B., & Joubert, P. N. (1966). Velocity and temperature profiles in adverse pressure gradient turbulent boundary layers. *J. Fluid Mech.* **25**, 299–320.

Perry, A. E. & Chong, M. S. (1982). On the mechanism of wall turbulence. *J. Fluid Mech.* **119**, 173–217.

Perry, A. E., Henbest, S. M., & Chong, M. S. (1986). A theoretical and experimental study of wall turbulence. *J. Fluid Mech.* **165**, 163–199.

Perry, A. E. & Li, J. D. (1990). Experimental support for the attached eddy hypothesis in zero-pressure-gradient turbulent boundary layers. *J. Fluid Mech.* **218**, 405–438.

Perry, A. E. & Li, J. D. (1991). Theoretical and Experimental studies of shear stress profiles in two dimensional turbulent boundary layers. *Rep.* FM-18. Dept. of Mech. Eng., University of Melbourne.

Perry, A. E., Li, J. D., & Marusic, I. (1991). Towards a closure scheme for turbulent boundary layers using the attached eddy hypothesis. *Phil Trans. R. Soc. Lond. A* **336**, 67–79.

Rotta, J. C. (1962). Turbulent boundary layers in incompressible flow. *Prog. Aero. Sci.* **2**, 1–219.

Townsend, A. A. (1961). Equilibrium layers and wall turbulence *J. Fluid Mech.* **11**, 97–120.

Townsend, A. A. (1976). *The structure of turbulent shear flow.* Cambridge University Press.